

**Editor-in-Chief B.E.Paton**

**EDITORIAL BOARD**

Yu.S. Borisov, A.Ya. Ishchenko,  
B.V. Khitrovskaya (*exec. secretary*),  
V.F. Khorunov, I.V. Krivtsun,  
S.I. Kuchuk-Yatsenko (*vice-chief editor*),  
V.I. Kyrian, Yu.N. Lankin,  
V.N. Lipodaev (*vice-chief editor*),  
L.M. Lobanov, A.A. Mazur,  
O.K. Nazarenko, I.K. Pokhodnya,  
V.D. Poznyakov, I.A. Ryabtsev,  
K.A. Yushchenko,  
A.T. Zelnichenko (*exec. director*)

**INTERNATIONAL EDITORIAL  
COUNCIL**

N.P. Alyoshin (Russia)  
Guan Qiao (China)  
V.I. Lysak (Russia)  
B.E. Paton (Ukraine)  
Ya. Pilarczyk (Poland)  
O.I. Steklov (Russia)  
G.A. Turichin (Russia)  
M. Zinigrad (Israel)  
A.S. Zubchenko (Russia)

**Founders**

E.O. Paton Electric Welding Institute  
of the NAS of Ukraine,  
International Association «Welding»

**Publisher**

International Association «Welding»

*Translators:*

A.A. Fomin, O.S. Kurochko,  
I.N. Kutianova

*Editor*

N.G. Khomenko  
Electron galley  
D.I. Sereda, T.Yu. Snegiryova

**Address**

E.O. Paton Electric Welding Institute,  
International Association «Welding»  
11, Bozhenko Str., 03680, Kyiv, Ukraine  
Tel.: (38044) 200 60 16, 200 82 77  
Fax: (38044) 200 82 77, 200 81 45  
E-mail: journal@paton.kiev.ua  
www.patonpublishinghouse.com  
URL: www.rucont.ru

State Registration Certificate  
KV 4790 of 09.01.2001  
ISSN 0957-798X

**Subscriptions**

\$348, 12 issues per year,  
air postage and packaging included.  
Back issues available.

All rights reserved.

This publication and each of the articles  
contained herein are protected by copyright.  
Permission to reproduce material contained in  
this journal must be obtained in writing from  
the Publisher.

## CONTENTS

### SCIENTIFIC AND TECHNICAL

- Lobanov L.M., Pashchin N.A., Timoshenko A.N., Mikhoduj O.L.*  
and *Goncharov P.V.* Effect of preliminary deforming and  
electrodynamic treatment on stressed state of circumferential  
welded joints of AMg6 alloy ..... 2
- Kozulin S.M., Lychko I.I. and Podyma G.S.* Structure and  
properties of steel 35L welded joints produced using  
multilayer electroslag welding ..... 7
- Marchenko A.E. and Skorina N.V.* Influence of technological  
factors in manufacture of low-hydrogen electrodes on  
hydrogen content in the deposited metal ..... 13
- Chernobaj S.V.* Welding of titanium aluminide alloys (Review) ..... 25
- Bryzgalin A.G.* Calculation of parameters of explosion  
treatment for reduction of residual stresses in circumferential  
welds of pipelines ..... 31

### INDUSTRIAL

- Kaleko D.M.* Welding of steel studs to aluminum sheets ..... 37
- Maksimov S.Yu. and Lyakhovaya I.V.* Wet underwater welding  
of low-alloy steels of increased strength ..... 42
- Kuskov Yu.M., Bogajchuk I.L., Chernyak Ya.P. and Evdokimov*  
*A.I.* Electroslag surfacing of parts, made of high-chrome cast  
iron, using cast iron shot ..... 46
- Stefaniv B.V.* Peculiarities of induction brazing of  
diamond-hard alloy cutters to blade of body of complex drill  
bit ..... 49
- Rudenko P.M. and Gavrish V.S.* Thyristor direct converters for  
supply of resistance welding machines ..... 54

«The Paton Welding Journal» abstracted and indexed in Ukrainian refereed journal «Source», RJ VINITI «Welding» (Russia), INSPEC, «Welding Abstracts», ProQuest (UK), EBSCO Research Database, CSA Materials Research Database with METADEX (USA), Questel Orbit Inc. Weldasearch Select (France); presented in Russian Science Citation Index & «Google Scholar»; abstracted in «Welding Institute Bulletin» (Poland) & «Rivista Italiana della Saldatura» (Italy); covered in the review of the Japanese journals «Journal of Light Metal Welding», «Journal of the Japan Welding Society», «Quarterly Journal of the Japan Welding Society», «Journal of Japan Institute of Metals», «Welding Technology».



# EFFECT OF PRELIMINARY DEFORMING AND ELECTRODYNAMIC TREATMENT ON STRESSED STATE OF CIRCUMFERENTIAL WELDED JOINTS OF AMg6 ALLOY

L.M. LOBANOV, N.A. PASHCHIN, A.N. TIMOSHENKO, O.L. MIKHODUJ and P.V. GONCHAROV

E.O. Paton Electric Welding Institute, NASU

11 Bozhenko Str., 03680, Kiev, Ukraine. E-mail: office@paton.kiev.ua

At the present time the methods of control of welded and technological stresses based on preliminary deforming of elements being welded and also electrodynamic treatment (EDT) of welds using pulsed current become ever more developed. The aim of the work is the investigation of influence of preliminary unclamping of edges being welded and EDT on control of stressed state of circumferential welded joints specimens of aluminium alloy AMg6, made using automatic welding in argon. Control of stressed state of specimens was performed using method of electron speckle-interferometry with use of a specialized rigging. The preliminary unclamping of edges was performed using original device for force loading. The values of preliminary tensile stresses reached the yield strength of AMg6 alloy. The EDT was conducted at the surface of deposited metal in the direction «from middle to edges» at a charged voltage of capacitive storage up to 450 V. As a result of carried out investigations it was established that preliminary unclamping and EDT allow significant decreasing of level of residual stresses in circumferential welded joints. 10 Ref., 6 Figures.

**Keywords:** *electrodynamic treatment, preliminary unclamping of edges being welded, aluminium alloy, tensile stresses, compressive stresses, circumferential welded joint, automatic welding, capacitive storage, current discharge, plane inductor*

Welded structures of aluminium alloys find ever wider application in different branches of modern industry. One of the factors negatively influencing the service efficiency of welded joints is residual stresses, high level of which decreases the service life of structures at fatigue and dynamic loads, characteristic of products of transport machine-, air- and ship-building. Therefore the problem of control of welding residual stresses is challenging in welding of circumferential butt joints of light alloys.

The existing methods for control of stresses of large elements of structures, for example, preliminary deforming of parts assembled for welding, have the certain limitations, connected with the presence of a specialized fixture and not always can be realized under the conditions of unit-by-unit or module-block assembly-welding of a product [1].

At the present time the methods for control of welding and technological stresses based on treatment of metallic materials and structures using pulsed electromagnetic fields of different duration and configuration find the ever more spreading [2–6].

It is shown in work [7] that interaction of mechanical and electromagnetic pulses influences the movement of dislocation clusters in crystalline materials which causes change in their stressed state.

One of the methods of realization of mutual interaction of pulse electric field of a plane inductor and dynamic loading on welded joint is electrodynamic treatment (EDT) [8]. The EDT equipment, characterized by compactness and mobility, allows using this type of treatment to control the stressed state of welded joints in erection or repair large-size thin-wall products. The application of EDT showed its efficiency in repair welding of ship-hull structures of AMg6 alloy and allowed prolonging their service life [9].

The aim of this work is the investigations of efficiency of control of residual stresses in circumferential butt joints of aluminium AMg6 alloy at their preliminary deforming and EDT.

As the object for investigations, the authors used specimens of circumferential butt-welded joints of AMg6 alloy. Before welding the specimens were subjected to heat treatment to eliminate technological stresses in them caused by mechanical treatment.

The specimens of circumferential joint, butt-welded, (Figure 1, *a*) were assembled of two cylindrical billets of AMg6 alloy of 100 mm diameter, 150 mm height and wall thickness of

3 mm. To provide preset assembly gaps, complete penetration and formation of reverse bead the specialized assembly device was applied, the appearance of which is presented in Figure 1, *b*. The principle of operation of the device is based on transformation of forward movement of screw pair into radial force of distance levers of unclamping hinge system, where at the places of coupling the cut out backing rings with forming groove were mounted. The value of unclamping force of backing rings was controlled by loading nut which provided the guaranteed mutual alignment of cylindrical billets, backing rings and optimal orientation of assembly gap, relative to the welding head.

In the zone of edges being welded of circumferential butts two levels of values of initial stressed state  $\sigma_0$  were preset using their radial unclamping. The level of component of initial stressed state in the circular direction at the distance of 10 mm from the butt was controlled by mechanical deformation meter.

In the specimens of the first type the values of initial stresses did not exceed 10–15 MPa, which allowed providing both necessary accuracy of assembly of circumferential butt for welding as well as distribution of residual stresses characteristic of full-scale structures welded without application of force devices.

In the specimens of the second type the initial stresses reached the value  $\sigma_{0,2}$  for AMg6 alloy which provided formation of plastic tensile deformations in welding and, as a consequence, fields of compressive stresses in a weld.

The welding of circumferential butts using non-consumable electrode was performed in the installation «MAGIC WAVE-3000» (Figure 2) at the «backward welding» position of torch with 60° angle to horizontal. At the smaller values of angle the instable arc burning takes place accompanied by periodic splashes of metal from the weld pool. The angle between the longitudinal axes of non-consumable electrode and bunch with filler wire amounted to 90°. The process was performed at the linear speed of 5.4 mm/s, welding current of 165 A and arc voltage of 18 V.

The initial stressed state of specimens of circumferential welded joints was measured using contact-free method of electron speckle-interferometry. The method was used, which is based on measurement of deformations at elastic unloading of metal volume in the investigated spots at the surface of specimen caused by drilling of blind holes of 1.0 mm diameter [10]. The optical scheme of interferometer was applied in the places where investigated area of the specimen

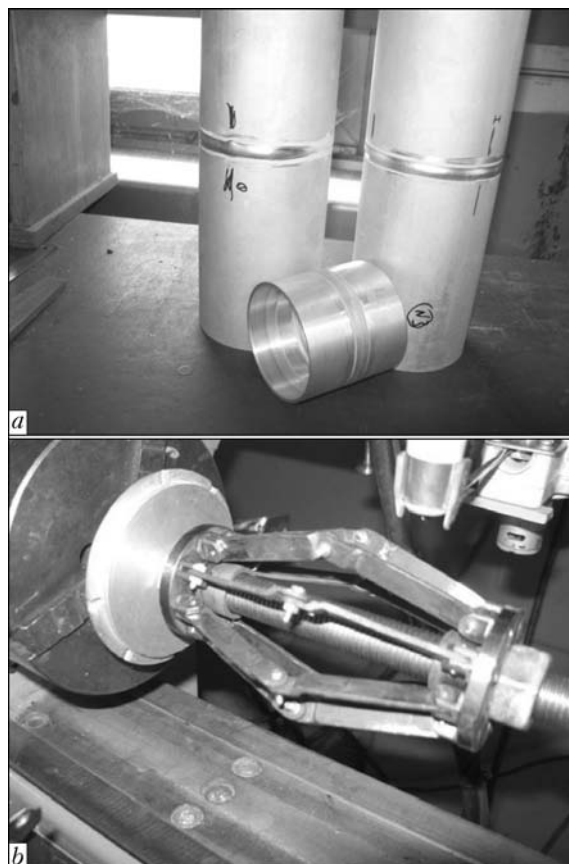


**Figure 1.** Appearance of specimens of AMg6 alloy circumferential butts (*a*) and assembly device for their welding (*b*) (on the right – loading nut)

was illuminated by the laser beam at the same angle from the both directions and, thus, plane components of movement vector were determined, characterizing deformation of specimen in the plane. The angle between the normal to the spot of investigated surface and illumination direction was 57°. The choice of this method was predetermined by need in preserving integrity of specimen after registration of its initial stressed state. The specimens with known level of initial stresses were subjected to pulse treatment and then the resulting values of stresses were repeat-

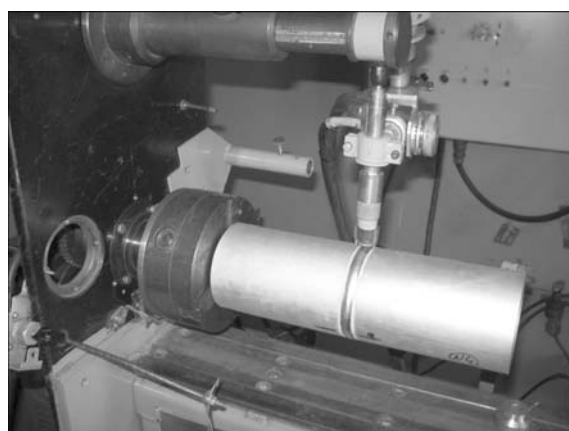


**Figure 2.** Argonarc welding of specimens of AMg6 alloy circumferential butts



**Figure 3.** Device and specialized fixture for measurement of residual stresses of welded circumferential joints of AMg6 alloy using method of speckle-interferometry

edly measured. Having combined the parameters of stressed state before and after the pulsed treatment on the specified specimen of welded joint it is possible to judge about efficiency of EDT process. To determine changes of level of stressed state of welded joints using speckle-method the small interferometer was used which was installed directly at the surface of investigated specimen (Figure 3). The device is composed of such basic components as speckle-interferometer, CCD-camera, light-guide, basement with three cone supports. For quality mounting of device on the cylindrical surface of circumferential weld a specialized fixture was designed. The parameters of stressed state of specimens of circumferential welds were recorded only at the external surface of joints.

Measurement of stresses using speckle-interferometry method was performed after mounting of interferometer on the surface of the specimen. The reflected light wave characterizing the initial stressed state of metal was entered to the memory of computer. Later in the specified spot of the surface of welded joint the blind hole of diameter and depth of 1.0 mm was drilled. After elastic unloading of stresses caused by drilling, the reflected light wave was also entered to the memory of computer. After computer processing of light waves received before and after the local elastic unloading of residual stresses, in the vicinity of a hole the fringe pattern was obtained by visualization means containing the information about parameters of stressed state in the controlled spot at the surface of specimen. During treatment of metal of welded joint using current pulses the stressed state is changed in it, the parameters of which are determined in the following measurement cycle. The cycle includes record of parameters of reflected light wave before and after the

drilling, obtaining of fringe pattern containing the characteristics of stressed state. Difference in values of stresses obtained in the first and second measurement cycles is the value of efficiency of EDT process as-applied to the welded joints.

Distribution of stressed state was studied on the external surface of circumferential joints by change of values of two its components – along  $\sigma_x$  and perpendicularly to  $\sigma_y$  of a weld line.

To treat the specimens using current pulses the installation was used, the basic element of which is a capacitive storage, and working device was a plane inductor coupled with a disc of non-ferromagnetic material and cylindrical electrode, the spherical edge of which is the zone of energy generation at the contact with treated surface of welded joint at the moment of discharge. The disc is intended for realization of dynamic component of electrodynamic effect on the metal. The principles of operation of the installation are given in the work [8], based on the transition electrodynamic processes which run in the metal of specimen at the discharge of the capacitive storage.

For EDT of specimens the assembly device was used (Figure 4) designed for positioning of inductor relatively to the specimen being treated and also for fixed contact of electrode edge with the surface of metal at the pressing force of up to 60 kg.

The device (Figure 4, *a*) is composed of a support beam 2 with a cradle of electrical copper of grade M1 which is the element of discharge circuit. The cradle, located on the face side of beam and coupled with a contact wire of capacitive storage, is designed for guaranteed clamping of specimen 1 at the moment of current discharge. To fix the plane inductor 6, a pressing beam 5 was used, the positioning of which relatively to the specimen was performed by guiding pins and vertical clamping force was created by loading nuts 4. The magnified fragments of positioning zone of electrode on the treated surface in EDT of circumferential joints are presented in Figure 4, *b*, where arrangement of plane inductance coil 7 is shown relatively to the disc of non-ferromagnetic material 8 and electrode 9. The force control of vertical loading of nuts 3 was performed using dynamometric key. It was established that the optimal pressing force providing the guaranteed contact of electrode edge in the absence of damage of the surface being treated, is the loading value close to 40 kg.

The EDT of butt welds of circumferential joints was performed at charge voltage of 450 V

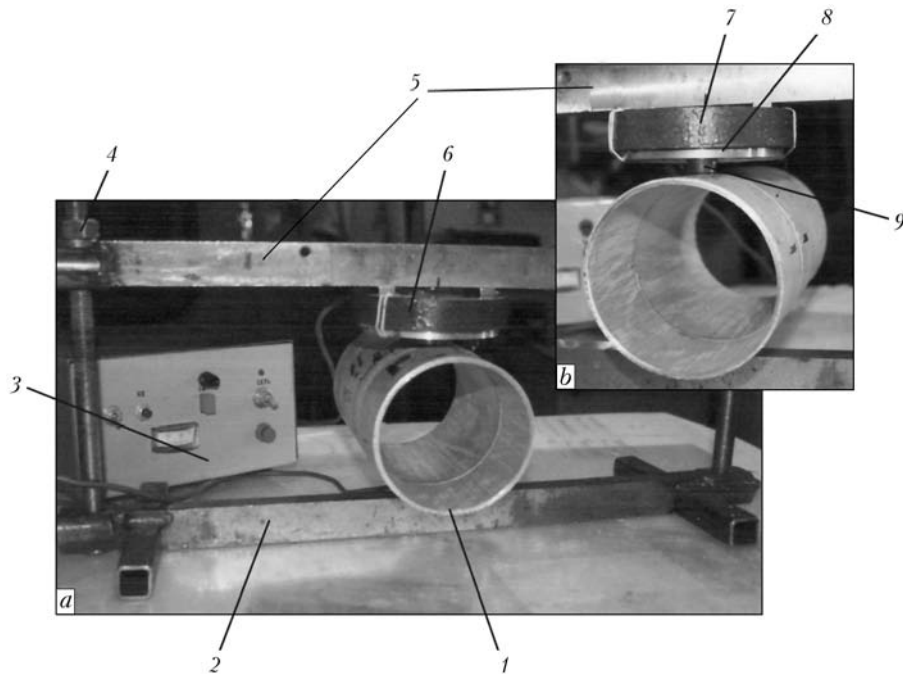


**Figure 4.** Assembly device for EDT of welded circumferential joints of AMg6 alloy (a) and inductor positioning (b): 1 – specimen; 2 – support beam; 3 – EDT power source; 4 – guiding pin with loading nut; 5 – pressing beam; 6 – inductor; 7 – inductance coil; 8 – disc; 9 – electrode

and in the storage capacity of 6600  $\mu\text{F}$ . The treatment was performed along the weld centre in the direction «from the middle to the edges» at a pitch of 10 mm in such a way that the first two zones of pulse effects were arranged on both opposite sides of a circumferential weld and the next two ones – within 90° as applied to the previous ones. Each area of the surface near the fusion line was exposed up to five electrodynamic effects.

At the circumferential welded butts, made without elastic-plastic unclamping of edges, the residual stressed state was recorded which is characterized by maximum values of longitudinal  $\sigma_x = 175$  MPa and transverse component  $\sigma_y = 125$  MPa (Figure 5, a). Here, if the tensile stresses  $\sigma_x$  are monotonously decreased almost to zero values in near-weld zone, then for  $\sigma_y$  stresses the non-monotonous distribution of values in weld area varied from 0 to 50 MPa is characteristic.

In the specimens welded applying the preliminary unclamping of edges, the stressed state is characterized by transformation of longitudinal component of tensile stresses  $\sigma_x$  to the compression area up to the values of 125 MPa at some lowering of tensile stresses  $\sigma_y$  down to 75 MPa (Figure 5, b). Thus, the preliminary force effect on the circumferential joint edges being welded results in increase of their diameter, positively influencing the distribution of  $\sigma_x$  at practically negligible influence on  $\sigma_y$ . It can be explained by the similarity of mechanisms of preliminary

unclamping of circumferential elements and tension of plane plates and panels [1].

In the specimens welded without unclamping of edges with the further EDT the longitudinal component  $\sigma_x$  also changed not only the value, but also the character and, as a result, its values amounted down to -100MPa, whereas values  $\sigma_y$  decreased to 100 MPa (Figure 6) which is comparable with the variant of welding under the conditions of edges unclamping (see Figure 5, b).

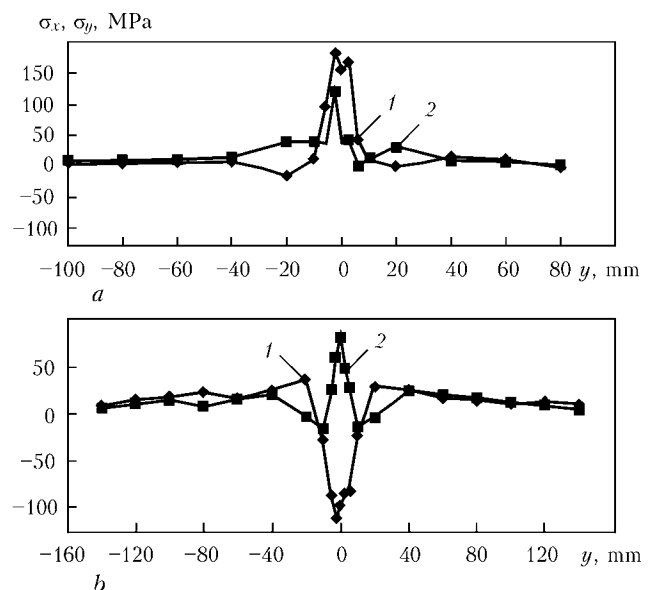


**Figure 5.** Residual stressed state in AMg6 alloy circumferential welded joint of longitudinal (1) and transverse (2) component of stresses without elastic-plastic unclamping (a) and after welding with preliminary unclamping of edges (b)

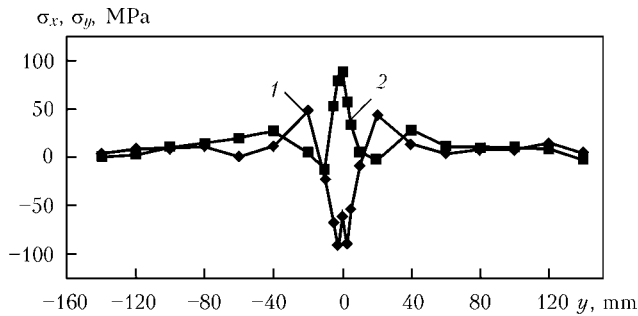


**Figure 6.** Stressed state in the specimen of circumferential joint after EDT of longitudinal (1) and transverse (2) stress component

It should be noted that the peculiar feature of unclamping method is the fact that it is the complex of technological effects on the joint, made both before welding as well as in the process of its performance. To realize the method, it is necessary to provide an access for fixture of unclamping device inside the edges being welded, performance of unclamping and removal of device.

The EDT is applied after producing a welded joint and for its realization the access to inner hollows of welded circumferential joint is not required. The labor consumption of EDT of circumferential joints is compatible with those, consumed in use of device for unclamping.

Thus, comparing the distribution of  $\sigma_x$  and  $\sigma_y$  for both variants of producing specimens of circumferential joints, shown in Figure 5, b and 6, one can conclude that EDT can be applied under the conditions when the method of preliminary unclamping of edges can not be realized.

### Conclusions

1. The experimental method for evaluation of effect of preliminary unclamping of edges and electrodynamic treatment on change of residual stressed state of circumferential welded joints was developed.

2. It was established that in preliminary unclamping of welded edges of AMg6 alloy circum-

ferential joints, when circumferential stresses reach the yield strength, transition of tensile stresses occurs at the external surface of circumferential weld of up to 175 MPa into compressive ones, the values of which reached 125 MPa.

3. It was shown that in electrodynamic treatment the decrease of longitudinal component of stresses reaches more than by 100 %.

1. Lobanov, L.M., Makhnenko, V.I., Trufiyakov, V.I. et al. (1993) *Welded building structures*. In: Vol. 1: Principles of structural design. Kiev: Naukova Dumka.
2. Tang, F., Lu, A.L., Mei J.F. et al. (1998) Research on residual stress reduction by a low frequency alternating magnetic field. *J. Mater. Proc. Technol.*, **74**, 255–258.
3. Stepanov, G.V., Babutsky, A.I., Mameev, I.A. (2004) Redistribution of residual welding stresses due to the treatment by pulsed electromagnetic field. *Problemy Prochnosti*, **4**, 60–67.
4. Stepanov, G.V., Babutsky, A.I., Mameev, I.A. (2011) Nonstationary stress-strain state in long bar caused by electric current pulses of high density. *Ibid.*, **3**.
5. Baranov, Yu.V., Troitsky, O.A., Avramov, Yu.S. et al. (2001) *Physical principles of electropulse and electroplastic treatments and new materials*. Moscow: MGIU.
6. Strizhalo, V.A., Novogrudsky, L.S., Vorobiov, E.V. (2008) *Strength of materials in cryogenic temperatures with action of electromagnetic fields*. Kiev: Ins-te for Problems of Strength.
7. Alshits, V.I., Darinskaya, E.V., Legenkov, M.A. et al. (1999) Motion of dislocations in NaCl crystals under combined action of mechanical and electromagnetic pulses produced by electron beam. *Fiz. Tsvorodogo Tela*, **41**(Issue 11), 2004–2006.
8. Lobanov, L.M., Pashchin, N.A., Cherkashin, A.V. et al. (2012) Efficiency of electrodynamic treatment of aluminium alloy AMg6 and its welded joints. *The Paton Welding J.*, **1**, 2–6.
9. Lobanov, L.M., Pashchin, N.A., Loginov, V.P. et al. (2010) Repair of ship hull structures of aluminium alloy AMg6 using electrodynamic treatment. *Ibid.*, **9**, 31–32.
10. Lobanov, L.M., Pivtorak, V.A., Savitsky, V.V. et al. (2006) Procedure for determination of residual stresses in welded joints and structural elements using electron speckle-interferometry. *Ibid.*, **1**, 24–29.

Received 04.06.2013



# STRUCTURE AND PROPERTIES OF STEEL 35L WELDED JOINTS PRODUCED USING MULTILAYER ELECTROSLAG WELDING

S.M. KOZULIN<sup>1</sup>, I.I. LYCHKO<sup>1</sup> and G.S. PODYMA<sup>2</sup>

<sup>1</sup>E.O. Paton Electric Welding Institute, NASU

11 Bozhenko Str., 03680, Kiev, Ukraine. E-mail: office@paton.kiev.ua

<sup>2</sup>NTUU «Kiev Polytechnic University»

6/2 Dashavskaya Str., 03056, Kiev, Ukraine. E-mail: meganom8@ukr.net

In multilayer electroslag welding the heat generated in the process of producing each layer effects the earlier welded areas of a groove performing its partial heat treatment and improving its mechanical properties. The aim of the work is the study of effect of thermal cycle on the structure and mechanical properties of welded joint in multilayer electroslag welding using consumable nozzle. The measurements of thermal cycles of the metal of heat affected zone were carried out. To study the effect of self-heat treatment on the structure and properties of welded joints the investigations were carried out including macro- and microanalysis of weld layers and their heat affected zones as well as mechanical tests of the characteristic areas of welded joints. It was found that in the overheating zone of base metal, not exposed to the reheating, the growth of grains reaches  $N^2$  and  $N^1$  according to the GOST 5639-82 and in the zones of reheating (self-heat treatment) –  $N^7$  and  $N^8$ . The hardness of metal of layers and areas of heat affected zone exposed to reheating is on average by 20 % lower than that of the areas of heat affected zone with base metal not exposed to reheating. It was shown that in multilayer electroslag welding alternatively from one edge of a butt to another one the volume of self-heat treatment of the layers of multilayer electroslag weld reaches 38.4 %. In multilayer electroslag welding with deposition of layers from the middle of a butt to its edges, the volume of self-heat treatment of the first (central) layer reaches 87 % and the rest (except of the external layers) is 30–43 %. It was established that the width of heat affected zone scarcely depends on specific energy input in the investigated range of its values. 19 Ref., 10 Figures.

**Keywords:** *multilayer electroslag welding, thermal cycle, self-heat treatment, heat affected zone, mechanical properties, impact toughness*

The quality of welded joint depends greatly on the structure and properties of a weld metal and heat affected zone (HAZ), which are determined by thermal cycle [1]. Except of melting and crystallization of weld metal the change of temperature results in structural transformations, volumetric changes, elastic-plastic deformations of product material, which at unfavorable thermal cycle in HAZ causes arising of brittle hardened structures for carbon and alloyed steels which predetermined the increased tendency of metal of this zone to cracks and brittle fracture of welded joint as a whole [2]. Therefore in welding of carbon structural steels the task is put to produce welded joint of a full strength.

For the thermal cycle of HAZ in electroslag welding (ESW) the delayed heating of this zone, its long exposure at the temperatures of overheating and next delayed cooling in the region of temperatures of pearlite, intermediate and martensite transformations are characteristic [2].

In multilayer electroslag welding (MESW) the heat generated in the process of producing each next layer affects the earlier welded areas of a groove, making their partial heat treatment and improving the mechanical properties [3–5]. The same heat creates the preliminary heating of base metal in not-welded part of a groove and decreases the cooling rate of welded part of a butt, which, as is known, creates favorable conditions for ESW of steels with increased carbon content. The investigations showed [5] that thermal cycles of HAZ metal in MESW have a complicated nature and remind of the thermal cycle of metal in multilayer manual welding [1].

ESW, unlike the known methods of fusion welding, is characterized by the highest heat inputs per a unity of thickness of welded butt [3], which leads to abrupt increase of HAZ width and growth of grains in it, zone of residual stresses and also higher deformations. It considerably influences the accuracy of geometric sizes of a product after its restoration. With increase of thickness of welded metal it is more difficult to minimize the negative effect of mentioned phenomena on the quality of welded joint due to increase of volume of liquid slag and metal pool. Therefore



the application of MESW can be considered to be the most preferable process to provide the quality of welded joint especially in repair of expensive large-size products where it is important to preserve their designed sizes [4, 6–8].

It is known that recrystallization of the metal structure during heating to the point higher than the critical ones results in grains refining at the areas of HAZ and weld overheating and also decrease in concentration of alloying elements and impurities at the grain boundaries [9]. In the metal of each previous layer the HAZ from deposition of the previous layer is observed. In the process of producing each next layer the heat, generating in the welding zone produces heat treatment of metal of the previous layer and HAZ [4, 10]. The data about nature of such heat treatment, its influence on structure and properties of welded joints in ESW with plug welds of circular blind holes of 60 mm diameter and 100 mm depth are given in work [5]. It is shown that impact toughness of deposited metal exposed to accompanying normalization is twice increased

and overheating area of HAZ exposed to recrystallization increases by 2.5–3 times as compared to deposited metal and HAZ of the last weld which were not exposed to self-heat treatment. At the areas of overheating zone exposed to heating in intercritical range of  $A_{c1}$ – $A_{c3}$  temperatures the impact toughness is 1.5 times increased.

Considering the non-conventional shape of edges preparation for investigated MESW [11] and presence of not one, but two heating centers in a slag pool [12], it became necessary to study the influence of self-heat treatment effect on the structure and mechanical properties of welded joints of the steel 35L. The investigations were carried out including experiments with measurement of thermal cycles of HAZ metal, macro- and microanalysis of layers of welds and their HAZ and also mechanical tests of characteristic areas of welds.

One of the specimens of the size  $290 \times 940 \times 520$  mm of steel 34L-ESh which is widely applied for manufacture by electroslag casting of welded-in bands of rotary furnaces [13], was welded in four passes using two-electrode consumable nozzle. MESW was performed with specific energy  $E_w = 110\text{--}170$  kJ/cm<sup>2</sup>. Welding up of holes was purposely performed without preheating of specimen. The measurements of thermal cycles were performed according to the method described in work [3], using six-channel self-recording device KSP-4 (Figure 1, a). The tungsten-rhenium thermocouples of grade VR 5/20 were used which were mounted along the axes of rectangular holes of edge groove for MESW at the equal distance from the end of one of the edge being welded (Figure 1, b). The results of measurements of thermal cycles of HAZ metal are given in Figure 2. The analysis of thermal cycles showed that cooling rates of HAZ metal of each layer in the range of temperatures of 600–500 °C ( $w_{6/5}$ ) do not exceed the critical values for the steel 35L [14] and also decrease with deposition of the layers  $N$  (Figure 2, b). According to the diagram of the structure components of HAZ metal given in work [15] the danger of martensite formation in this zone is absent. However at the beginning of producing of the first layer, i.e. at the non-steady electroslag process the accelerated cooling of metal occurs which under the conditions of increased rigidity of fastening of edges being welded can result in initiation of cracks-spallings and cracks-tears [10, 16]. The efficient method to prevent such cracks for steels, whose carbon equivalent  $C_{eq} > 0.5$ , is preliminary and concurrent heating of edges being welded up to the temperature of 150–

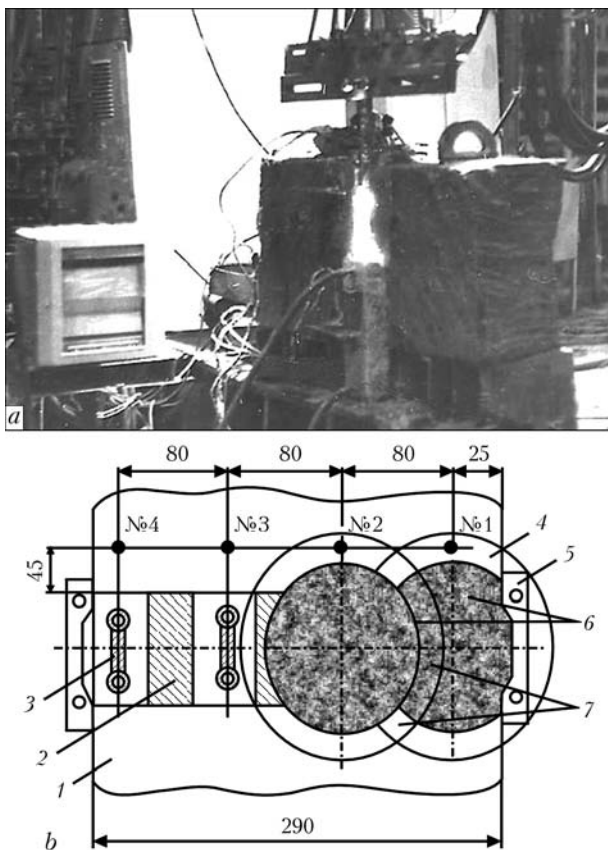


**Figure 1.** Fragment of measurement of thermal cycles of HAZ metal (a) and scheme of thermocouples arrangement in the specimen of steel 34L-ESh (b): 1 – edge being welded; 2 – forming plate; 3 – consumable nozzle; 4 – HAZ; 5 – water-cooled cover plate; 6 – layers of multi-layer electroslag weld; 7 – zones of reheating (self-heat treatment); No 1–4 are the ordinal numbers of points of thermocouples arrangement

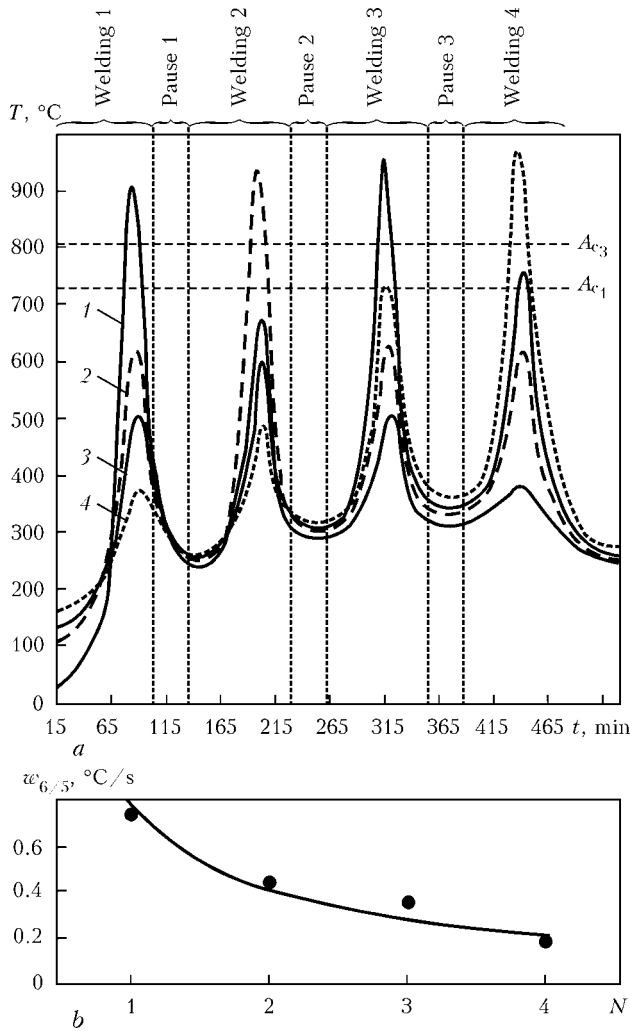


**Figure 2.** Thermal cycles of HAZ metal in MESW using consumable nozzle (a) and dependence of cooling rate of HAZ metal on number of produced weld layers (b): 1-4 – thermal cycles of HAZ metal corresponding to the numbers of thermocouples;  $A_{c1}$  and  $A_{c3}$  are the temperatures of critical points

200 °C [10]. During MESW the concurrent heating of edges being welded can be not performed, as during welding process the periodical heating of a product being welded occurs due to the heat generation in producing of previous layers (Figure 2, a).

During analysis the multilayer macrostructure of weld was revealed for which the column crystallization with predominant development of axial crystals is characteristic. In the first layer of weld the fine crystals of small section are detected and also uniaxial crystals are met. In the second layer the crystals are elongated and enlarged ones near the fusion zone. In the third layer the coarser, branchy crystals were detected. In the fourth layer the coarsest branches of crystals are observed. Such structure of crystals is characteristic for electroslag processes. In the investigated case the change of shape of crystals in the succession of producing layers of multilayer weld

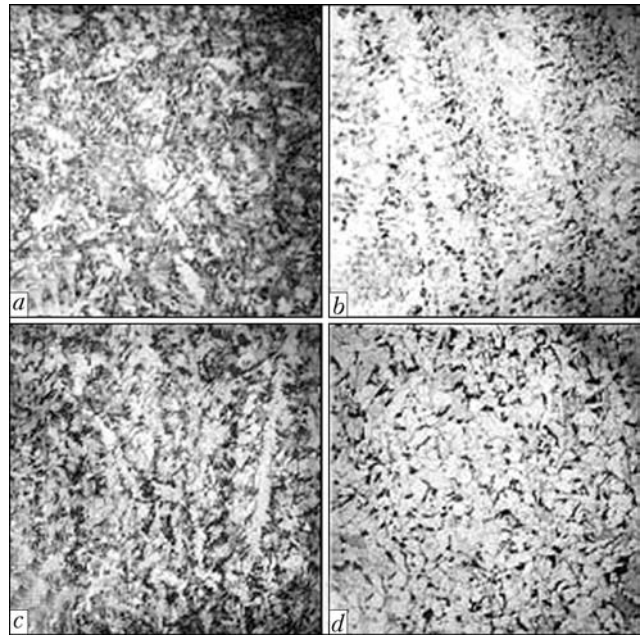


**Figure 3.** Microstructures ( $\times 100$ ) of interfaces of HAZ and deposited metal (steel 34L-ESh): a-c – of 1st–3rd layers; d – metal of 2nd layer exposed to reheating higher than the temperatures of  $A_{c3}$  point in making the 3rd layer

is caused by gradual heat saturation of specimen and corresponding decrease in speed of cooling of crystallizing metal of layers.

The investigation of microstructure of metal of layers of multilayer electroslag welds showed that in the overheating zone of base metal not exposed to reheating, the value of grains reaches  $N^2$  and  $N^1$  according to the GOST 5639–82 (Figure 3, a–c). In the zones of reheating (self-heat treatment) the growth of grains corresponds to  $N^7$  and  $N^8$  (Figure 3, d, Figure 4, c).

The analysis of micro- and macrostructures showed that similarly to the data given in the work [5], one regions of previous layers and their HAZ during producing next ones were heated higher than the temperature corresponding to the point  $A_{c3}$ , i.e. passed heat treatment as normalization, and other passed heat treatment in intercritical range of temperatures  $A_{c1}$ – $A_{c3}$ . For the steel 34L-ESh (analogue of the steel 35L) the temperatures of critical points  $A_{c1} = 730$ ,  $A_{c3} = 802$  °C [17]. Therefore the metal of layers and their HAZ, got into the zone of normalization, had to pass the complete recrystallization and have the fine-grain structure [5, 18], and also to possess the improved mechanical properties [10, 18]. In this connection, it is most desirable in MESW to maximum overlap the overheated areas of previous layers by the normalization zone.

To evaluate the effect of self-heat treatment on change of hardness of metal of welded joint, its measurements were made along the overheat areas of HAZ between the base and deposited

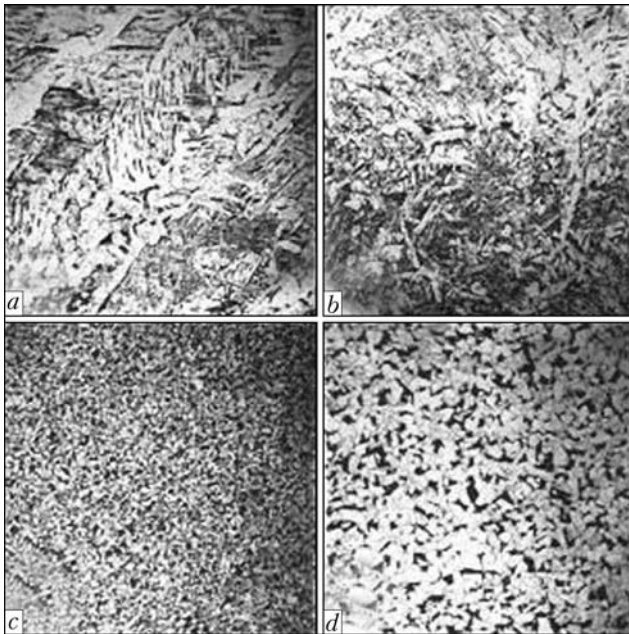


**Figure 4.** Microstructures ( $\times 100$ ) of base and deposited metal of layers of multilayer weld produced using MESW (steel 35L): *a* – deposited metal; *b* – fusion zone; *c* – deposited layer of metal exposed to reheating higher than the temperature of point  $A_{c3}$ ; *d* – base metal

metal and also centre of deposited metal. The analysis of obtained results showed that character of change of hardness of metal of multilayer electroslag welds has a common regularity. In Fi-

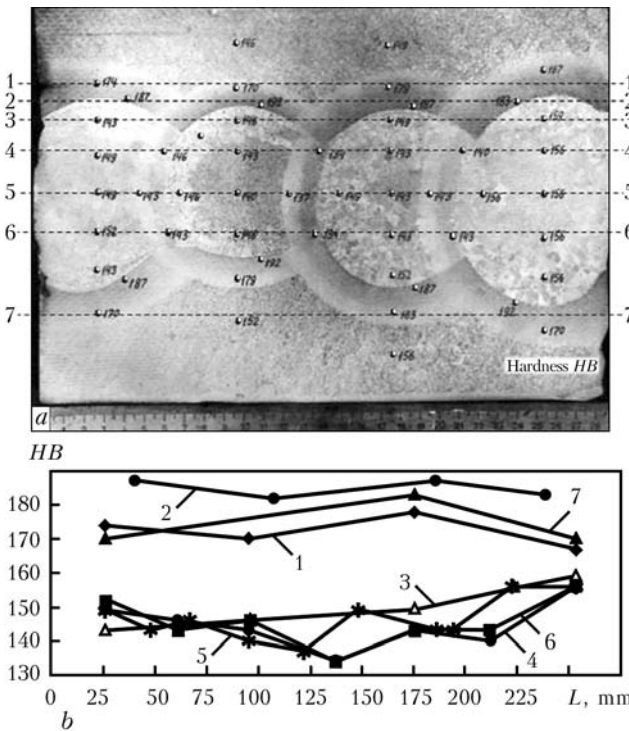


**Figure 5.** Macrostructure of cross section of multilayer electroslag weld at the depth of 120 mm from the surface of specimen of steel 34L-ESh (*a*) and character of change of hardness along its zones (*b*): 1, 2 and 7 – the lines of measurements of hardness along the zones of overheating the weld layers; 3 – the same in periphery regions of layers; 4–6 – the same in the centre of multilayer weld

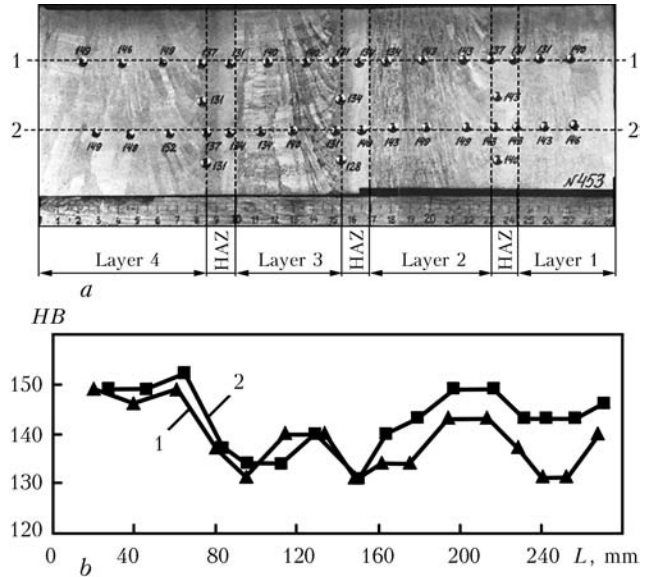


**Figure 6.** Macrostructure of central part of longitudinal section of multilayer electroslag weld at the specimen of steel 34L-ESh (*a*) and character of change of hardness along its zones (*b*): 1 and 2 – the lines of measurements of hardness; 1–4 – succession of producing weld layers

gures 5 and 6 the change of hardness in typical zones of cross and longitudinal sections of multilayer electroslag weld is shown. It is seen that hardness at the overheating area of each layer not exposed to reheating reaches maximum value of corresponding hardness of overheated zone of the last layer (Figure 5, lines of measurements 1, 2 and 7). The areas exposed to self-heat treatment and located at the central part of multilayer weld have the lowest values of hardness, which practically correspond to hardness of base metal (Figure 5, lines of measurements 3–6). The difference between the values of hardness at the area of overheating and central part of deposited metal is amounted, on average, to HB 20–30. The hardness of deposited metal in the layers of multilayer weld, exposed to reheating, is changed with the same difference of values (HB 5–10) and has the smallest value as compared to the hardness of metal of the last produced layers not exposed to reheating (Figure 6). It was established that hardness of metal of layers and HAZ areas exposed to reheating is in average 20 % lower than that of HAZ areas with the base metal not exposed to reheating.

To determine the mechanical properties of multilayer welded joints of specimens the transverse and longitudinal templates of 50 mm thickness were cut out of the specimens. The specimens to conduct tests of characteristic areas of welded joints for tensile and impact bending tests (GOST 6996–66) were cut out according to the schemes showed in Figure 7. The test results showed that strength characteristics of welded

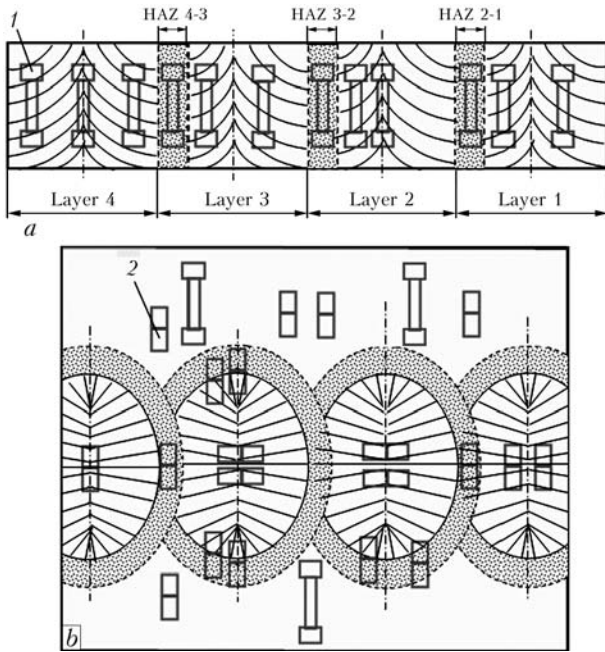


**Figure 7.** Scheme of cutting out of specimens for conductance of mechanical tests of welded joints produced using MESW: *a* – longitudinal; *b* – cross template of multilayer electroslag weld; 1, 2 – specimens for static tensile «gargin» and impact bend tests («Mesnager»), respectively

joints of steels 35L and 34L-ESh, rewelded by MESW, meet, in general, the requirements of standard documents [19]. Ductility of metal of weld layers has an increased values, especially in the zones exposed to concurrent self-heat treatment. The test results of welded joints on impact bending showed the following. The impact toughness  $\alpha_n$  in the zones of deposited metal which passed the concurrent self-heat treatment exceeds the values of test results of base metal and also standard requirements by 2–4 times (Figure 8). The values  $\alpha_n$  of metal in HAZ of weld layers at the boundary of fusion with the base metal correspond to the test results of base metal.

For quantitative evaluation of self-heat treatment effect on metal and corresponding HAZ of produced layers the measurements of HAZ width and also zone areas after reheating were carried out. The measurements were carried out in the following way. Scanned photos of transverse macrosections were placed on the working table of computer program «KOMPAS-3D V8» observing the scale. Then closed curves of Bezier were plotted following the visually observed lines of fusion and HAZ boundaries by which the areas of investigated regions with the accuracy of  $0.01 \text{ mm}^2$  were determined. It was established that in MESW the volume of self-heat treatment of layers of multilayer electroslag weld from one butt to another reaches 38.4 % (Figure 9). In MESW with deposition of layers from the middle of a butt to its edges the volume of self-heat

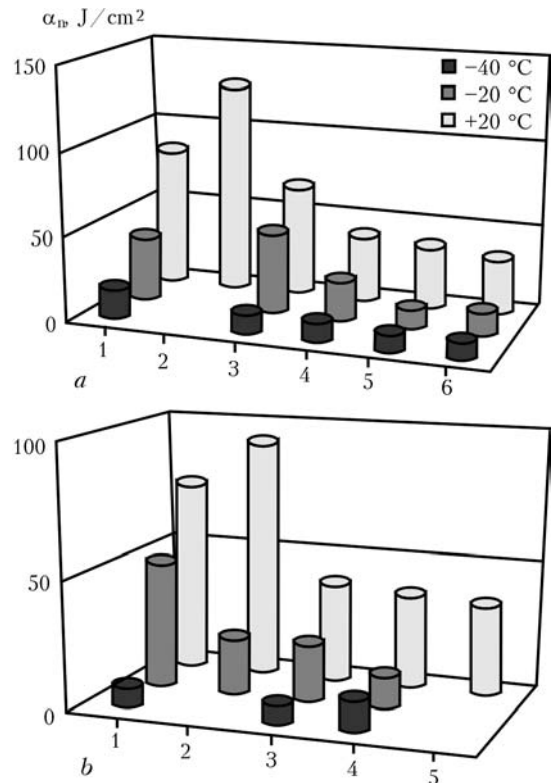


**Figure 8.** Impact toughness of welded joints and base metal: *a* – steel 35L (1 – deposited metal; 2 – HAZ in deposited metal; 3 – overheating zone at the distance of 0.75–3.0 mm from the fusion line; 4 – normalization zone at the distance of 10–15 mm from the fusion zone; 5 – base metal; 6 – GOST 977–88); *b* – steel 34L-ESh (1 – deposited metal; 2 – HAZ in deposited metal; 3 – normalization zone at the distance of 8–12 mm from the fusion line; 4 – base metal; 5 – TS 22102-61–81)

treatment of the first (central) layer reaches 87 % and the rest ones (except the external layers) is 30–43 %. Consequently, to improve the quality

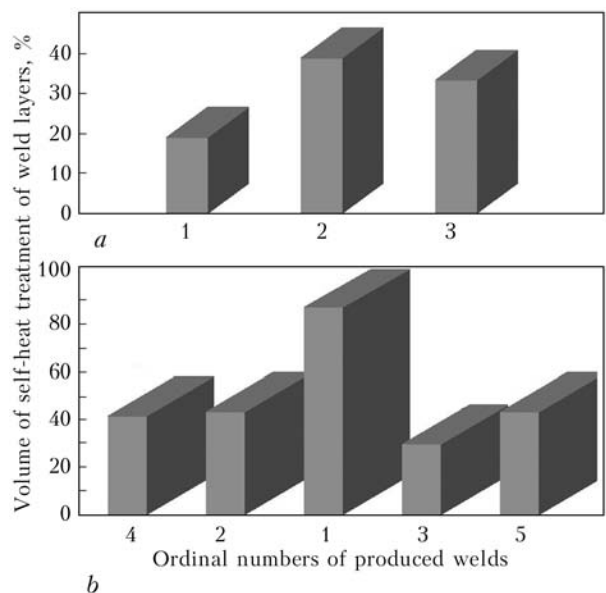


**Figure 9.** Dependence of volumes of self-heat treatment of layers of multilayer electroslag weld on the sequence of their producing: *a* – successively from one end of butt to another; *b* – the same from the middle of butt to its edges

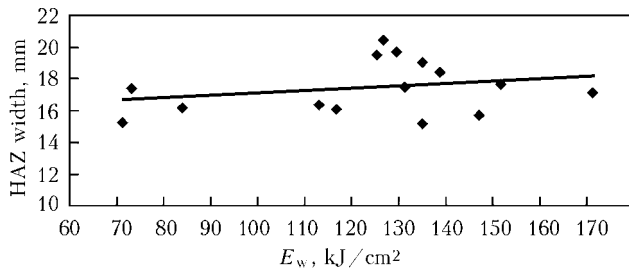


**Figure 10.** Dependence of HAZ width on specific energy of MESW

of welded joint produced using MESW the most preferable method is random deposition of layers from middle of a butt to its edges.

The carried out measurements showed that the width of HAZ is gradually increased in the direction from the first layer to the last one and reaches 14–20 mm. The width of HAZ of external (the last produced) layers reaches 22.6 mm which is explained by the presence of edge effect [1].

To evaluate the effect of specific energy of MESW on the width of HAZ the dependence was plotted (Figure 10) from which it follows that width of HAZ scarcely depends on  $E_w$  in the investigated range of its values. The obtained dependence can be used to predict volumes of self-heat treatment of layers of multilayer weld.

## Conclusions

1. It was established that as a result of effect of self-heat treatment of layers of multilayer weld the recrystallization of structure occurs facilitating the grains refining at the area of HAZ overheating and weld layer.

2. Mechanical tests of the characteristic areas of welded joints produced using MESW showed that in these zones the improvement of mechanical properties took place. The impact toughness  $\alpha_n$  in the zones of deposited metal passing the concurrent self-heat treatment exceeds the values of test results of base metal and also standard requirements by 2–4 times. The values  $\alpha_n$  of metal in HAZ of weld layers at the fusion boundary with base metal correspond to the test results of base metal.

Thus, in the process of repair of damaged parts at the site of their service using MESW it is possible to be limited by applying a local high tempering, that is most important in making these operations in site-field conditions.

3. The width of HAZ scarcely depends on specific energy input of the process in the investigated range of its values. It was shown that width of HAZ is increased in the direction from the first layer to next ones and reaches 14–20 mm.

1. Rykalin, N.N. (1954) *Calculations of heat processes in welding*. Moscow: Mashgiz.
2. Makara, A.M., Gotalsky, Yu.N. (1955) Investigation of thermal cycle of near-weld zone in electroslag welding in connection with problem of hardenable steels. *Avtomatich. Svarka*, **5**, 25–32.
3. Sushchuk-Slyusarenko, I.I. (1964) Deformation compensation in electroslag welding. *Ibid.*, **1**, 28–33.
4. Sushchuk-Slyusarenko, I.I. *Electroslag welding and cladding*. Moscow: VINITI.
5. Filchenkov, D.I., Kozulin, M.G. (1979) Calculation of thermal cycle for near-weld metal in electroslag plug welding. *Svarochm. Proizvodstvo*, **1**, 1–2.
6. Sushchuk-Slyusarenko, I.I., Lychko, I.I., Kozulin, M.G. et al. (1989) *Electroslag welding and cladding in repair operations*. Kiev: Naukova Dumka.
7. Sushchuk-Slyusarenko, I.I., Vergela, A.G., Shevchenko, N.T. (1969) Electroslag welding-up of cracks. *Avtomatich. Svarka*, **4**, 72–73.
8. Kozulin, S.M., Lychko, I.I. (2011) Deformations of welded joints in multilayer electroslag welding. *The Paton Welding J.*, **1**, 23–27.
9. Zemzin, V.N., Shron, R.Z. (1978) *Heat treatment and properties of welded joints*. Leningrad: Mashinostroenie.
10. (1959) *Electroslag welding*. Ed. by B.E. Paton. Kiev: Mashgiz.
11. Yushchenko, K.A., Kozulin, S.M. (2012) Specifics of electroslag welding technology for repair of defects in large parts of machine building units on-site of their operation. In: *Proc. of 3rd Sci.-Techn. Conf. on Welding Production in Machine Building: Prospects of Development* (2–5 Oct. 2012). Kramatorsk: DGMA, 2012.
12. Kozulin, S.M. (2011) Selection of the groove shape for repair of through cracks by multilayer electroslag welding. *The Paton Welding J.*, **3**, 32–35.
13. Kozulin, S.M., Lychko, I.I., Kozulin, M.G. (2007) Methods of reconditioning rotary kilns (Review). *Ibid.*, **10**, 33–39.
14. Popov, A.A., Popova, L.E. (1961) *Reference book of heat-treater. Isothermal and thermokinetic diagrams of decomposition of supercooled austenite*. Moscow: Mashgiz.
15. Shorshorov, M.Kh., Belov, V.V. (1972) *Phase transformations and change of properties of steel in welding*. Moscow: Nauka.
16. Makara, A.M., Kovalyov, Yu.Ya., Novikov, I.V. (1972) Tears on near-weld zone in electroslag welding of structural steels. *Avtomatich. Svarka*, **5**, 1–5.
17. Sorokin, V.G., Volosnikova, A.V., Vyatkin, S.A. et al. (1989) *Reference book of steel and alloy grades*. Ed. by V.G. Sorokin. Moscow: Mashinostroenie.
18. Livshits, L.S. (1979) *Metals science for welders*. Moscow: Mashinostroenie.
19. GOST 9770–88: Steel casts. General specifications. Intergovernmental standard. Introd. 01.01.90.

Received 30.05.2013



# INFLUENCE OF TECHNOLOGICAL FACTORS IN MANUFACTURE OF LOW-HYDROGEN ELECTRODES ON HYDROGEN CONTENT IN THE DEPOSITED METAL

A.E. MARCHENKO and N.V. SKORINA

E.O. Paton Electric Welding Institute, NASU

11 Bozhenko Str., 03680, Kiev, Ukraine. E-mail: office@paton.kiev.ua

PWI department of «Physico-chemical processes in the welding arc», led by Prof. I.K. Pokhodnya, academician of NASU, celebrated its 50th anniversary in 2012. Alongside the work on arc welding metallurgy and development of welding consumables, a considerable scope of research conducted by the department staff during this period deals with improvement of the technology of mechanized production of welding electrodes. This work enables clarifying the nature of the phenomena which are the basis for technological processes of manufacturing this kind of mass products, as well as improving the metallurgical, technological and service characteristics of electrodes and their quality. Given below are the results of investigation of the influence of such technological factors of manufacturing low-hydrogen electrodes as composition and amount of water glass in the electrode compound, its interaction with marble in the electrode coating, as well as organic hydrocolloids (carboxymethyl cellulose and alginates) on dehydration of electrode coating and hydrogen content in the deposited metal. It is found that alkali hydrosilicates remaining in the electrode coating after dehydration of its water glass binder during electrode heat treatment, are a potential source of hydrogen in the deposited metal. There exists a direct relationship between water-retaining capacity of sodium-potassium hydrosilicates, dependent on the module and  $\text{Na}_2\text{O}:\text{K}_2\text{O}$  ratio, potential hydrogen content in the coating and hydrogen content in the deposited metal. However, at evaluation of the degree of potential hydrogen «assimilation» by the deposited metal, we should take into account the possible influence of potassium and sodium ions contained in the hydrosilicate, on fluorine removal from the reaction of hydrogen fluoride formation and on kinetic conditions of hydrogen sorption and desorption by electrode metal drop. Marble powder, contained in the electrode coating, and water glass which is the coating binder, interact with each other in a heterophase fashion. Calcium ions coming to the water glass binder lower the water-retaining capacity of alkali hydrosilicates. Products of interaction on marble particle surface hinder their thermal dissociation up to higher temperatures, compared to the temperature of pure calcite dissociation. Both promote lowering of hydrogen content in the deposited metal. Organic hydrocolloids such as sodium modifications of carboxymethyl cellulose (CMC) and sodium or potassium alginates, are sorbed by the surface of marble particles and, blocking water glass access to it, they hinder the heterophase transition of calcium ions into the water glass. This has a favourable effect on the technological properties of electrode compounds, but at the same time improves the water-retaining capacity of alkali hydrosilicates in the electrode coating and hydrogen content in the deposited metal. Calcium ions are capable of moving from calcium-containing CMC modifications and alginates into the water glass binder as they do from calcite particle surface. Therefore, they should be considered as technological additives, which not only increase the plasticity of electrode compounds, but also lower the potential hydrogen content in the coating and hydrogen content in the deposited metal. 15 Ref., 8 Tables, 7 Figures.

**Keywords:** manual arc welding, welding electrodes, electrode coating, water glass, hydrogen in the deposited metal, cold cracks, technological causes for hydrogen lowering

Factors influencing hydrogen content in the deposited metal are conditionally subdivided into the metallurgical and technological ones. Metallurgical factors determine the thermodynamic and kinetic conditions of the process of hydrogen dissolution in the molten metal (hydrogen partial pressure in the arc atmosphere, its solubility in the metal and slag, temperature and size of spe-

cific surface separating the molten metal and water-containing gas or slag phase, duration of melt interaction with the environment, etc.). Technological factors characterize the intensity of sources of hydrogen coming to the welding zone and deposited metal and include potential content of hydrogen in the coating differentiated by the strength of the bond with coating materials, in particular in the form of:

- constitution moisture of mineral components;
- residual moisture of alkali silicate binder;
- remnants of organo-colloidal plastifying additives;



- moisture absorbed by the coating from air during electrode storage;
- atmospheric moisture penetrating into the arc zone from air.

In principle, they complement each other and should be considered jointly at assessment of the results of the deposited metal hydrogenation. Influence of technological factors becomes quite significant in the case of electrodes capable of ensuring hydrogen content below 5 ml/100 g of deposited metal, determined by mercury or chromatographic method.

The main source of hydrogen is dry residue of the binder consisting of alkali hydrosilicates with different degrees of dehydration. It and, to a certain extent, filler materials (organic, mineral ore components with constitution moisture, ferroalloys), fulfill this function, if hydrogen, initially present in their composition, is not removed from them at 400 °C temperature, used for baking low-hydrogen electrodes.

Water-retaining capacity of alkali hydrosilicates depends on chemical composition. They act as fire-retardants relative to organic ingredients. Ore-mineral components can slow down or accelerate alkali hydrosilicate dehydration, depending on their substantial and granular composition and on the degree to which the temperature range of their dehydration facilitates running of the reaction of polycondensation of silicon-oxygen anions of alkali hydrosilicates in the coating.

**Water-retaining capacity of alkali hydrosilicates and hydrogen content in the deposited metal.** Free moisture contained in water glasses (silicate solvent proper) evaporates at soaking in air (room temperature), and moisture associated with alkali hydrosilicate is preserved in the solidified residue. Part of it in the form of water molecules is coordinated in the hydration shell of alkali cations, and the other (in the form of

hydroxyl groups) is part of the structure of silicon-oxygen anions (SOA). As temperature is increased both kinds of moisture are removed from alkali hydrosilicate, the first easier than the second. Therefore, at the temperature above 400 °C (right up to melting), predominantly SOA hydroxyl moisture remains in it.

Moisture removal from SOA structure occurs by polycondensation reaction, and moisture is considered to be not only its product, but also a catalyst. In terms of kinetics, the reaction proceeds faster, and the dehydration process is realized more completely, if the evolving moisture is not removed immediately from the material, but contacts the condensing anions for a certain time, participating in their regrouping. Its development is the more difficult, the more is the anion polymerized. Therefore, in highly polymerized SOA, for instance, of potassium, rubidium and cesium silicates, despite their higher permeability for water vapour removed during dehydration, more moisture remains, nonetheless, than in lithium and sodium hydrosilicates, subjected to the same heat treatment. This is confirmed by comparison of energies of dehydration activation of potassium and sodium hydrosilicates (Table 1), determined by us by processing the results of thermogravimetric analysis with the method described in [1]. Residual moisture of the coating made with application of such glasses, as well as with higher content of diffusible hydrogen in the deposited metal  $[H]_{\text{dif.d.m}}$  also turns out to be higher (Table 2).

Increase of  $[H]_{\text{dif.d.m}}$  content should be promoted, to a certain extent, by fluorine losses in the fused coating, caused by formation of alkali metal fluorides, the probability of which rises at transition from lithium to cesium glass.

Influence of modulus  $M$  on water-retaining capacity and residual moisture of sodium-potas-

**Table 1.** Thermokinetic characteristics of dehydration of sodium, potassium and sodium-potassium hydrosilicates

Kind of hydrosilicate	Dehydration indices	
	$T_s$ , °C	$E$ , kJ/mol
$\text{Na}_2\text{O}\cdot 3.0\text{SiO}_2$	115	3.1
$\text{K}_2\text{O}\cdot 3.2\text{SiO}_2$	140	10.0
$0.7\text{Na}_2\text{O}\cdot 0.3\text{K}_2\text{O}\cdot 2.7\text{SiO}_2$	125	4.4
$0.7\text{Na}_2\text{O}\cdot 0.3\text{K}_2\text{O}\cdot 2.9\text{SiO}_2$	95	1.5
$0.7\text{Na}_2\text{O}\cdot 0.3\text{K}_2\text{O}\cdot 3.0\text{SiO}_2$	120	2.5

Note.  $T_s$  and  $E$  are the temperature of maximum rate and activation energy of the dehydration process.

**Table 2.** Influence of the kind of water glass on coating moisture and hydrogen content in the deposited metal (glycerin method)

Kind of water glass	$C_m$ , mol/100 g	$W_T$ , wt. %	Weight fraction in deposited metal, %		$[H]_{\text{dif}}$ , ml/100 g of deposited metal
			Mn	Si	
$\text{Li}_2\text{O}\cdot 3.5\text{SiO}_2$	0.030	0.10	1.45	0.60	3.9
$\text{Na}_2\text{O}\cdot 3.0\text{SiO}_2$	0.030	0.10	1.40	0.50	5.1
$\text{K}_2\text{O}\cdot 3.0\text{SiO}_2$	0.030	0.30	1.40	0.40	6.1
$\text{Cs}_2\text{O}\cdot 3.1\text{SiO}_2$	0.015	0.30	1.10	0.30	8.3

Note.  $C_m$  is the molar fraction of silicate in the coating;  $W_T$  is the residual moisture of the coating;  $[H]_{\text{dif}}$  is the average value of the results of three parallel measurements.



sium hydrosilicates is also attributable to presence of two kinds of moisture contained in them. Fraction of moisture related to alkali cations, decreases with increase of modulus, whereas it grows in SOA structure. Resulting effect is described by an extremal curve, the minimum of which falls on the modulus approximately equal to 3.0 un. [2]. Minimum values of thermokinetic dehydration characteristics also correspond to it (see Table 1).  $[H]_{\text{dif.d.m}}$  content should depend also on the fraction of dry residue of water glass in the coating, which usually decreases with modulus increase. Combined hydrosilicates of  $0.7\text{Na}_2\text{O}\cdot 0.3\text{K}_2\text{O}\cdot \text{MSiO}_2$  have lower water-retaining capacity than pure sodium or potassium analogs, as the reaction of their polycondensation proceeds more readily and completely than that of pure components of which they consist [2].

We attributed it to the increased probability in combined hydrosilicates of meeting of various SOA structural forms, which are located in the field of action of sodium and potassium cations, the polycondensation of which results in release of bound water.

The filler separates binder fragments in electrode coating, which participate in polycondensation reaction and, as a rule, hinders moisture removal from the coating at electrode baking. Moisture is present in the structure of many electrode compound fillers, the greater part of which is preserved at the temperature of low-hydrogen electrode baking. Nonetheless, at favourable combinations of dehydration ranges, evolution of this moisture can to some extent facilitate run-

ning of the reaction of polycondensation of alkali hydrosilicates [2]. Constitution moisture of such aluminosilicates, as mica-muscovite, kaoline and talc, remains in their structure after electrode baking and promotes an increase in  $[H]_{\text{dif.d.m}}$  content. Synthetic mica, in the structure of which hydroxyl ions are replaced by fluorine during its pyrogenic synthesis, is an exception [3].

In view of the above, the concepts of the influence of water glass composition and dose on hydrogen content in the metal deposited with low-hydrogen electrodes can be precised, using the results of investigations derived in [4].

Test electrodes close by their coating composition to UONI-13/55 electrodes, were produced using sodium-potassium ( $M = 2.7\text{--}3.4$  un.) and potassium-sodium ( $M = 2.7\text{--}3.1$  un.) water glasses of different density (Table 3). Electrodes manufactured with application of sodium-potassium water glass and marked by C and D indices, were baked at 400 °C for 30, 60 and 120 min that enabled assessment of coating dehydration kinetics. Electrodes of A and B series made with application of potassium-sodium water glass, were baked at the same temperature for 30 and 120 min.  $W_T$  was assessed by heating a sample in an oxygen flow at 1100 °C (IIW method), and  $[H]_{\text{dif.d.m}}$  — by glycerine method [4].

Weight fraction of  $W_T$  varied from 0.07 to 0.5 %, and  $[H]_{\text{dif.d.m}}$  content was proportional to coating moisture, being within 2.6 to 12 ml/100 g of deposited metal. The interaction between  $[H]_{\text{dif.d.m}}$  and  $W_T$  can be described by linear regression equations given in Table 3, judg-

**Table 3.** Composition, characteristics and weight fraction of water glass in test electrode coating

Electrode series and weight fraction of $\text{Na}_2\text{O} + \text{K}_2\text{O}$ in the coating, %	Kind of glass	Modulus, units	Density, g/cm <sup>3</sup>	Weight fraction of water glass, %	$[H]_{\text{dif.d.m}} = f(W_T)$
A 3.10–3.60	Potassium-sodium	2.7	1.40	27	$[H]_{\text{dif.d.m}} = 1.08 + 18.60W_T$
		2.9			
		3.1			
B 3.30–3.80	Potassium-sodium	2.9	1.36	30	$[H]_{\text{dif.d.m}} = 0.20 + 24.40W_T$
			1.40		
			1.44		
C 2.45–2.85	Sodium-potassium	2.7	1.40	27	$[H]_{\text{dif.d.m}} = 1.05 + 17.85W_T$
		3.1			
		3.4			
D 2.85–3.40	Sodium-potassium	2.9	1.36	30	$[H]_{\text{dif.d.m}} = 1.30 + 21.10W_T$
			1.40		
			1.44		
			1.48		



ing by which  $[H]_{\text{dif.d.m}} = f(W_T)$  straight lines differ from each other by their inclination to abscissa axis and are shifted along the vertical relative to each other. At the same coating moisture level (for instance, 0.2 %) hydrogen content varies from 4.80 to 6.40 ml/100 g of deposited metal, i.e. by 30 %. In the case of low hydrogen levels, such scatter should be regarded as quite significant.

In order to clarify its causes, we used the techniques described below. We will assume that all the moisture in the coating is concentrated in the residue of alkali hydrosilicate. With the change of composition and dose of water glass in the electrode coating the dose and degree of silicate hydration in the baked electrode coating, i.e. amount of moisture associated with it, changed at the same time. In physical chemistry moisture is calculated from dry substance and is presented in molar units as the quantity of water moles per one mole of dehydrated silicate,  $\varpi$ . Quantity of silicate moles in the coating is found as quotient of division of dry residue weight by its molecular mass. Quantity of  $H_2O$  moles is calculated as quotient of division of the mass of moisture preserved in the silicate, by molecular mass of water.

The data lacking in [4] (silicate dry residue and its molar moisture content, depending on the kind, modulus and density of water glasses) was calculated using formulas given in [5], having

converted them by additivity rule, for combined water glasses:

$$\frac{1}{\rho - \rho_0} = \frac{\varpi + \omega_0}{b}, \quad (1)$$

where  $\rho$  and  $\rho_0$  is the density of water glass and solvent (equal to a unity for water);  $b$  and  $\omega_0$  are the constants additively dependent on the composition of alkali silicate;  $b = 4.701 + 2.130M$ ;  $\omega_0 = 1.109 = 1.537$  (sodium-potassium glasses);  $b = 5.082 + 2.050M$ ;  $\omega_0 = 0.750 + 1.780M$  (potassium-sodium glasses).

$\varpi$  value calculated by formula (1) in sum with silicate molecular mass is the mass of water glass in the coating, and the fraction of silicate molecular mass in it is the dry residue of water glass. Knowing the dose of water glass in the electrode compound, weight fraction of silicate (dry residue) in the coating was calculated. It remains in the coating as the coating is dehydrated during electrode baking without changes in the mass and mole units. Only  $W_T$  determined during experiments decreases [4].

Figure 1 gives dependence of  $[H]_{\text{dif.d.m}}$  content on molar moisture content of hydrosilicate in the coating of electrodes baked during selected time intervals at 400 °C, which was derived as a result of our calculations. It is seen that with such an interpretation the experimental results are quite clearly stratified into two groups. In each group they are approximated by straight lines, starting from the origin of coordinates, which differ from each other only by the angle of inclination to  $\varpi$  axis. The lower straight line belongs to electrodes of A and C series, in which the glass modulus was changed. Upper curve 2 belongs to electrodes of B and D series with  $M = 2.9$  un., and varying density. At the same  $\varpi$  value electrodes of B and D series provide higher  $[H]_{\text{dif.d.m}}$  content than electrodes of A series. This can be explained as follows.

Electrodes, the application of which provides higher  $[H]_{\text{dif.d.m}}$  content, also have a higher fraction of alkali oxides in the coating. Reaction of formation of alkali metal fluorides should neutralize part of active fluorine and, thus, weaken its role in lowering of partial pressure of hydrogen by binding it into hydrogen fluoride.

Stabilizing action of potassium and sodium on the arc discharge can cause expansion of the arc column (and of fraction of the surface of that part of the drop through which hydrogen absorption from the arc atmosphere occurs). Increase of the ratio of surface areas, through one of which hydrogen absorption from the plasma by the electric arc takes place, and through the other, lo-

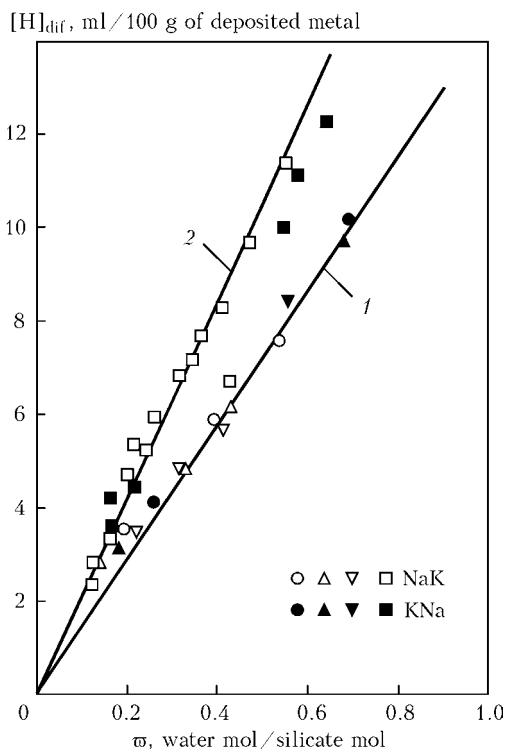


**Figure 1.** Interrelation of hydrogen content in the deposited metal and moisture content of sodium-potassium and potassium-sodium hydrosilicates in test electrode coating: 1 –  $\rho = \text{const}$  (27 % glass); 2 –  $M = \text{const}$  (30 % glass)



cated outside the active spot, hydrogen evolves simultaneously from molten metal, is an important kinetic characteristic of the process of setting of final concentration of diatomic gases in the deposited metal [6]. Influence of this factor is similar to reduction of concentration of fluorine binding hydrogen in the arc atmosphere.

Figure 2 gives the results of assessment of dehydration kinetics in coatings of electrodes of C series, made with sodium-potassium water glass with different modulus values. It is seen that dehydration of electrode coatings really proceeds very slowly. Molar moisture content of the coating decreases, becoming close to equilibrium value for 400 °C temperature only after 2 h soaking of electrodes made with water glass with  $M = 3.3$  un. (temperature curve of dehydration comes to a horizontal section). Equilibrium moisture content of coatings of two other studied variants of electrodes from this series is not achieved. The lowest moisture content (0.14 %) was obtained in a coating made with water glass with the modulus of 3.1 un. In coatings made with water glass with the modulus of 2.7 and 3.3 un., it is approximately 1.5 times higher at 0.18 and 0.22 water mol/silicate mol, respectively. It is important that hydrogen content in the metal deposited with the same electrodes, changes in proportion to coating moisture content, being equal to 3.3, 2.6 and 3.1 ml/100 g of deposited metal, for moduli of 2.7, 3.1 and 3.3 un., respectively.

In other words, residual moisture of sodium-potassium hydrosilicate changes, depending on the modulus value by an extremal law, both in the free state and in the electrode coating composition.  $[H]_{\text{dif.d.m}}$  also changes in an extremal fashion, accordingly, although in this experimental series, part of fluorine removed by alkali from the reaction of formation of hydrogen fluoride was the greater, the lower the water glass modulus.

No such relationship of  $[H]_{\text{dif.d.m}}$  content and final moisture level of hydrosilicate in the coating was established for electrodes of A series.

Therefore, when searching for methods to lower  $[H]_{\text{dif.d.m}}$  content, alongside the residual moisture of the coating, the concurrent factors influencing hydrogen partial pressure in the arc atmosphere should be taken into account.

**Influence of marble interaction with water glass in the coating on hydrogen content in the deposited metal.** From the very start of mastering full-scale low-hydrogen electrode production by the press method, their manufacturers had to deal with unsatisfactory technological properties

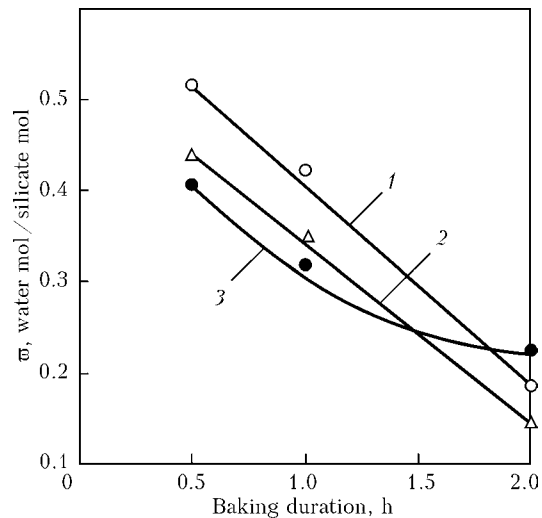
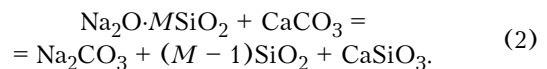


**Figure 2.** Kinetics of dehydration of low-hydrogen electrode coating at the temperature of 400 °C, made with application of sodium-potassium glass with modulus of 2.7 (1); 3.1 (2); 3.3 (3) units

of electrode compounds and assumed that this is caused by chemical interaction of marble with water glass by the following exchange reaction:



The validity of such an assumption was called into question [7], however, it was not possible to establish the real cause of this phenomenon for many years.

We have found out that marble indeed interacts with water glass, but by a much more complex mechanism. Calcium from marble (similar to other calcium-containing minerals difficult-to-dissolve in water) dissolves in water glass and is capable of causing its curing in the process [8].

In physical chemistry the mechanism of such curing is considered in terms of heterophase interaction, as the reaction proceeds between the solid substance and water solution of inorganic polymer. Products responsible for curing of the system, can form only after completion of the slow, i.e. quite prolonged incubation period, during which calcium concentration in water glass will reach oversaturation, sufficient for nucleation of new hydrosilicate phases, amorphous as to their structure [9].

The above-mentioned period includes chemisorption [10] and ion-exchange stages. Silicon-oxygen anions of alkali hydrosilicates, which are present in water glass, absorbing calcium ions in exchange for hydroxyl ions, act as cationite [11]. Calcium which has passed into solution during the incubation stage forms intermediate compounds with silicate ions on  $\equiv\text{Si}-\text{O}-\text{Ca}-\text{O}-\text{Si}\equiv$  binders. They become the new phase nuclei. Hy-

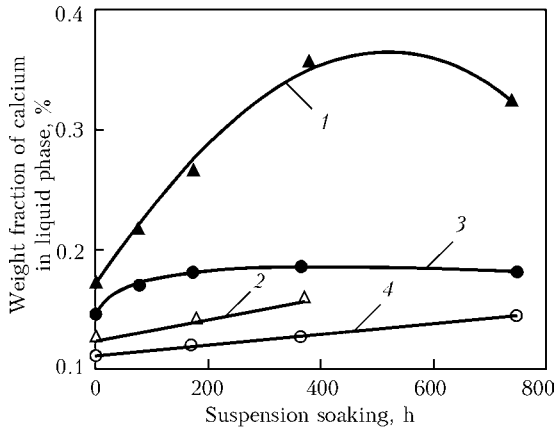


**Figure 3.** Kinetics of calcium transition from marble powder into water glass (weight fraction in suspension is 25 %): 1, 3 – modulus of 2.6 units, viscosity of 400 (1) and 50 MPa·s (3); 2, 4 – modulus of 3.6 units, viscosity of 330 (2) and 50 MPa·s (4)

droxyl ions are released from alkali hydrosilicates with free moisture formation.

Activity of natural calcium carbonates in water glass compositions depends on their structure formed during prolonged geological periods. Quarry chalk is an inert material in relation to water glass. Marble is more active than limestone, although its activity is lower than that observed in calcium silicates, which make up the basis of silicate cements. Even more active is natural aragonite having a denser hexagonal structural cell, unlike the cubic cell, characteristic for the structure of other above-mentioned kinds of calcites. Aragonite structure forms also at fine grinding of marble [12]. Together with amorphization of particle surface and energy, accumulated by them during grinding, it becomes the cause for increased chemical activity of fresh refined marble powders. Natural seasoning for 7 to 10 days partially phlegmatizes them. However, the activity, which is directly related to appearance of aragonite, can be suppressed only by powder heating up to 400 °C.

Calcium solubility in water glass at the moment of oversaturation, does not depend on the nature of the mineral, from which it comes to water glass. When recalculated to calcium weight fraction for sodium glasses it varies from 0.6 up to 1.3 %, growing within these ranges at modulus lowering from 3.3 to 2.6 units and increase of alkali silicate concentration in water glass right up to 5–6 moles of SiO<sub>2</sub>/l [9]. Mineral nature and its particle dispersity influence only the calcium dissolution rate.

Analyzing the above-said, it may be assumed that electrode compositions should react to running of the incubation period of marble interaction with water glass, at the end of which new hardening phases are formed due to:

- more intensive improvement of raw (plastic) strength compared to coatings, not having calcium-containing minerals in their composition and this, indubitably, should be accompanied by deterioration of their plasticity;

- additional release of moisture from the structure of alkali hydrosilicates and lowering of potential content of hydrogen in the coating after electrode heat treatment;

- changes of surface structure of marble particles participating in the reaction, that may result in the change of kinetic indices of their thermal dissociation during electrode heating and melting.

During experiment performance we observed hardening of electrode compounds under the impact of calcium transition into water glass [13]. Role of the last two factors in regulation of [H]<sub>dif.d.m</sub> content was revealed by us during investigations, the results of which are given below.

Calcium from marble dissolves in sodium-potassium water glass to a somewhat smaller extent, than in sodium glass. For instance, limit solubility of calcium in low-modulus sodium-potassium glass, is equal to 0.20 and 0.55 wt.% at SiO<sub>2</sub> concentration of 5.85 and 6.35 mol/l, respectively. It is even lower in high-modulus glass and is not higher than 0.15 wt.% at SiO<sub>2</sub> equal to 5–6 mol/l. As follows from Figure 3, it grows with viscosity increase and lowering of water glass modulus. Calcium transition during the incubation period is accompanied by improvement of water glass viscosity. The effect is the more pronounced, the higher its initial viscosity (Figure 4).

Incubation period is over at the moment of achievement of maximum concentration of calcium in the solution and viscosity of water glass. Both the indices decrease with the start of new phase precipitation and will not be restored as long as the new phase precipitates.

Rate of calcium dissolution rises, when freshly ground marble is used. So, at the same duration of marble powder mixing with water glass, calcium transition decreases from 0.25 wt.% (freshly ground marble) to 0.15 wt.% (same powder soaked in air for 15 days). Increasing calcium transition is promoted by application of intensive modes of powder mixing with water glass or increasing marble particle dispersity.

Influence of calcium impurity on water-retaining capacity of alkali hydrosilicates was studied by derivatography method [2].

Samples of sodium-potassium hydrosilicates (modulus of 2.80; 3.05; and 3.30 un.) with cal-



cium content not exceeding its limit solubility, were prepared. For this purpose a saturated water solution of calcium hydrate oxide  $\text{Ca}(\text{OH})_2$  in the amount from 0.05 up to 0.20 wt.% was added to water glasses, in order to obtain the pre-specified molar concentration of calcium in the solution in the range from 2.5 up to 12 mmol  $\text{Ca}/\text{mol SiO}_2$ . Samples for comparison were hydrosilicates without calcium. During water glasses mixing with  $\text{Ca}(\text{OH})_2$  solution, colloidal lime precipitated, which, being gradually compressed in its volume through syneresis, rejected the solvent. Slow evaporation was used to bring all the samples to solidlike state (with moisture content of 20–35 wt.%). Then thermogravimetric analysis (TGA) method was used to find in each of them the share of moisture remaining after hydrosilicate heating up to 400 °C. Figure 5 gives the results of experiments.

It is seen that calcium ions  $\text{Ca}^{2+}$  indeed influence water-retaining capacity of alkali hydrosilicates. At water glass moduli of 2.80 and 3.05 units small  $\text{Ca}^{2+}$  additives lower hydrosilicate residual moisture content (effect similar to mixed alkaline one, observed in combined sodium-potassium silicates, but  $\text{Ca}^{2+}$  action is manifested at concentrations by three orders of magnitude smaller than the concentration of accompanying alkali cation). At concentrations, exceeding the optimum ones, calcium causes an opposite effect, and water-retaining capacity of hydrosilicate rises. In the real electrode compounds  $\text{Ca}^{2+}$  concentrations can, apparently, be both greater and smaller than the found optimum. Hence the unpredictability of the induced result as regards the achieved degrees of coating dehydration.

At water glass modulus of 3.30 units the dissolved calcium monotonically increases the hydrosilicate water-retaining capacity in the entire range of its obtained concentrations.

It is important to note that at molar concentrations exceeding 7.5 mmol  $\text{Ca}/\text{mol SiO}_2$ , the value of alkali silicate modulus no longer influences its water-retaining capacity. The role of dissolved calcium in ensuring the residual moisture content of alkali hydrosilicates becomes the determinant one here.

Investigation of water vapour mass-spectra in the gas phase over the heated samples of hydrosilicates showed that intensive dehydration of hydrosilicates under calcium influence gradually shifts to the region of ever higher temperatures, thus confirming that ever greater amount of bound moisture remains in the hydrosilicate, baked at 400 °C.

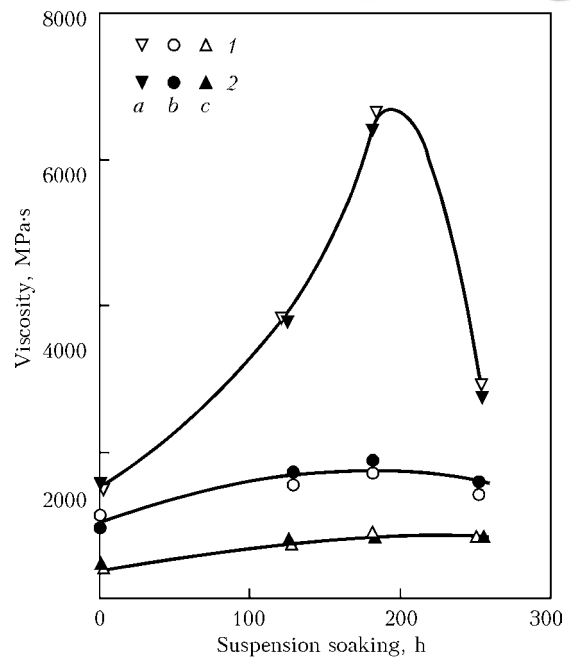


**Figure 4.** Change of viscosity of marble suspensions in sodium-potassium glass with modulus of 2.87 (1) and 3.11 units (2) in time. Initial viscosity of water glass is 1800 (a), 1000 (b) and 500 (c) MPa·s [13]

So, at weight fraction of calcium in water glass, %: 0; 0.11; 0.22; 0.43  $[\text{H}]_{\text{dif}}$  content, ml/100 g of deposited metal is as follows: 4.6; 3.7; 3.0; 3.6, respectively. Here and further on  $[\text{H}]_{\text{dif}}$  value was calculated as the average value of three parallel measurements, made by chromatographic method by A.P. Paltsevich, Cand. of Sci. (Eng.).

It was noted above that calcium transition from marble powder into water glass increases with increase of its dispersity. Data given in  $W_T$ , wt.%

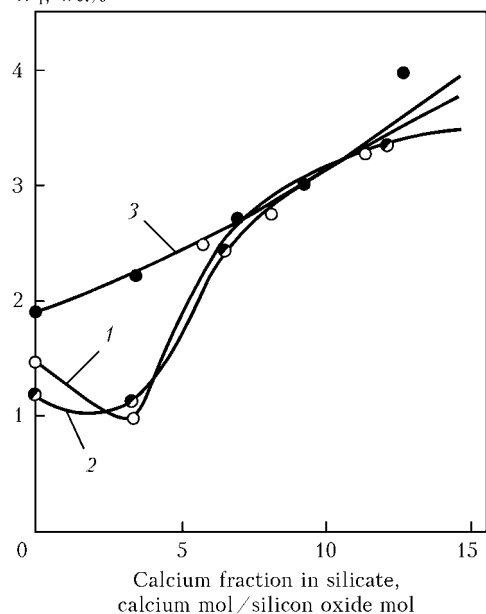


**Figure 5.** Influence of  $\text{Ca}^{2+}$  ions on water-retaining capacity of sodium-potassium hydrosilicates with modulus of 2.80 (1): 3.05 (2); 3.30 (3) units [13]



**Table 4.** Influence of charge dispersity on composition and content of hydrogen in the deposited metal

Weight fraction of -0063 particle size in the charge, %	Weight fraction in deposited metal, %		[H] <sub>diff</sub> , ml/100 g of deposited metal
	Mn	Si	
0	0.51	0.14	3.3
20	0.71	0.30	3.4
40	0.65	0.37	3.1
60	0.54	0.29	2.8
80	0.47	0.24	2.5

ble 4, confirm that hydrogen content in the deposited metal also decreases in this case.

The following experiments and their results are a convincing proof of the fact that [H]<sub>diff.d.m</sub> decrease is related exactly to calcium transition into water glass. In the coating of test electrodes UONI-13/55 the content of Trilon B (komplexon) was gradually increased up to 0.12 wt.%. Trilon is disodium salt of ethylenediaminetetraacetic acid, which is usually used for absorption of calcium ions at water softening. Unlike ion-exchange resins (ionites) it is capable of removing calcium ions not only from water, but also from solutions containing the concurrent potassium and sodium ions. Adding komplexon to coating compound during charge mixing with water glass, we remove calcium from the solution. Here, water-retaining capacity of calcium-pure alkali hydrosilicate in the coating is restored and [H]<sub>diff.d.m</sub> content is increased. At increase of komplexon weight fraction, %: 0; 0.04; 0.08; 0.12, [H]<sub>diff</sub> content, ml/100 g in the deposited metal changes as follows: 4.6; 5.8; 5.3; 6.7, respectively.

Effect similar to the one obtained with komplexon, is anticipated at application of potassium oxalate [8]. Comparison of effects due to calcium spontaneously moving into the solution from marble, on the one hand, and calcium, deliberately added to the compound in the form of volumetric solution of calcium chloride CaCl<sub>2</sub>, on the other hand, revealed that the above calcium sources are to some extent antagonistic in water glass. When coarse-grained charge is used, and the anticipated transition of calcium into the solution from marble is minimum, adding CaCl<sub>2</sub> solution to the compound turns out to be quite effective in terms of lowering [H]<sub>diff.d.m</sub> content. Contrarily, at application of fine-grained charge, when the anticipated coming of calcium into the solution from marble is maximum, adding CaCl<sub>2</sub> to the compound is no longer effective.

Proceeding from the results of these experiments, we came to the conclusion that marble should be regarded not only as a source of calcium, which allows adjustment of water-retaining capacity of alkali hydrosilicate, but also as coating ingredient, the gas-forming capacity of which, essentially lowering partial pressure of hydrogen in the arc atmosphere, rises at its heterophase interaction with water glass for a reason not clear so far.

This can be assessed by comparing the process of thermal dissociation of marble powder in the pure form and in compositions with water glass. Powders of marble from Koelgin field were studied, in particular in a mixture with sodium-potassium silicate block in the amount of 13 wt.% or with fluorspar powder, taken in the molar ratio of CaCO<sub>3</sub>:CaF<sub>2</sub> = 1:1. Coarseness of ingredient particles did not exceed 0.25 μm.

A sample of a mixture of marble powder with sodium-potassium water glass (M = 2.7 units, 22 % weight fraction in the mixture, 8 % recalculated to dry residue) brought to air-dry state, was studied separately.

Total pattern of thermal dissociation of powderlike marble at proportional heating is in good agreement with the published data of other authors. Its dissociation starts at the temperature of 650 °C, maximum rate of thermal dissociation reaction is found at 890 °C, and the process is over at 940–950 °C. Losses of sample mass are very close to theoretical content of carbon dioxide gas CO<sub>2</sub> in marble and are equal to 43.2 % (44 % in pure calcium carbonate CaCO<sub>3</sub>).

In mixtures with fluorite and with silicate block the running of marble dissociation almost does not change. The revealed very slight differences are in agreement with published data, in which the facilitating influence of additives in the form of alkali oxides and fluorides on calcium decomposition is noted. The found thermoeffects behind the decarbonization peak are caused by the reaction of ordering of the formed metastable oxide.

Sample mass losses recalculated by the method of [1] and graphically presented in Figure 6, show that the seeming energy of activation of the process of thermal dissociation of marble for all the three variants of the studied dry mixtures remains constant (experimental points fall on the same curve). Apparently, in all these cases the rate of calcium dissociation is limited not so much by its initial stage, dependent, primarily, on the condition of its grain surface, but also by subsequent stages of the process, on which the studied additives cannot have any influence.



Water glass turned out to be an additive, which essentially affects the activation energy of the process of marble dissociation. We mean not the threshold stage or the characteristic temperature  $T_s$ , which are hidden from direct observation by effects accompanying the alkali silicate dehydration proceeding at this moment of time, but the main stage, during which  $\text{CO}_2$  is actively released. As follows from Figure 6, starting from 720 °C this stage becomes the dominating one in its influence on reduction of sample weight, caused by  $\text{CO}_2$  release and runs with greater energy impediments than in hydrosilicate absence. Below this temperature the sample mass losses are, apparently, determined predominantly by dehydration of hydrosilicate binder, and if its energy is assessed by the inclination of the respective section of the straight line, than it can be assumed that its running is more difficult than carbonate dissociation in the absence of hydrosilicate film on its particle surface.

The following designations are used in Figure 6:  $G_0$ ,  $G_t$ , and  $G$  are the initial, final and current mass of the sample;  $\theta = T - T_s$ , where  $T$  and  $T_s$  are the current temperature and temperature of maximum rate of dissociation reaction.

Considering that dehydration of silicate binder, coating  $\text{CaCO}_3$  grains, which involves high energy consumption, goes on also above 720 °C, its inhibitory action on carbonate dissociation under the conditions of high-rate proportional heating can be quite substantial (reports of positive role of water vapours in realization of calcite dissociation are related to long-term isothermal variants of heating [14]).

Another possible cause of inhibitory action of hydrosilicate film on thermal dissociation of calcium carbonate can be the consequences of interaction of its particle surface with water glass at the stage of electrode compound preparation. Judging by the concentration of calcium ions detected by chemical analyses in water glass, and by the results of calculation estimates, up to 10 elementary surface layers of calcite grains could become involved in the dissolution process. This results in a kind of their phlegmatization, i.e. delayed reaction to the initial heating phase.

Recently published investigation results [15] on the whole confirm our conclusions that application of finely-dispersed marble in the coating of low-hydrogen electrodes promotes lowering of  $[\text{H}]_{\text{dif.d.m}}$  content. Experiments were conducted with electrodes, in the coating composition of which marble with regular grain composition (31 wt.%) was gradually replaced by marble powder, consisting of nanosized particles. As a

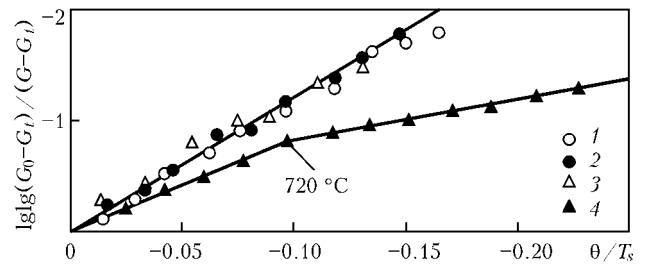


**Figure 6.** Dependence of the change of sample weight on reduced temperature in the coordinates of Gorovits–Mettlinger equation [1]: 1 – marble; 2–4 – mixture of marble with silicate block, with fluorite, and with water glass, respectively

result of such a replacement  $[\text{H}]_{\text{dif.d.m}}$  content decreased from 3.8 to 2.45 ml/100 g of deposited metal at 50 % replacement and down to 2.3 ml/100 g of deposited metal at complete replacement of regular marble by its nanosized analog. The authors of the work explained this phenomenon by lowering of hydrogen partial pressure in the arc atmosphere caused by more intensive evolution of  $\text{CO}_2$  from the surface of nanosized  $\text{CaCO}_3$  particles. Judging by the deposited metal composition, oxidizing potential of the arc atmosphere remained unchanged. From our point of view, lowering of  $[\text{H}]_{\text{dif.d.m}}$  content occurring under the influence of finely-dispersed marble powders in the coating (including also nanosized modifications), is caused by the processes of their heterophase interaction with water glass, which lead to reduction of potential content of hydrogen in the coating and its partial pressure in the arc atmosphere.

#### **Role of organic hydrocolloids in regulation of hydrogen content in the deposited metal.**

Traditionally such organic hydrocolloids as carboxymethylcellulose (CMC) and alginates were regarded only as technological additive, effectively plastifying the electrode compound. After that at the stage of compound preparation and application on the rods it is «burnt out» of the coating during electrode heat treatment. In the case of Na-CMC, one can see that coating moisture found by IIW method in electrodes made with application and without application of Na-CMC, is indeed homogenized by value (Table 5) after their baking at the temperature of 400 °C.

At the same time, it is experimentally established that hydrogen content in the metal, deposited by electrodes initially containing Na-CMC in their coating, often is higher than for electrodes which were manufactured without CMC application (Table 6). Here  $[\text{H}]_{\text{dif.d.m}}$  content changes much less than the initial CMC content in the coating.

We can assume that organic hydrocolloids with a non-symmetrical molecule structure, can



**Table 5.** Depth of dehydration of low-hydrogen electrode coatings during their baking

Electrode baking temperature, °C	Coating moisture, $W_T$ , %		$\Delta W_T = W_T(A) - W_T(B)$ , %
	A	B	
20	4.67	6.08	1.41
290	0.71	0.93	0.22
325	0.48	0.63	0.15
360	0.30	0.34	0.03
405	0.23	0.24	0.01

Note. Coating with A index — without CMC content, with B index — CMC content of 1.5 %.

be sorbed by the surface of marble solid particles similar to, for instance, salts of fatty acids in flotation processes, that allows suppressing calcium dissolution in water glass.

This is confirmed by the nature of IR-spectra of marble powders, contacting the water glass, after their pre-treatment by water solutions, as well as by water-glass Na-CMC dispersions. Na-CMC concentration in the dispersions is 2 %. Marble powder was sifted through a sieve with 63  $\mu\text{m}$  cell size. Weight ratio of powder and liquid is 1:5. Sodium-potassium water glass with 2.9 un. modulus and 1000 MPa·s viscosity was used. Experiments were performed by V.G. Vojtkевич, Cand. of Sci. (Phys-Math.) and E.E. Fedorina, Eng.

CMC chemical and molecular composition was varied in broad ranges. In addition to Na-CMC with extreme values of substitution degree (SD) (from 65 to 130) and polymerization degree (PD) (from 350 to 1300), calcium CMC (Ca-CMC) was also used.

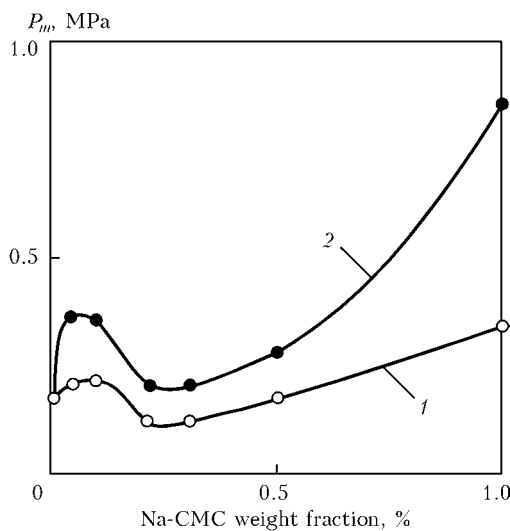


**Figure 7.** Influence of Na-CMC with different molecular composition on plastic strength of UONI-13/55 electrode compound: 1 — CMC 68/350; 2 — CMC 68/920

Marble powder interacted with the above-mentioned preparations for 30 min at periodical shaking of the suspension. Then it was separated by decantation from excess liquid phase, rinsed several times with water, and after 5 hour drying at 105 °C was studied on IR-spectra in the mode of incomplete compensation [9].

It is established that the adsorption pattern which is observed on the surface of marble particles treated by pure water glass, coincides with that which is described in [9]. Na-CMC, irrespective of SD and PD, being present in water glass, suppresses water glass sorption on calcite surface. Reflections in IR-spectra caused by out-of-plane deformation vibrations of carbonite anion under the influence of CMC return to their normal state (880  $\text{cm}^{-1}$ ), and the silica gel band at 1069  $\text{cm}^{-1}$  disappears completely. Bands characteristic for adsorbed CMC gel appear instead of it.

So, presence of a blurred band in 1300–1100  $\text{cm}^{-1}$  region, observed after marble powder treatment by Na-CMC water solution and its dispersions in water glass, can be due to transoriented methyl groups of sorbed CMC which either oust water glass SOA from the sorbent surface, or prevent their sorption. The thus blocked calcite surface naturally loses its capacity to supply calcium ions into water glass. In addition to that, the influence of water glass on the structure of calcium carbonate particle surface, on the condition of which the nature of their dissociation at heating depends, is weakened.

As hydrocolloids are in a powderlike form in the dry mixture, phlegmatization of the surface of marble particles during electrode compound preparation proceeds by not such an ideal mechanism. Before the hydrocolloid particles, while absorbing moisture from water glass, acquire the capacity of blocking the surface of marble grains,

**Table 6.** Hydrogen content in the metal, deposited with UONI 13/55 electrodes with organic additives in the coating, depending on their baking duration at the temperature of 400 °C

Additive kind and grade	Additive weight fraction, %	Glass weight fraction, %	$[H]_{\text{diff}}$ , ml/100 g of deposited metal at baking duration of, h		
			0.5	1.0	2.0
Without additive	—	24	7.1	6.3	5.2
Na-CMC, Cecol DVY	1.0	25	11.5	11.6	11.8
	1.5		15.5	11.3	10.8
	2.0		14.6	12.9	12.2
Ca alginate, C/YSF	1.5	24	5.4	5.6	2.8
	2.0	25	5.4	5.2	4.4



a certain part of calcium has enough time to dissolve in water glass and influence  $[H]_{\text{dif.d.m}}$  content. This is, in particular, confirmed by the results of experiments with komplexon.

The opposition of alkali silicate and Na-CMC in their tendency to take some place in the sorbed layer on the surface of calcite grains can be assessed by non-linear variation of plastic strength of UONI-13/55 coating at gradual increase of its content of powderlike CMC from 0 up to 1 % (Figure 7).

Low-viscosity (68/352) and high-viscosity (68/920) Na-CMC and sodium-potassium water glass with modulus of 2.9 units and viscosity of 0.175 Pa·s, which is readily sorbed by marble and dissolves calcium, were used. Water glass weight fraction was 22.5 %.

As follows from Figure 7, plastic strength of electrode compound  $P_m$ , which is equal to 0.19 MPa in the initial condition, first rises and then, having reached a small maximum, it is minimized at CMC content of 0.2–0.3 %. And only after that it continues monotonically growing exponentially at further increase of CMC content right up to 1 % (result caused predominantly by swelling of CMC particles through water glass moisture absorption by them). CMC molecular composition almost does not affect the position of extreme points along the concentration axis, but the high-viscosity preparation (68/920), on the one hand ensures greater  $P_m$  value, in particular in the maximum point, and, on the other hand, leads to a higher rate of its initial and post-minimal rise. Supposedly,  $P_m$  maximums are achieved, when the structuring impact of CMC and calcium ions is equalized by value, and the minimums are reached, when CMC absorption suppresses calcium transition from marble into the solution.

In the case of Ca-CMC application, IR-spectra bands in the region of 1300–1100  $\text{cm}^{-1}$  are not observed. Silica gel bands are preserved, even though in a weakened form. Both of them are attributable to hindered adsorption of carbomethyl radicals of Ca-CMC on calcite particle surface. Apparently, strongly cross-linked by calcium ions, the above radicals have a more ramified structure, which is difficult-to-sorb by calcite surface, and, therefore, is not capable of reliably shielding it from direct contact with water glass.

It can be anticipated that in this case water-retaining capacity of alkali hydrosilicate should be influenced by calcium coming to it both from marble (not blocked by hydrocolloid from contact with water glass), and from the hydrocolloid

proper. Ca-CMC modification formed as a result of its interaction with alkali cation, should have a plastifying impact on the electrode compound.

In addition to that, delayed dissociation of marble particles, the surface of which is «phlegmatized» by adsorbed alkali silicate, should influence lowering of partial content of hydrogen in the arc atmosphere.

In other words, calcium form of organic hydrocolloids should be regarded not only as plastifying (structure-forming) additive to electrode compound, but also as a quite effective means of lowering hydrogen content in the metal, deposited with low-hydrogen electrodes.

This is confirmed by the data given in Table 6, which were obtained when using calcium alginate — a hydrocolloid, which unlike Ca-CMC, is made from alginic acid — a product of processing sea weed.

## Conclusions

1. Alkali hydrosilicates remaining in electrode compound after dehydration of water glass binder during electrode heat treatment, are a potential source of hydrogen in the deposited metal. There exists a direct relationship between water-retaining capacity of sodium-potassium hydrosilicates, dependent on modulus value and  $\text{Na}_2\text{O}:\text{K}_2\text{O}$  ratio, potential hydrogen content in the coating and hydrogen content in the deposited metal. However, at assessment of the degree of potential hydrogen «assimilation» by the deposited metal the possible influence of potassium and sodium ions contained in the hydrosilicate on fluorine removal from the reaction of hydrogen fluoride formation and on kinetic conditions of hydrogen sorption and desorption by an electrode metal drop, should be taken into account.

2. Marble powder, contained in the electrode coating, and water glass which is the coating binder, interact with each other in a heterophase fashion. Calcium ions coming to water glass binder, lower the water-retaining capacity of alkali hydrosilicates. Products of interaction on marble particle surface delay their thermal dissociation till higher temperatures, compared to that of pure calcite dissociation. The impact of these factors results in lowering of hydrogen content in the deposited metal.

3. Organic hydrocolloids such as sodium modification of CMC and alginates, are sorbed by marble particle surface, blocking water glass access to it, and transition of calcium ions into it. This has a favourable influence on the technological properties of electrode compounds, but enhances the water-retaining capacity of alkali



hydrosilicates in the electrode coating, and hydrogen content in the deposited metal. Calcium-containing modifications of CMC and alginates, from which calcium ions can go into the water glass binder, as they do from calcite particle surface, are technological additives, which not only increase electrode compound viscosity, but also lower the potential content of hydrogen in the coating and hydrogen content in the deposited metal.

1. Horowitz, H.H., Metzger, G.A. (1963) New analyzes of thermogravimetric traces. *Anal. Chem.*, 35(10), 1464–1468.
2. Marchenko, A.E., Skorina, N.V., Suprun, S.A. (1987) Water-retaining capacity of alkali silicates and its effect on electrode coating degradation. In: *Inform. documents of CMEA*. Kiev: Naukova Dumka, Issue 1.
3. Pokhodnya, I.K., Marchenko, A.E., Koritsky, G.G. *Compound for coating of welding electrodes*. USSR author's cert. 288961. Int. Cl. B 23 k, 35/36. Fil. 12.09.69. Publ. 08.11.70.
4. Pokhodnya, I.K., Yavdoshchin, I.R., Yurlov, B.V. (1981) Influence of some technological factors on diffusion hydrogen content in welds made with basic electrodes. *Avtomatich. Svarka*, 1, 31–33.
5. Matveev, M.A., Rabukhin, A.I. (1961) Relation between water solution density of alkali silicates and their composition. *Steklo i Keramika*, 6, 21–26.
6. Lakomsky, V.I. (1998) About macrokinetics of process of interaction between nitrogen from electric arc plasma and molten metal. *Problemy Spets. Elektrometallurgii*, 1, 56–65.
7. Petran, K.V. (1951) Manufacturing of UONI-13, UP-1 and UP-2 electrodes in powerful presses under high pressure. *Avtogen. Delo*, 8, 31–33.
8. Korneev, V.I., Danilov, V.V. (1996) *Water and soluble glass*. St.-Petersburg: Strojizdat.
9. Uvarova, I.Yu., Lukyanova, O.I. (1996) Examination of induction period of solidification in interaction of Na and K silicates in concentrated suspensions. In: *Physicochemical mechanics of dispersion structures*. Moscow: Nauka.
10. Lavrenov, L.V., Marchenko, A.E., Shkurko, S.A. (1975) Peculiarities of alkali silicate adsorption from water glass by marble and fluorite in electrode coatings. *Avtomatich. Svarka*, 3, 34–38.
11. Dushina, A.P., Aleskovsky, V.B. (1963) *Silica gel – inorganic cationite*. Moscow: Strojizdat.
12. Burns, J.H., Bredig, M.A. (1956) Transformation of calcite to aragonite by grinding. *J. Chem. Phys.*, 25(6), 1281.
13. Marchenko, A.E., Skorina, N.V., Voroshilo, V.S. et al. (1979) About some technological problems caused by interphase processes in manufacturing of welding electrodes. In: *Inform. materials of CMEA*. Kiev: Naukova Dumka, Issue 1.
14. Katler, A.I. (1965) Kinetics of thermal decomposition of some minerals. In: *Kinetics of high temperature processes*. Ed. by V.D. Kindzheri. Moscow: Strojizdat.
15. Chen, B., Han, F., Huang, Y. et al. (2009) Influence of nanoscale marble (calcium carbonate CaCO<sub>3</sub>) on properties of D600D surfacing electrodes. *Welding J.*, 88(5), 99–103.

Received 29.04.2013



# WELDING OF TITANIUM ALUMINIDE ALLOYS (Review)

S.V. CHERNOBAJ

E.O. Paton Electric Welding Institute, NASU  
11 Bozhenko Str., 03680, Kiev, Ukraine. E-mail: office@paton.kiev.ua

One of the most promising directions in the field of development of new metallic materials with a high level of heat resistance and thermal stability is development of intermetallic alloys of Ti–Al system. In the near future these alloys can create serious competition to nickel-based superalloys, as titanium aluminides are lighter and do not require expensive and deficit elements for alloying. In addition, they have a high corrosion resistance, high-temperature oxidation resistance, and also have a high modulus of elasticity and strength. Titanium aluminides can be successfully applied in the form of cast products, for instance of valves of super-power internal combustion engines; as high-temperature resistant coatings on gas turbine blades, exposed to high-temperature gas flows; as structural material operating at static loads and high temperatures. Wide industrial application of titanium aluminides is hindered by their low ductility at room temperature. This greatly complicates technological processing and slows down industrial application of the above alloys. Therefore, application of titanium aluminides in various-purpose structures is dependent on development of effective technologies of their processing, including welding. In this connection the purpose of this review is analysis of currently available developments of joining processes for titanium aluminide based materials by various kinds of welding. Analysis of published data given in the review showed that formation of welded joints with application of traditional welding processes based on local melting of material has several drawbacks, which can be eliminated at application of various solid-phase welding processes. Results given in the publications, are indicative of the good prospects for application of intermediate inserts for joining difficult-to-weld titanium aluminide based alloys. 36 Ref., 5 Figures.

**Keywords:** *titanium aluminide, fusion welding, temperature, joining processes, pressure welding, structure, insert, weld, microstructure*

Aircraft engine manufacture is an extremely complicated process based on the latest advances in the field of aero- and thermodynamics, materials science, technology, strength, electronics and informatics. Important tasks solved when designing new generation engines are lowering of the cost of manufacture and operation, in particular by simplifying the design and reducing the number of parts and components [1].

Improvement of the effectiveness of aircraft engines and similar power units is becoming impossible without application of fundamentally new structural materials. Such materials include alloys based on  $\gamma$ -TiAl intermetallic phases. Owing to a unique set of physical and mechanical properties [2, 3] (high strength and modulus of elasticity, low density, high-temperature strength and high-temperature resistance, high anticorrosion properties, good fatigue fracture and creep resistance), they have for many years preserved their positions in the category of attractive materials for aerospace, transportation industries and in power engineering.

Wide introduction of titanium aluminides into industry is prevented by their low room tempera-

ture ductility [4], related to low crystallographic symmetry and insufficient number of slip systems; low cleavage strength; weak grain boundaries, as well as low technological properties [2].

Improvement of technological properties of these materials can be ensured not only by micro- and macroalloying [5], but also by alloy microstructure. Reference [6] shows three main types of titanium intermetallic structures: lamellar (platelike), recrystallized and mixed (duplex). Authors of [7] show that finely-dispersed two-phase duplex structure of Ti–Al based alloys has the best ductility, while another, not less important characteristic, namely, alloy viscosity, is lowered. An optimum variant is producing alloys with a completely lamellar two-phase  $\gamma + \alpha_2$  structure with a certain quantity of  $\gamma$  and  $\alpha_2$  phases in the alloy [7].

Titanium aluminide based alloys with different structure types, in addition to aircraft industry [5, 8–10], can be used in various industrial sectors, namely gas- and oil-processing, chemical, as well as in nuclear and transportation engineering [11, 12].

Wider acceptance of  $\gamma$ -TiAl based alloys is promoted by current intensive investigations of their weldability and development of effective measures to improve the strength and reliability of welded joints.



In this connection the purpose of this review is analysis of modern developments of joining processes for titanium aluminide based materials using various kinds of welding.

**Arc welding.** Reference [3] gives the results of investigation of weldability of an alloy with  $\gamma$ -TiAl cast structure (48 at.% Al and 2 at.% Cr and Nb). Welding of titanium aluminides was conducted without preheating with current adjustment in the range of 50–1500 A. As a result, it was established that microstructure of weld metal zone consists of columnar and equiaxed dendritic structures.

Mechanical properties of weld metal turned out to be lower than those of base metal. This is exactly what was established as a result of tensile testing (Figure 1). At the same time, at low current welding cracks were found in the joint, which formed as a result of increase of  $\alpha_2$ -phase amount.

Weldability of the above-mentioned alloy was studied in [14]. Before welding all the samples were subjected to hot isostatic pressing, part of them were heat-treated at the temperature of 1300 °C for 20 h. This resulted in formation of a crystalline structure, consisting of  $\gamma$ -phase,  $\gamma + \alpha_2$  colony and Laves phases. Cracking was observed in all the welds, both after their isostatic pressing, and without it.

Bharani and Acoff conducted welding of the above titanium aluminide alloy and wrought  $\gamma$ -TiAl alloy (46 at.% Al, 2 at.% Cr, 2 at.% Nb, 0.9 at.% Mo) without preheating. It is established that shortening of crack length in the welded joint can be achieved only due to performance of postweld heat treatment at 615 °C temperature [15].

**Electron beam welding.** In the opinion of the authors of [16, 17], fusion welding of titanium

aluminide can be performed only with preheating up to 250–650 °C. This is related to the fact that in view of the low ductility (right up to 700 °C) titanium aluminides are quite sensitive to stresses, which develop under the conditions of non-uniform heating in welding and, therefore, are prone to appearance of transverse cold cracks in welded joints.

References [16, 17] give preheating temperature without any additional details, and in [18] it is recommended to preheat the samples to be welded up to 400–500 °C to prevent development of transverse cracks in welded joints. On parts of local welds or deposits for repair purposes preheating temperature should be not less than 600 °C. However, these parameters are established only for  $\gamma$ -TiAl alloy (31 at.% Al and 2 at.% Nb and Mn each), while sample preheating is performed in the welding chamber.

**Pressure welding in vacuum.** During performance of research work authors of [19] used for experimental purposes aluminide samples (20 mm diameter and height titanium) cut out of an ingot subjected to isostatic processing at the temperature of 1260 °C and pressure of 170 MPa for 4 h with subsequent stabilizing annealing at 1000 °C (50 h). Weight fraction of alloying elements and additives in the alloy was equal to, %: 60.95 Ti; 31.15 Al; 4.65 Nb.

Welding was performed at the temperature below  $\alpha + \gamma$  transition, so that material structure practically did not change. This enabled eliminating the phenomena, which are due to rapid cooling of the joint. A clear-cut boundary is registered at contact of the joined surfaces. No common grain formation was found. Both single macropores and linear porosity were present in a number of samples.

Further investigations were performed with the purpose of revealing the features of structural transformations in titanium aluminide under the impact of thermodeformational cycle of welding in the following modes: temperature  $T = 900$  and 1100 °C, welding time  $t = 4$ –5 h, pressure  $P = 200$ –300 MPa [20]. It is established that at welding temperature below 900 °C transcrystalline cracks without any visible traces of plastic deformation develop in the alloy under the impact of a compressive welding force. With increase of welding temperature from 900 up to 1100 °C, structural element morphology changes from coarse-grained platelike to fine-grained globular. At the temperature of 1100 °C, common grains are observed in the joint zone, forming as a result of plastic deformation and subsequent recrystallization of near-contact metal volumes.

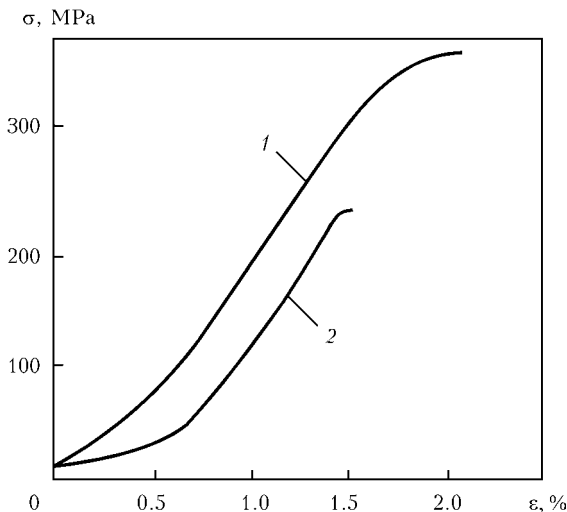


Figure 1. Dependence of deformations  $\sigma$  on stresses  $\epsilon$  [13] of base metal (1) and weld zone (2)

Possibility of welding titanium aluminide using a «soft» interlayer was studied later on [19]. The authors assumed that part annealing after welding with an interlayer will lead to its dissolution in the base metal and to diffusion-induced homogenizing of the composition in the joint zone. Therefore, aluminium and titanium as the main alloying elements of the alloy were selected as interlayers. Thickness of aluminium and titanium interlayers was equal to 0.15 and 0.20 mm, respectively. Samples of titanium aluminide (20 mm height and diameter) were used for experiments.

Microstructures of welded joints made with application of aluminium and titanium foil as an interlayer, are given in Figures 2 and 3. It is established that welding of  $\gamma$ -TiAl based alloy with application of aluminium and titanium foil as interlayers does not ensure the required quality of the joints. At application of aluminium interlayer it is possible to produce (after welding and annealing) phase and chemical compositions of metal along the fusion line close to those of base metal. However, these joints are not operable because of the presence of defects which arise in welding (Figure 2). Now in the case of application of titanium foil, welded joints, both after welding and after welding and annealing, feature a certain level of strength at normal temperature. However, it does not seem possible to ensure high-temperature strength of such joints close to that of  $\gamma$ -TiAl, as the joint zone has single-phase structure of  $\alpha_2$ (Ti<sub>3</sub>Al) (Figure 3).

**Friction welding.** The main problems at production of operable joints of titanium aluminides in friction welding [21–23] is microcracking in the zone of thermomechanical impact during deformation [21], weld metal cracking during cooling [22], considerable increase of joint zone hardness [21–23], as well as absence of optimum parameters of welding mode [21–23].

Description of structural and phase changes proceeding in the plane of interaction and in the HAZ in two different modes (convection and combined) is given in [24]. It is established that metal structure in the plane of the joint produced at convection welding, differs from that of joint zone metal in the combined mode, in which extremely fine dynamically recrystallized  $\gamma$ -TiAl grains are formed without the presence of the lamellar component, by insufficient quantity of  $\alpha_2$ -phase and structural gradient in the radial direction.

It is known that welded joint quality depends on welding time and upset length. References [25, 26] describe investigations on weldability

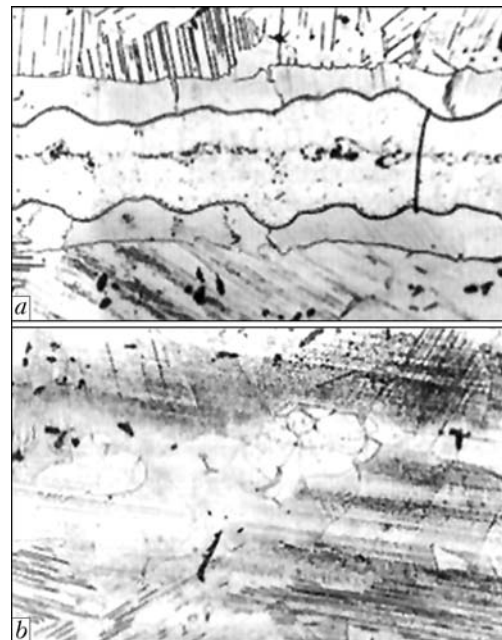


**Figure 2.** Microstructures of welded joints of  $\gamma$ -TiAl alloy with aluminium interlayer: *a* – after welding ( $\times 400$ ); *b* – after welding and annealing ( $\times 200$ ) [19]

of  $\gamma$ -TiAl and  $\alpha_2$ -TiAl alloys using nanointerlayer of Ti/Al foil with different heating times. It is established that in joints produced at heating duration  $t_h = 1.0$  s, an interlayer of up to 100  $\mu\text{m}$  width with a fine-grained structure is observed. With increase of time  $t_h$  up to 4.0 s the observed structure in the joint plane and in the HAZ of welded alloys is characterized by presence of extremely fine dynamically recrystallized grains. The authors of the work supposed that formation of fine-grained metal structure in the joint plane

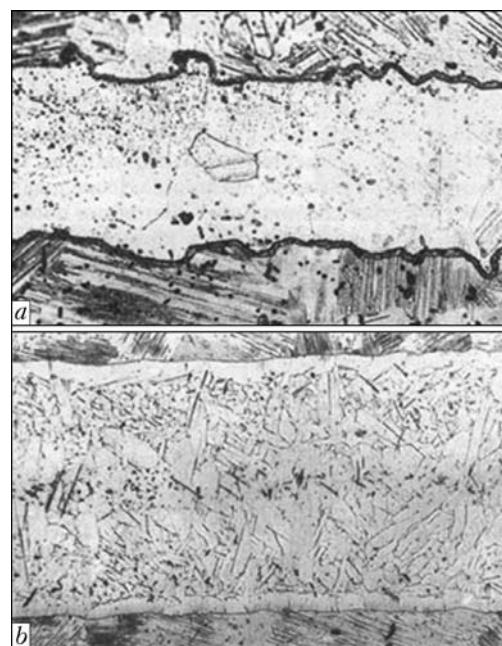


**Figure 3.** Microstructures of welded joint of  $\gamma$ -TiAl alloy with titanium interlayer: *a* – after welding ( $\times 250$ ); *b* – after welding and annealing ( $\times 100$ ) [19]

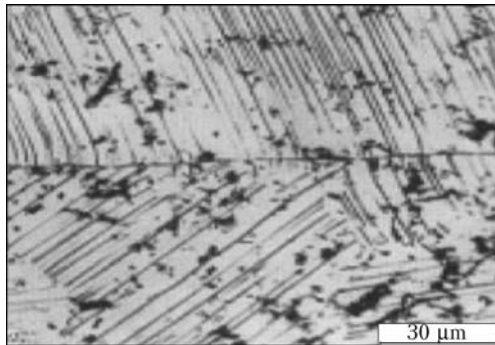


**Figure 4.** Microstructure of metal of the zone of  $\gamma$ -TiAl alloy welded joint produced by vacuum diffusion welding [28]

promotes an increase of butt metal resistance to cracking during cooling.

**Diffusion welding.** Reference [27] deals with  $\gamma$ -TiAl alloy (49 % Ti, 47 % Al and 4 % Cr, Mn, Nb, Si, B each) produced by the process of precision casting and hot pressing with subsequent homogenizing annealing. As shown by investigation results, formation of a lamellar structure in the vicinity of the weld is provided in the following welding mode:  $T = 1000\text{--}1100\text{ }^{\circ}\text{C}$ ,  $t = 3\text{ h}$ ,  $P = 20\text{--}40\text{ MPa}$  with subsequent heat treatment.

Reference [28] presents the results of investigations, conducted on Ti – 48 at.% Al alloy alloyed with niobium and manganese. Titanium aluminide joints were produced by diffusion welding in vacuum without the interlayer at  $T = 1200\text{ }^{\circ}\text{C}$  and  $P = 70\text{ MPa}$  with subsequent soaking for 20 min. Figure 4 shows the microstructure of joint zone metal.

The authors of the work found that the interface is an interlayer of intermetallic, the composition of which, by the data of local chemical analysis, is close to that of  $\text{Ti}_3\text{Al}$  intermetallic. Presence of a brittle intermetallic interlayer lowers welded joint strength, thus leading to lowering of its service characteristics.

In order to improve the welding processes and properties of permanent joints of  $\gamma$ -TiAl alloys, the authors of [29–32] applied nanostructured

interlayers, which were placed between the item surfaces to be welded. Such interlayers can be one- or multilayer coatings [29–31] or foils [32].

In [29–31] weldability of  $\gamma$ -TiAl alloy was studied at application of various nanolayered coatings, which were applied on the surfaces being welded by magnetron sputtering. Reference [31] shows application of coatings of titanium, vanadium, chromium and manganese  $0.5\text{--}1.5\text{ }\mu\text{m}$  thick, and [29–30] describe application of coatings of Ti/Al system of Ti – 48–50 at.% Al composition, the thickness of which was equal to  $2.0\text{--}2.5\text{ }\mu\text{m}$  at individual layer thickness of up to 4 nm.

It was established [31] that application of vanadium, chromium and manganese coatings improves ductility of welded joints of  $\gamma$ -TiAl alloys, at atomic fraction of the above elements in the welded joints on the level of 1–3 %.

In [29, 30] it is shown that deposition of thin nanolayered Ti/Al coatings on the surfaces being joined provides formation of a uniform microstructure in the joint zone during diffusion welding at the temperature of  $1000\text{ }^{\circ}\text{C}$ . The authors came to the conclusion that formation of a strong welded joint in the temperature range of  $700\text{--}1100\text{ }^{\circ}\text{C}$  is related to dynamic recrystallization of  $\gamma$ -TiAl alloy which leads to structure refinement and ensures running of plastic deformation.

Investigation of weldability of  $\gamma$ -TiAl based alloy with application of nanolayers produced by the technology described in [33], was performed by the authors of [32]. Welding was conducted on  $10 \times 10 \times 6\text{ mm}$  samples from  $\gamma$ -TiAl intermetallic (48 at.% Al, 2 at.% Nb, 2 at.% Mn), for which the following interlayers were chosen: Ti/Al (Ti – 38 at.% Al), Ni/Ti (Ti – 44 at.% Ni) and Ni/Al (Al – 46 at.% Ni) (Figure 5).

The authors established that during diffusion welding of  $\gamma$ -TiAl samples with application of Ni/Ti and Ni/Al nanolayers, a transition zone of heterogeneous structure and composition

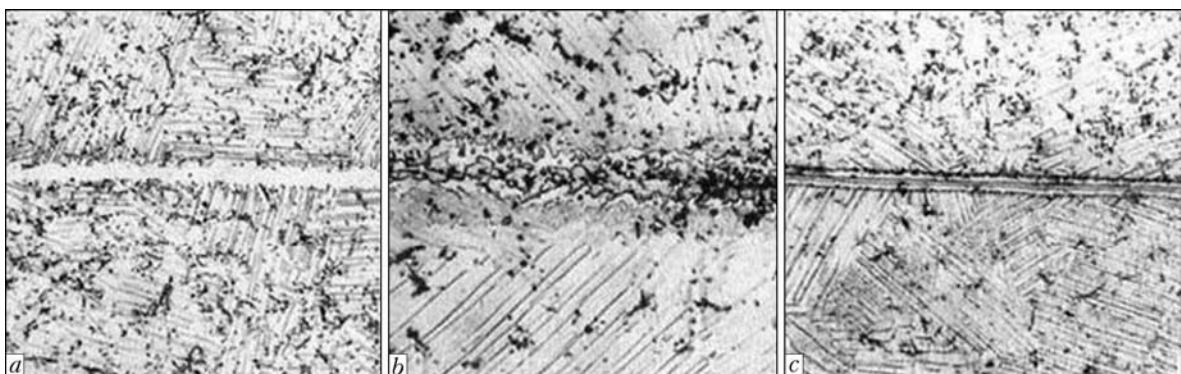


**Figure 5.** Microstructures of  $\gamma$ -TiAl alloy joint zone at diffusion welding with application of nanolayers [32]: *a* – Ti/Al ( $\times 200$ ); *b* – Ni/Ti ( $\times 200$ ); *c* – Ni/Al ( $\times 400$ )



forms in the joint zone [32]. At application of Ti/Al nanolayers an intermetallic forms in the joint zone, the composition of which corresponds to the initial  $\gamma$ -TiAl intermetallics, layer-by-layer transforming into  $\gamma$ -TiAl with nanometric periods (less than 200 nm). Such changes of metal composition and structure in the joint zone are indicative of a high diffusion mobility of components that may be due to the processes of heat generation accompanying solid-phase reactions, initiated in nanolayered foil at heating [34].

**Resistance welding.** Reference [35] gives the results of investigations of the features of formation of  $\gamma$ -TiAl based welded joints by resistance welding technology. Such a technology provides local high-rate application of heat to the joint zone [36] that prevents metal softening. Considering the experience of previous developments on flash-butt welding of difficult-to-weld materials [37], welding of  $\gamma$ -TiAl alloys was conducted with application of nanostructured foils of Ti/Al system. At application of foil consisting of titanium and aluminium layers, additional heat evolution in the contact zone takes place that is due to running of an exothermal reaction between metals, that results in welding time shortening by 0.5–0.7 s on average. It is additionally shown in the work that nanolayered foils should be applied in order to ensure uniform heating, improve welded joint formation and properties. Foil thickness can vary from 60 up to 100  $\mu\text{m}$ .

## Conclusions

1. Applications of traditional welding processes, based on local melting of material in the joint zone showed that the quality of the produced welded joint essentially depends on phase transformations in the HAZ zone. At deviation of welding mode from the optimum one in the joint zone phase transformations take place, which are accompanied by volumetric effects leading to development of stresses in the HAZ zone and, as a result, cracks form in its vicinity.

2. The highest values of mechanical properties of titanium aluminide joints were produced in diffusion welding with application of thin interlayers. This welding process, however, was not accepted by industry. One of the main disadvantages of diffusion welding is the need for long-term heating up to high temperatures ( $T = 1000\text{--}1100\text{ }^\circ\text{C}$ ) of the entire item to be welded and presence of vacuum.

3. Application of composite interlayers in resistance welding provides a more uniform and concentrated heating, and, as a result, sound joints of parts of a small cross-section (100–

200  $\text{mm}^2$ ) from titanium aluminides that is indicative of applicability of such technologies at industrial-scale manufacture of various components.

4. Results presented in the published works, are indicative of high efficiency of application of nanostructured interlayers for joining difficult-to-weld  $\gamma$ -TiAl alloys.

1. Mukhin, V.S. (2007) *Principles of technology of machine building (aircraft engine engineering)*. Ufa: UGATU.
2. Pavlinich, S.P., Zajtsev, M.V. (2011) Application of intermetallic titanium alloys in casting of assemblies of gas turbine engines and blades with lightened high strength structures for aircraft engines of new generations. *Vest. Ufim. Gos. Aviats. Tekhn. Un-ta*, 15(4), 200–202.
3. Ivanov, V.I., Yasinsky, K.K. (1996) Efficiency of application of heat resistant alloys based on Ti<sub>3</sub>Al and TiAl intermetallics for service at 600–800  $^\circ\text{C}$  temperatures in aircraft engineering. *Tekhnol. Lyogk. Splavov*, 3, 7–12, 93.
4. Lipsitt, H.A., Shechtman, D., Schafrik, R.E. (1975) The plastic deformation of TiAl. *Met. Transact. A*, 6, 1991–1998.
5. Froes, F.H., Suryanarayana, C., Eliezer, D. (1991) Production, characteristics and commercialization of titanium aluminides. *ISIJ Int.*, 31(10), 1235–1248.
6. Polkin, I.S., Kolachev, B.A., Iliin, A.A. (1997) Titanium aluminides and alloys on their base. *Tekhnol. Lyogk. Splavov*, 3, 32–39.
7. Kazantseva, N.V., Grinberg, B.A., Gulyaeva, N.P. et al. (2003) Microstructure and plastic deformation of orthorhombic Ti<sub>2</sub>AlNb alloys II. Structure and phase transformations in strong deformation. *Fiz. Metalla i Metallovedenie*, 96(4), 23–32.
8. Kim, Y.-W., Dimiduk, D.M. (1991) Progress in the understanding of gamma titanium aluminides. *JOM*, 8, 40–47.
9. Bannykh, O.A., Povarova, K.B., Braslavskaya, G.S. et al. (1996) Mechanical properties of cast alloys  $\gamma$ -TiAl. *Metallovedenie i Term. Obrabotka Met.*, 4, 11–14.
10. Boggs Robert, N. (1989) Titanium aluminide true space-age material. *Des. News*, 45(12), 51–53.
11. Antashaev, V.G., Ivanov, V.I., Yasinsky, K.K. (1996) Development of technology for producing of cast parts from intermetallic alloy TiAl and their application in structures. *Tekhn. Lyogk. Splavov*, 3, 20–23.
12. Hino, H., Nisiyamo, Yu. (1990) Application of titanium aluminides. *Metals Technol.*, 60(7), 70–76.
13. Arenas, M.F., Acoff, V.L. (2003) Analysis of gamma titanium aluminide welds produced by gas tungsten arc welding. *Welding J.*, 5, 110–115.
14. Kelly, T. (1992) Repair welding of gamma titanium aluminide castings. In: *Proc. of the 3rd Int. SAMPE Metals Conf.* (Covina, 25–30 May 1992). Covina: SAMPE, 1992.
15. Bharani, D.J., Acoff, V.L. (1998) Autogenous gas tungsten arc weldability of cast alloy Ti–48Al–2Cr–2Nb (atomic percent) versus extruded alloy Ti–46Al–2Cr–2Nb–0.9Mo (atomic percent). *Met. and Mater. Transact. A*, 29(13), 927–935.
16. Patterson, R.A. et al. (1990) Titanium aluminide : electron beam weldability. *Welding J.*, 1, 39–44.
17. Jensen, C.M., Zhang, H., Baeslack, W.A. et al. (1998) The effect of postweld heat treatment on the structure and properties of electron beam welded Ti–48Al–2Cr–2Nb alloy. In: *Abstr. of Papers of 79th AWS Annual Meeting* (Miami, AWS).
18. Kharchenko, G.K., Ustinov, A.I., Falchenko, Yu.V. et al. (2001) Choice of preheating temperature of  $\gamma$ -



- aluminide titanium in EBW. *The Paton Welding J.*, **11**, 20–23.
19. Yushtin, A.N., Zamkov, V.N., Sabokar, V.K. et al. (2001) et al. (2001) Pressure welding of intermetallic alloy  $\gamma$ -TiAl. *Ibid.*, **1**, 33–37.
  20. Zamkov, V.N., Markashova, L.I., Kireev, L.S. (1992) Peculiarities of structural changes of heat resistant alloy based on Ti<sub>3</sub>Al in vacuum pressure welding. *Avtomatich. Svarka*, **9/10**, 13–16.
  21. Baeslack, W., Threadgill, P., Nicholas, E. (1992) Linear friction welding of alpha-two titanium aluminide. *TWI Research Report*, **442**, 204–210.
  22. Miyashita, T., Hino, H. (1994) Friction welding characteristics of TiAl intermetallic compound. *J. Japan Inst. Metals*, **58(2)**, 215–220.
  23. Baeslack, W., Threadgill, P., Nicholas, E. et al. (1995) Linear friction welding of Ti–48Al–2Cr–2Nb (at.%) titanium aluminide. In: *Proc. of the 8th World Conf. on Titanium* (Birmingham, 22–26 Oct. 1995). Birmingham: Inst. of Materials, 1995.
  24. Kuchuk-Yatsenko, S.I., Zyakhov, I.V. (2009) Specifics of friction welding of titanium aluminides. In: *Proc. of 9th Math. Annual Int. Conf. on Efficiency of Implementation of Scientific, Resource and Industrial Potential in Current Conditions* (Slavskoe, 9–13 February 2009). Kiev: UIC Science. Technique. Technology, 2009.
  25. Zyakhov, I.V., Kuchuk-Yatsenko, S.I., Ustinov, A.I. (2009) Application of nanolayered foil of Ti–Al system in friction welding of titanium aluminide based alloys. In: *Proc. of Conf. on Slavic Lectures* (Lipetsk, 4–5 June 2009). Lipetsk: LGTU, 2009.
  26. Zyakhov, I.V., Kuchuk-Yatsenko, S.I. (2009) Structure of titanium aluminide compounds in friction welding using nanolayered foil of Ti–Al system. In: *Proc. of 8th All-Russ. Sci.-Techn. Conf. with Internat. Participation* (Moscow, 30 November–1 December, 2009). Moscow: MATI, 2009.
  27. Cam, G., Bohm, K.-H., Kocak, M. (1999) Diffusionsschweißen feingegossener Titanaluminide. *Schweißen und Schneiden*, **8**, 470–475.
  28. Ustinov, A.I., Falchenko, Yu.V., Ishchenko, A.Ya. et al. (2009) Producing permanent joints of  $\gamma$ -TiAl based alloys using nanolayered Ti/Al interlayer by vacuum diffusion welding. *The Paton Welding J.*, **1**, 12–15.
  29. Duarte, L.I., Ramos, A.S., Viera, M.F. et al. (2006) Solid-state diffusion bonding of gamma-TiAl alloys using Ti/Al thin films as interlayers. *Intermetallics*, **14**, 1151–1156.
  30. Ramos, A.S., Viera, M.T., Duarte, L.I. et al. (2006) Nanometric multilayers: A new approach for joining TiAl. *Ibid.*, **14**, 1157–1162.
  31. Yan, R., Somekh, R.E., Wallach, E.R. (1992) Solid-state bonding of TiAl with interlayers. In: *Proc. of the 3rd Int. Conf. on Trends in Welding Research* (Gattinburg, Tennessee, USA, 1–5 June, 1992). Ohio: ASM International, Materials Park, 1992.
  32. Kharchenko, G.K., Ustinov, A.I., Falchenko, Yu.V. et al. (2011) Diffusion bonding of  $\gamma$ -TiAl base alloy in vacuum by using nanolayered interlayers. *The Paton Welding J.*, **3**, 2–6.
  33. Ustinov, A.I., Olikhovskaya, L.A., Melnichenko, T.V. et al. (2008) Solid phase reactions in heating of multilayer Al/Ti foils produced by electron beam deposition method. *Advances in Electrometallurgy*, **2**, 19–26.
  34. Kuchuk-Yatsenko, S.I., Shvets, V.I., Sakhatsky, A.G. et al. (2009) Features of resistance welding of titanium aluminides using nanolayered aluminium-titanium foils. *Ibid.*, **3**, 11–14.
  35. Kochergin, A.K. (1987) *Resistance welding*. Leningrad: Mashinostroenie.
  36. Kuchuk-Yatsenko, V.S., Shvets, V.I., Sakhatsky, A.G. et al. (2007) Specifics of resistance butt welding of aluminium alloys by using nanostructural aluminium-nickel and aluminium-copper foils. *Svarochn. Proizvodstvo*, **9**, 12–14.

Received 01.03.2013



# CALCULATION OF PARAMETERS OF EXPLOSION TREATMENT FOR REDUCTION OF RESIDUAL STRESSES IN CIRCUMFERENTIAL WELDS OF PIPELINES

A.G. BRYZGALIN

E.O. Paton Electric Welding Institute, NASU

11 Bozhenko Str., 03680, Kiev, Ukraine. E-mail: office@paton.kiev.ua

Reduction of residual stresses in circumferential welds of pipelines is laborious and expensive process. Explosion treatment as an alternative to heat-treatment provides for significant time and expenses reduction. Experiment-calculation method is developed for determination of modes of explosion treatment of circumferential pipe welds of different dimension-type. The method is based on application of general form dependence of deformation of cylindrical shell wall on external static load, obtained in scope of elasticity theory, applicable to solution of problem on determination of value of dynamic load necessary for development of plastic strains, providing reduction of residual stresses in circumferential pipe welds. Dependences for calculation of main parameters of explosion treatment are derived based on this method. Experimental investigations verifying suitability of obtained dependencies for practical application without participation of technology developers were carried out. 13 Ref., 2 Tables, 3 Figures.

**Keywords:** explosion treatment, heat treatment, residual stresses, deformations, circumferential weld, pipelines

Residual welding stresses (RS) from circumferential welds can significantly reduce working capacity of the pipelines operating under low temperature conditions, influence of corrosive medium and other unfavourable factors [1, 2]. Reduction of RS is performed with the help of heat treatment being expensive and laborious technology [3]. Explosion treatment (ET) providing lower prime cost and high efficiency can be an alternative to heat treatment.

ET technology has found wide application in providing of safety and service life of technological pipelines of aluminous production and gas fields with increased content of hydrogen sulphide, providing transportation of corrosive media which promotes cracking of circumferential welds. Unique experience of ET application for prevention of avalanche-like cracking was obtained during laying of Taas-Tumus-Yakutsk gas pipeline, on which 295 erection joints made by manual arc welding under field conditions were treated. Absence of damages on treated joints of the gas pipeline, including under extremely severe winter conditions, shows efficiency of application of ET structures operating under low temperatures. Obvious advantage of ET compared to heat treatment is an absence of necessity of application of special equipment and power sources. The technology can be used not only in

pipeline assembly, but in performance of on-line tasks on repair and replacement of damaged sections.

On-line selection of modes of ET of circumferential pipe welds has important practical value, in particular, when its accuracy provides selection of modes close to optimum ones allowing eliminating expensive experimental investigations.

Considered are the peculiarities of ET process using charges representing them self specific quantity of winds of explosive cord (EC) located on outer surface of the pipe close to weld. Figure 1, *a* shows generalized diagram of elastic tangential strains of pipe wall from circumferential weld. Loading from explosion effect in accepted scheme is considered equal to distributed one and should be applied to zone of compression RS effect [4] (area AB, Figure 1, *b*). Cross section of the charge from EC is shown in Figure 1, *c* in form of circles.

Unique determination of ET mode of circumferential weld of pipe of known dimension-type requires searching of charge mass  $m$ , charge width  $a$  and distance from axis of treated circumferential weld to end of charge  $b$  nearest to it [b]. Value of pipe wall deformation created by explosion is determined by mass of charge, therefore, selection of latter should depend on pipe deformation resistance, i.e. on cylindrical rigidity (geometric parameters) and material yield strength. Location of created deformations is determined by charge parameters  $a$  and  $b$ .

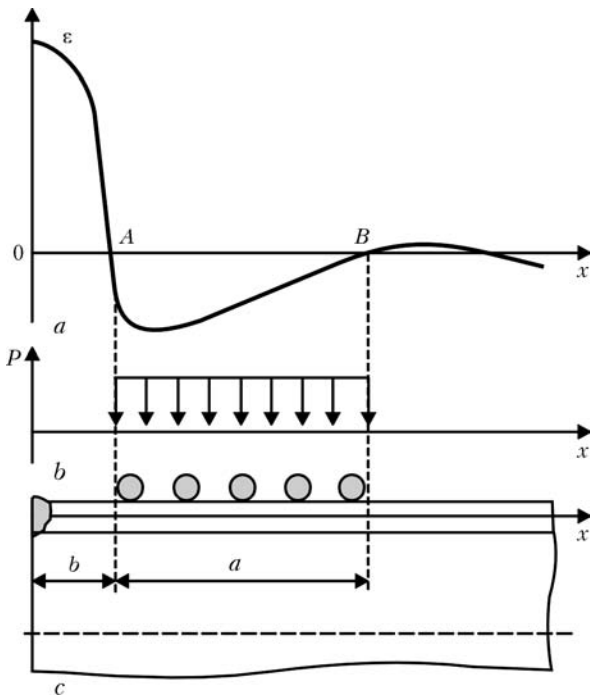


**Figure 1.** Scheme of charge positioning during ET: *a* – general diagram of tangential residual elastic strains; *b* – distribution of loading from explosion; *c* – positioning of charge from EC

There are analytical as well as numerical methods of solving of dynamic problems [6, 7]. These methods and form of representation of solutions obtained with their help are, as a rule, very bulky and difficult, and require application of precisising experiments in each specific case. It is reasonable to develop sufficiently easy method allowine for on-line calculation of optimum values of ET parameters for circumferential welds of pipes of different dimension-types using existing results of calculation investigations and accumulated experience of practical methods of selection of charge parameters.

Considering that circumferential stresses (operational and welding) in pipelines are, as a rule, significantly higher of axis ones, and that ET obviously results in reduction of axial welding

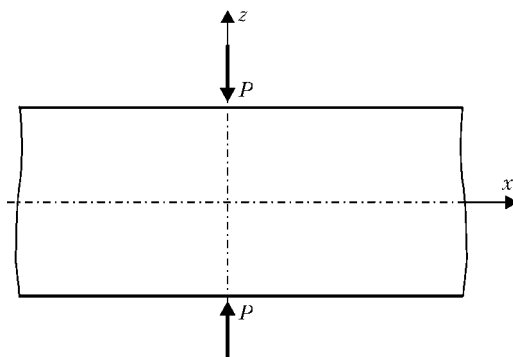


**Figure 2.** Scheme of calculation of charge width for ET of circumferential pipe weld: *P* – distribution of load on circle; *x* – distance along the generatrix of pipe from place of load application

residual stresses [7], present paper studies distribution of only circumferential RS in welds.

**Calculation of charge width.** The reason of appearance of residual deformations and stresses in welded joint is formation of plastic shortening strain in the process of welding heating, width of which is indicated as  $b_p$ . The charge width  $a$  should be so as to provide deformation of pipe wall in zone of formation of elastic welding contraction strains, i.e. equal the width of [AB] area (Figure 1). Therefore, ET parameter  $b$  should equal  $b_p$ , position of point A corresponds to  $x = b_p$  coordinate, position of point B is determined by coordinate of transfer into zero of diagram of elastic welding contraction strains. Further, increase of charge width will not result to significant increase of ET efficiency, although provide no negative consequences, except for over-expenditure of EC and time for charge assembly.

Practice of RS measurement in pipes shows that width of this zone even for pipes of one dimension-type can be different since it depends on conditions of welding of circumferential weld, conditions of pipe manufacture, measurement error and other factors. At the same time, multiple experiment investigations and industrial application of ET indicate that applied ET scheme provides for high efficiency even at some deviations of selected charge width from that accepted in considered scheme. This testifies that accuracy of calculation data can be leveled by random factors which couldn't be considered in the calculation model even with the most well-set problem.

In this connection the simplest scheme for calculation of width of zone of compression strain is taken.

Influence of weld on the rest of pipe will be modeled based on external contraction load  $P$  (Figure 2) uniformly distributed on circumference of pipe cross section and concentrated in direction of longitudinal axis  $x$ . Symbolically  $b_p = 0$  is taken at such statement of problem.

Equation of deflected axis of shell for present case takes on the following form [8]:

$$w = 0.125Pe^{-\beta x}(\sin\beta x + \cos\beta x)/D_\beta\beta^3, \quad (1)$$

where  $\beta = [3(1 - \nu^2)/R^2h^2]^{0.25}$  is an auxiliary geometric parameter of the pipe;  $\nu$  is a Poisson's ratio;  $R$  is a radius;  $h$  is a thickness;  $D_\beta = Eh^3/12(1 - \nu^2)$  is a cylindrical rigidity of the shell;  $E$  is a modulus of elasticity of steel of pipe being treated.

Width of ET charge is determined on coordinate  $x$ , at which  $w = 0$ :



$$\sin\beta x + \cos\beta x = 0.$$

Since only first positive root of equation (1) is interesting for us, it is finally found:

$$a = x|_{w=0} = 0.75\pi/\beta, \tag{2}$$

or in more simple form

$$a = 1.8 \sqrt{Rh}. \tag{3}$$

**Determination of charge mass.** Mass of the charge equal the mass of explosive material (EM) in EC and can be expressed in the following way:

$$m = 2\pi Rnj, \tag{4}$$

where  $n$  is the quantity of EC winds;  $j$  is the portion of EM per unit of length in EC.

Considering that charges for ET of circumferential pipe welds are manufactured from EC which is characterized by sufficiently stable detonating specifics, it can be assumed that dynamic yield strength  $\sigma_y^d$  is proportional to static yield strength  $\sigma_y$ :

$$\sigma_y^d = K\sigma_y. \tag{5}$$

It is also supposed that data of pipe calculation as elastic static shell will be sufficiently valid in moment of appearance of first plastic strains under the charge regardless the dynamic character of problem being solved.

Let's consider the following problem (Figure 3). Some part of infinitely long pipe with width  $a$  is loaded along the circle by uniformly distributed load  $p$  (Figure 1, b). Divide this pipe on three parts in  $x = 0.5a$  and  $x = -0.5a$  sections, and balance their effect on each other by distribution of bending moments  $M$  and intersecting forces  $Q$  acting in these sections.

Functions of shell bending are found by means of solving of differential equation of symmetric deformation of circular cylindrical shell with constant thickness [8]:

$$\frac{d^4 w}{dx^4} + 4\beta^4 w = \frac{p}{D\beta} \tag{6}$$

and have form

$$w_1 = e^{-\beta x}(C_1 \cos \beta x + C_2 \sin \beta x) + e^{\beta x}(C_3 \cos \beta x + C_4 \sin \beta x) + 0.25p/\beta^4 D\beta \tag{7}$$

for the first (central, final length) part of the pipe and

$$w_2 = e^{-\beta(x-0.5a)}[C_5 \cos \beta(x-0.5a) + C_6 \sin \beta(x-0.5a)] \tag{8}$$

for the second (right, semiinfinite length) of its part;  $C_1 - C_6$  are the unknown coefficients;

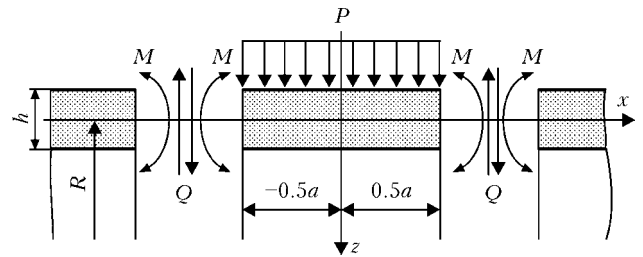


**Figure 3.** Calculation model for determination of charge value

$0.25p/\beta^4 D\beta$  is the partial solution of equation (3).

It is determined that  $C_3 = C_1$ ,  $C_4 = -C_2$  considering that  $w_1(x) = w_2(-x)$ .

$C_1$  and  $C_2$  are determined from condition of equality of bendings, angles of wall turning, moments and intersecting forces of the shells 1 and 2 in point  $x = 0.5a$ :

$$C_1 = -p \frac{1}{8\beta^4 D\beta k}; \quad C_2 = p \frac{tg(0.5\beta a)}{8\beta^4 D\beta k},$$

where  $k = (\cos 0.5\beta a + tg 0.5\beta a \sin 0.5\beta a)e^{0.5\beta a}$ . Then

$$w_1 = \frac{p}{8\beta^4 D\beta k} [e^{-\beta x}(-\cos \beta x + tg 0.5\beta a \sin \beta x) + e^{\beta x}(-\cos \beta x - tg 0.5\beta a \sin \beta x) + 2k]. \tag{9}$$

Maximum circumferential stresses (at  $x = 0$ )  $\sigma_{\beta\max}$  in the shell can be found on formulae [9]:

$$\begin{aligned} \sigma_{\beta\max} &= N/h + 6vM/h^2; \quad N = -Ehw/R; \quad M = -D\beta d^2 w/dx^2, \\ \sigma_{\beta\max} &= \frac{pR}{hk} [1 - k - \frac{3vtg 0.5\beta a}{\sqrt{3(1-v^2)}}] = pf(R, h, a), \end{aligned} \tag{10}$$

where  $f(R, h, a)$  is a function determined only by geometry parameters of the pipe and loading scheme.

The next reasons are given in order to evaluate possibility of application of solution of static problem for selection of parameters of corresponding dynamic loading of the pipe.

1. Based on that an expression for static maximum stress consists of two multipliers, namely force  $p$  and geometry  $f(R, h, a)$ , it is assumed that structure of expression for maximum dynamic stress will be similar in dynamic formulation (10):

$$\sigma_{\beta\max}^d = AdIf(R, h, a), \tag{11}$$

where  $I$  is a uniformly distributed pressure pulse at ET;  $A_d$  is a some function considering dynamic of the process and determined only by EM properties;



2. Achievement of high efficiency of ET requires development of dynamic stresses equal the dynamic yield strength.

The following is obtained from (5) and (11) considering made assumptions:

$$K\sigma_y = A_d I f(R, h, a).$$

$K$  and  $A_d$  are unknown as a rule, therefore, the expression can be written in the form:

$$\sigma_y = A I f(R, h, a). \quad (12)$$

Considering possible errors of above assumptions, experimentally received information about already well elaborated mode with  $I_0$  and  $a_0$  parameters is used for determination of function  $A$  for some pipe, which is called reference, with  $R_0$ ,  $h_0$  and  $\sigma_{y0}$  characteristics:

$$\sigma_{y0} = A I_0 f(R_0, h_0, a_0).$$

Write for reference pipe considering (10):

$$\sigma_{y0} = \frac{A I_0 R_0}{h_0 k_0} \left[ 1 - k_0 - \frac{3v \operatorname{tg} 0.5 \beta_0 a_0}{\sqrt{3(1 - v^2)}} \right],$$

for studied pipe:

$$\sigma_{yi} = \frac{A I_i R_i}{h_i k_i} \left[ 1 - k_i - \frac{3v \operatorname{tg} 0.5 \beta_i a_i}{\sqrt{3(1 - v^2)}} \right]$$

and after corresponding transformations the next is obtained:

$$I_i = I_0 \frac{\sigma_{yi} R_0 h_i}{\sigma_{y0} R_i h_0} \left( \frac{k_i}{k_0} \frac{1 - k_0 - 3v \operatorname{tg} 0.5 \beta_0 a_0 / \sqrt{3(1 - v^2)}}{1 - k_i - 3v \operatorname{tg} 0.5 \beta_i a_i / \sqrt{3(1 - v^2)}} \right).$$

It should be noted that pressure pulse  $I$  is inversely proportional to charge width and directly proportional to mass of EM charge falling on unit of pipe area and mass of charge is determined by equation (4), i.e.  $I \sim jn/a$ , considering what will get:

$$n_i = n_0 \frac{j_0 a_i \sigma_{yi} R_0 h_i}{j_i a_0 \sigma_{y0} R_i h_0} \times \left( \frac{k_i}{k_0} \frac{1 - k_0 - 3v \operatorname{tg} 0.5 \beta_0 a_0 / \sqrt{3(1 - v^2)}}{1 - k_i - 3v \operatorname{tg} 0.5 \beta_i a_i / \sqrt{3(1 - v^2)}} \right). \quad (13)$$

Expression (13) allows calculating direct quantity of EC winds which is necessary for efficient ET of circumferential welds of pipes of set dimension-type as well as determining optimum EC for specific case on portion per unit of length which can be 6, 12, 14, 18, 33 g/m for industrially manufactured cords [10].

It is shown that obtained condition of determination of charge width (2) allows simplifying expression (13). Part of this expression, in brackets, is presented through  $\varphi$ :

$$\varphi = \left( \frac{k_i}{k_0} \frac{1 - k_0 - 3v \operatorname{tg} 0.5 \beta_0 a_0 / \sqrt{3(1 - v^2)}}{1 - k_i - 3v \operatorname{tg} 0.5 \beta_i a_i / \sqrt{3(1 - v^2)}} \right).$$

Inserting here value of charge width, determined by equation (2), namely  $a_0 = 0.75\pi/\beta_0$ ,  $a_i = 0.75\pi/\beta_i$  then  $\beta_0 a_0 = \beta_i a_i = 0.75\pi$ ,  $k_0 = k_i$  for all dimension-types of pipes, including for reference one, means that  $\varphi = 1$  and expression 13 takes the form:

$$n_i = n_0 \frac{j_0 a_i \sigma_{yi} R_0 h_i}{j_i a_0 \sigma_{y0} R_i h_0}. \quad (14)$$

**Calculation of distance from weld axis to near end of the charge.** Examine Figure 1 for determination of this parameter. Distance from weld axis to near end of the charge should equal the width of zone of plastic shortening strains appearing in welding. Well-known calculation method determining the width of plastic strain zone, proposed by G.A. Nikolaev [11], is used:

$$b_p = \frac{B\rho}{\rho - \varepsilon_y}, \quad \rho = \frac{0.484 \alpha q_0}{c^*(x_1 + x_2 - 2B)}, \quad (15)$$

where  $B$  is a width of plates being welded;  $\varepsilon_y$  is a deformation, corresponding to stresses equal the yield strength of steel;  $\alpha$  is a coefficient of linear expansion in heating;  $q_0 = q/2vh$  is a welding heat input;  $q = \eta IU$  is an effective capacity of power source;  $\eta$  is an efficiency of power source;  $I$  is a welding current;  $U$  is an arc voltage;  $v$  is a welding speed;  $c^*$  is a heat capacity of steel under specific welding conditions which can be taken equal the heat capacity at constant volume;  $x_1, x_2$  is the position of spots of welded joint on axis  $x$  at which temperature  $T$  during welding achieves 600 and 500 °C, respectively, and is calculated on N.N. Rykalin formula [6] ( $x = 0.484 q_0 / c^* T$ ). Arc voltage in manual arc welding (MAW) according to GOST 35-75 is determined on formula  $U = 20 + 0.04I$ , welding current is set by welder; welding current in semi-automatic arc welding is determined on amperemeter of semiautomatic device or on formula given for MAW depending on arc voltage registered by voltmeter of semiautomatic device; welding parameters in automatic welding are determined on measurers of automatic device or power source.

Model of welded joint considered by G.A. Nikolaev assumes that effect of thermal-deformation processes in welding propagates along the whole width of plates being welded. In real joint the value of elastic strains (residual one and forming in welding) quickly reduces with increase of distance from weld axis, and only part of metal, adjacent to zone of shortening strains, gives re-



action to deformations and stresses. In our case width of this reaction zone (zone of residual elastic contraction strains) is determined by point *B* in Figure 1. The width of this zone is described above by expression (2). Insert of (2) in (15) gives expression for calculation of width of zone of plastic shortening strains in welding of circumferential pipe joints:

$$b_p = \frac{1.8\sqrt{Rh}}{1 - \frac{\sigma_y}{\alpha E} \left( \frac{1}{600} + \frac{1}{500} - 3.6 \frac{c^* \sqrt{Rh}}{0.484 q_0} \right)}. \quad (16)$$

Coefficients, showing properties of pipe material for low-carbon steels, have the following average values in SI dimension system [11]:

$$c^* = 5.2 \cdot 10^6 \text{ J/m}^3\text{C}, \quad \alpha = 15 \cdot 10^{-6} \text{ 1/}^\circ\text{C}, \\ E = 2 \cdot 10^{11} \text{ Pa}.$$

Efficiency of power source  $\eta$  is determined experimentally and being the reference value [7].

Taking into account given values of coefficients as well as that the welding power source has physical width and heating of base metal is virtually carried out from fusion line, the final expression for determination of distance from weld axis to near end of EM charge in MAW takes the form:

$$b = \frac{1.8\sqrt{Rh}}{1 - 1.53 \cdot 10^{-9} \sigma_y \left( 1 - 11.3 \cdot 10^9 \frac{\sqrt{Rh}}{q_0} \right)} + S_w, \quad (17)$$

where  $S_w$  is a half of width of circumferential weld.

Width of zone of plastic strains in the case of multipass welding is determined by pass with the largest  $q_0$ , welding parameters of which should be taken for calculation. As a rule, this is the last pass.

Checking of proposed method for calculation of ET modes of circumferential pipe welds was made using reference pipe of Kh46 strength class of Japan origin with the following parameters, namely radius  $R = 0.36$  m, wall thickness  $h = 0.0172$  m,  $\sigma_y = 440 \cdot 10^6$  Pa,  $S_w = 0.009$  m, quantity of winds of EC with portion of unit of length  $12 \cdot 10^{-3}$  kg/m is 8, total width of winding of charge being 0.14 m. Indicated mode of treatment of this pipe was elaborated in development of ET technology for Orenburg Gas Condensate Field. Considering this expression (14) takes the form:

$$n_i = 0.033 \cdot 10^{-6} \sigma_{y_i} a_i h_i / j_i R_i.$$

Taking into account that RS in reference pipe after ET were not equal zero and made 80 MPa

**Table 1.** ET modes for circumferential pipe welds

No.	Dimension-size of pipe ( $2R \times h$ ), mm	$\sigma_y$ , MPa	$n$ , winds of EC-A ( $j = 12$ g/m)	$a$ , mm	$b$ , mm
1	115×4	240	2	28	19
2	115×8	240	4	39	29
3	150×8	280	4	44	28
4	160×5	280	2	36	21
5	530×7	350	2	78	20
6	530×9	350	3	88	22
7	720×17.2	440	9.8/8	142/140	19/40
8	168×14	280	10	62	25

(results are given below) as well as considering existing experience of ET of circumferential welds, the numerical coefficient is taken equal  $0.04 \cdot 10^{-6}$  and final expression for determination of quantity of EC winds is written in the next way:

$$n_i = 0.04 \cdot 10^{-6} \sigma_{y_i} a_i h_i / j_i R_i. \quad (18)$$

Control experiments on calculation modes, given in Table 1, were carried out for validation of efficiency of proposed procedure. Table 2 shows the results of stress measurements. Measurement of stresses was carried out with the help of well-known method of fracture tensometry using strainmeter with scale interval 2  $\mu$ m. Line 7 of Table 1 shows in the numerator the modes of ET of reference pipe, calculated on developed method, and in denominator that ones on which real ET (before method development) were carried out.

Obtained experimental data indicate that ET improved stressed state not only of some sepa-

**Table 2.** Results of experimental check of calculation method

No.	Dimension-size of pipe ( $D \times h$ ), mm	Residual stresses, MPa		
		$\sigma_i$ , MPa	$\sigma_f$ , MPa	$\Delta\sigma$ , MPa
1	115×4	150	-30	180
2	160×5	200	-50	250
3	115×8	200	-20	220
4	150×8	250	0	250
5	530×7	300	50	250
6	530×9	300	50	250
7	168×14	250	0	250
8	720×17.2	440	80	360

Note.  $\sigma_i$  – initial (after welding) RS;  $\sigma_f$  – resulting after ET of RS;  $\Delta\sigma$  – value of reduction of RS (all given values of stresses relate to external pipe surface).



rately taken specimens, but on average all specimens used in given series of experiments. Besides, results of RS reduction are sufficiently close for all tested specimens, on average the RS were reduced to zero level for this group of pipes. Any of test experiments showed unallowable deviations of results, in particular, no cases of ineffective treatment from point of view of RS reduction as well as cases of excessive deformation of treated pipes were registered. Residual bending of pipes does not exceed allowable one [12, 13]. This confirms applicability of developed procedure in selection of ET modes for practical application.

1. Golikov, N.I. (2000) *Evaluation of state of welded joints in North pipelines*: Syn. of Thesis for Cand. of Techn. Sci. Degree. Yakutsk.
2. Perunov, B.V., Kushnarenko, V.M. (1983) *Corrosion prevention as a guarantee of effectiveness*. Chelyabinsk: Yuzhno-Uralskoe Knizhnoe Izd-vo.
3. Ponomaryova, I.N. (2009) Residual welding stresses in multipass welding of pipeline butts. *Svarochn. Proizvodstvo*, **1**, 7–11.
4. Petushkov, V.G. (2005) *Application of explosion in welding technique*. Kiev: Naukova Dumka.
5. Bryzgalin, A.G. (2006) *Reduction of residual welding stresses in circular welds of pipelines by using explosion treatment*. Kiev: PWI.
6. Kudinov, V.M., Petushkov, V.G., Berezina, N.V. et al. (1975) Determination of explosive charge parameters for removal of residual stresses in circular welds. *Avtomatich. Svarka*, **9**, 63–65.
7. Makhnenko, V.I. (1976) Computational methods for study of kinetics of welding stresses and strains. In: *Stress state in zones of circular pipe butts in explosion treatment*. Kiev: Naukova Dumka.
8. Timoshenko, S.P., Vojnovsky-Kriger, S. (1963) *Plates and shells*. Moscow: Gos. Izd-vo Fiz.-Mat. Lit-ry.
9. Rabotnov, Yu.N. (1962) *Strength of materials*. Moscow: Gos. Izd-vo Fiz.-Mat. Lit-ry.
10. *List of recommended commercial explosive materials, devices for explosion and control*. Moscow: Nedra.
11. Kasatkin, B.S., Prokhorenko, V.M., Chertov, I.M. (1987) *Stresses and strains in welding*. Kiev: Vyshcha Shkola.
12. *GOST 20295-74*. Steel welded pipes for main gas-and-oil pipelines.
13. *SNiP 2.05.06-85*. Main pipelines. Moscow: Goskomstroj.

Received 01.04.2013



# WELDING OF STEEL STUDS TO ALUMINUM SHEETS

D.M. KALEKO

E.O. Paton Electric Welding Institute, NASU  
11 Bozhenko Str., 03680, Kiev, Ukraine. E-mail: office@paton.kiev.ua

Technology for welding of steel studs to aluminum sheets and structure of stud being welded were developed considering economic and environmental appropriateness of replacement of steel structures by aluminum alloys in transport machine-building and construction and related with this necessity in steel fasteners providing required loading. It is shown that application for this of a heat barrier in a form of evaporated zinc coating at end face of the stud reduces possibility of formation of brittle intermetallic compounds in a transfer layer between steel stud and aluminum sheet, and increased surface of welding provides for uniform strength of joint with steel stud. 10 Ref., 6 Figures.

**Keywords:** *steel and aluminum welding, stud welding, heat barriers, coatings*

Replacement of steel by aluminum alloys, in particular in transport machine-building and during finishing works in construction of buildings and structures, finds wide application in recent years. It allows reducing mass and increasing corrosion resistance and related with this economic and environmental advantages of products. This, naturally, provokes a problem of fastening aluminum sheets to bearing structure or using surfaces of aluminum bodies for hanging devices and equipment, pipelines and wires on them. It is solved, as a rule, using drilling of the holes weakening aluminum body, or welding on of the fasteners without breaking structure integrity.

One of the widespread methods of fastener joining to parts of different designation is mechanized stud welding [1]. However, existing methods are mainly designed for joining of similar materials.

Studs for mass application, including from aluminum alloys, are manufactured using method of cold upsetting in accordance with ISO 13918. Selection of aluminum alloys is limited by aluminum Al 99.5 and alloy AlMg3 (AMg3) under the same standard. Considering material strength the practical application of studs from aluminum alloys suggests insignificant mass of element of the part being hanged.

Fastener loading can be increased applying steel studs instead of aluminum ones. However, application of standard steel studs and methods used for their welding to aluminum products is impossible due to known problem of welding zone embrittlement by insoluble iron and aluminum compounds.

Real methods of steel to aluminum joining using fusion appeared in recent years [2] which allow obtaining satisfactory result at reduction of heat input mainly into the steel part during the process.

Earlier work [3] showed that welding of steel and aluminum studs to the sheets from the same materials at their dissimilar combination using capacitor discharge provides the possibility of obtaining of satisfactory joining due to short time of the process. Regardless specific quantity of intermetallic phase in the joint zone, it does not reduce joint quality since it is not uniform layer, but only inclusion into a soft aluminum matrix.

Regardless number of advantages caused by short time of the discharge in capacitor-discharge stud welding, the short time of the process requires relatively high accuracy in manufacture of studs and performance of works. In particular, high surface cleanness and preservation of normality of axis of manual tool-welding gun-joint plane of high accuracy (approximately  $\pm 2^\circ$  for M6 stud) are necessary. Considering geometry, the latter requirement rises with increase of stud diameter and, respectively, diameter of shoulder on its end being welded. This condition played an important role in selection of method of stud welding based on reasons mentioned above.

Method of stud welding using short cycle direct-current arc is less demanding on welding procedure and is comparable on diameters of studs being welded by this method with capacitor-discharge welding. Welding of studs on oily or oxidized surface at allowable parallel misalignment of surfaces up to  $10^\circ$  is successfully performed due to significant increase of welding time (from units to tens of milliseconds). These peculiarities determined application of stud welding using short cycle, for example, in automobile industry. However, application of this method is



limited by sheet thickness (more than 1/4 of stud diameter) or problems in welding of dissimilar materials, including during welding of steel studs to aluminum sheets.

Thus, necessity in development of technology for joining of these metals by method of short-cycle stud welding considering demands of industry and building has drawn. At that, the task is divided on two parts, i.e. propose a technology, allowing eliminating or making difficult formation of iron-aluminum intermetallics in the joint metal, and suggest a shape of steel stud, increasing strength of the joint up to the requirements of ISO 14555 standard (the joint should withstand stud bending for angle not less than 60°).

As it was mentioned above, formation of intermetallic compounds of iron and aluminum in fusion welding, to which stud welding is related, can be prevented by means of reduction of time of interaction of these metals and providing of allowable partial content of liquid phase before process finishing. The most favorable conditions are at minimum content of iron in the melt and high speed of cooling promoting very low mutual diffusion of the elements. The second condition can be well fulfilled in short-cycle stud welding since heat input into parts being welded does not exceed 1 kJ and it is rejected into the cold parts.

Stud with barrier coating which is used to slow down the melting of stud material (in the discussed process — steel) by means of absorption of arc energy heating the surfaces being welded was proposed for fulfillment of the first condition.

Two variants of widely applied coatings, i.e. zinc and chromium having different heat properties were chosen for investigation. The temperature of zinc evaporation (906.2 °C) is lower than the steel melting temperature and that of chromium is higher (2672 °C), but the latter has

significantly higher evaporation temperature than zinc (~6.6 and ~1.7 kJ/g, respectively). Such a choice allowed comparing the role of thermo-physical parameters, i.e. temperature and heat of evaporation, in slowing down the melting of stud metal. The latter was evaluated on microstructures of welded joints.

The first series of experiments was carried out with standard (in accordance with ISO 13918) steel studs M6 without coating, with zinc and chromium coatings of 20 µm thickness. Short-cycle welding to A0 sheet of 3 mm thickness was performed on GLV 650 unit at current approximately 600 A (not regulated) and alternating values of welding time and arc length determining not only arc voltage, but speed of stud deepening into liquid metal pool on the surface of sheet in resistance arc welding with spring upsetting. Welding was carried out using argon shielding of joining zone at 15 l/min consumption of gas for all experiments.

Influence of stud coating on arc characteristics was studied using digital oscillograph C9-8. Analysis of oscillograms showed that application of zinc-coated studs provides some increase of arc voltage in comparison with welding of uncoated studs due to intensive evaporation of zinc coating and respective increase of pressure in a short arc gap.

As can be seen from Figure 1, joints with studs without coating have the lowest strength and zinc-coated studs have the highest one at optimum time of welding. Chromium coating does not provide such significant effect as zinc coating due to higher temperature of evaporation than of zinc. Therefore, the base metal of chromium-coated stud is melted before coating evaporation that causes increase of volume of liquid iron phase in the joint in comparison with welding of zinc-coated studs. At the same time, if welding duration is increased above the optimum, the strength of joints with chromium-coated studs is higher than in uncoated ones since part of the heat energy is consumed for chromium evaporation and lower in zinc-coated due to that the zinc coating completely evaporates during this time making bare steel core of the stud and resulting in balancing of strength of joints of zinc-coated and uncoated stud with aluminum sheet.

If duration of heating is less than the optimum one, the role of coating becomes insignificant due to insufficient evaporation and, respectively, reduction of cooling effect of steel base of the stud.

Figure 2, representing microstructures of joints obtained with steel stud M6 of standard shape and different coatings, shows well a heat-

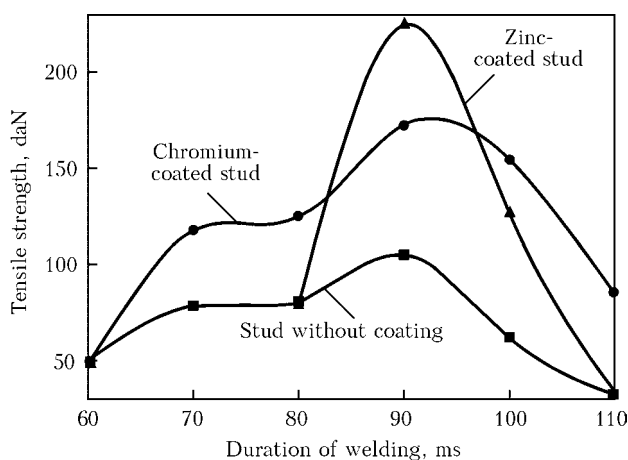


**Figure 1.** Dependence of strength of welded joints on coating composition and duration of welding

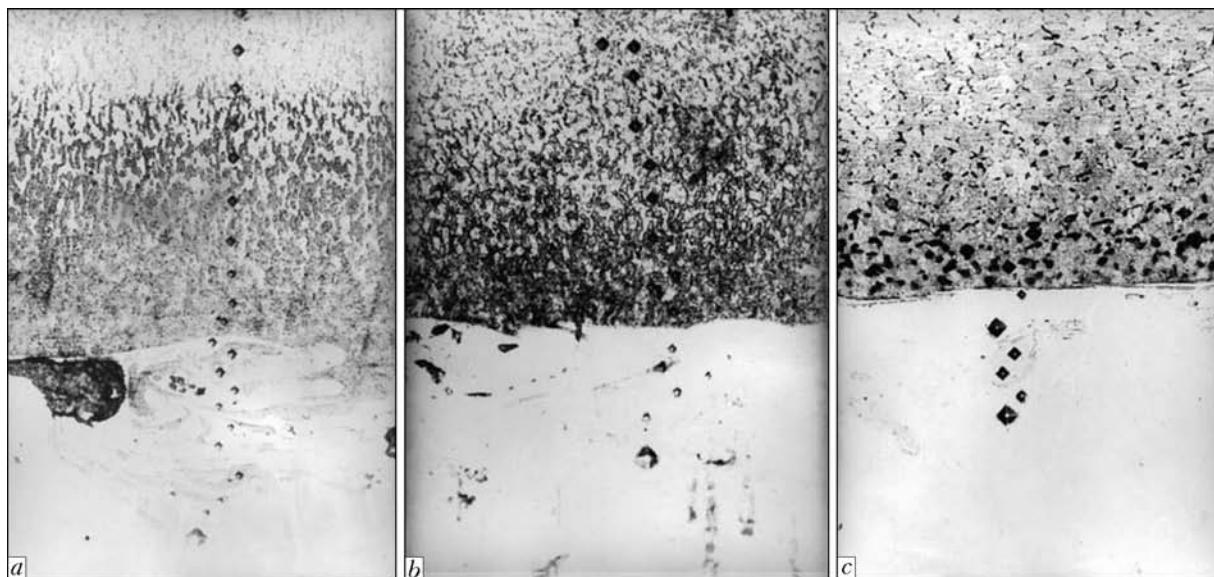


**Figure 2.** Microstructures ( $\times 200$ ) of joining zone of steel studs M6 to aluminum sheet of 3 mm thickness with different coatings before welding: *a* – without coating; *b* – chromium coating; *c* – zinc coating

affected zone (HAZ) of the arc reducing at transfer from uncoated stud to chromium-coated and further to zinc-coated one.

Microhardness measured at 50 g loading along the line normal to joint surface (Figure 3) shows that maximum registered hardness is two times lower the hardness of  $\text{FeAl}_3$  intermetallic (9600 MPa [5]) in all cases.

Thus, coating on surface of stud being welded allows controlling heat emission in the stud material and obtaining joint of steel stud to aluminum sheet having no brittle interface. However, strength of such a joint does not exceed strength of aluminum alloy (failure stress achieved 800 MPa in our experiments).

It should be noted that heat regulating coatings were used earlier as well, for example, aluminum coatings in niobium to zirconium welding [6]. However, at that the coating plays a role of heat sink cooling HAZ. While fusible electroplated coatings (zinc, silver) in steel to aluminum fusion welding were used for improvement of steel wetting by aluminum [7].

Since, as it is known, strength of the joint depends on its area (at other things being equal) then providing of uniform strength of the joint in steel stud requires increase in diameter of surface being welded proportionally to relation of tensile strength limits of steel and aluminum. Assuming that strength of steel 08, from which studs are mainly manufactured, is 325 MPa [8] and strength of aluminum alloy AD-60 being 60 MPa [9], a coefficient of increase in diameter of standard shoulder will be 2.3. Considering that a bead increasing area of the joint is formed on sheet around the shoulder as a result of stud upsetting into the molten metal pool, the calcu-

lated coefficient of shoulder diameter was reduced up to 2.1. Thus, diameter of the shoulder should be increased from 7.5 to 16 mm for obtaining of the joint not inferior to strength to steel stud M6, which is welded to aluminum sheet.

Welding of increased diameter studs to fusible aluminum is reasonable at arc rotation in magnetic field [10] that reduces density of heat emission on the sheet and, respectively, danger of its burning through. For this, the studs with different shape of surface being welded were manufactured (Figure 4).

Thickness of zinc coating meeting the requirement of minimum but necessary for melting (for elimination of inevitable deviations of technological conditions from ideal ones which were mentioned at the beginning of work) steel base of the stud was calculated with the help of spe-

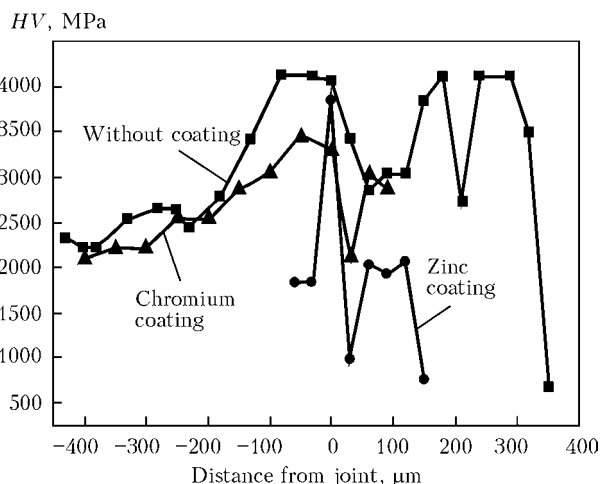


**Figure 3.** Distribution of microhardness normal to plane of joining of steel stud to aluminum sheet

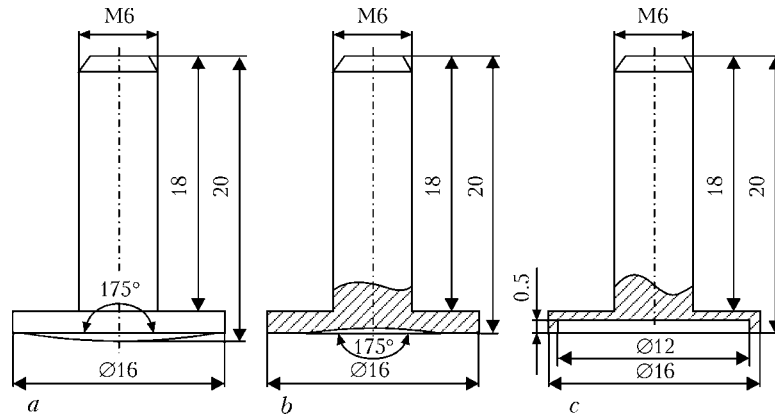


Figure 4. Sketches (a-c) of steel studs for welding to aluminum sheet using short-cycle welding with rotating arc

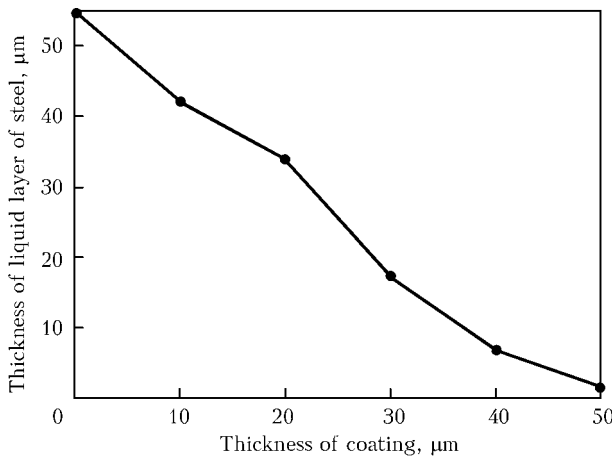


Figure 5. Calculated dependence of thickness of steel molten layer at the end of M6 stud of standard shape on thickness of deposited zinc coating (duration of welding 40 ms, welding current 600 A)

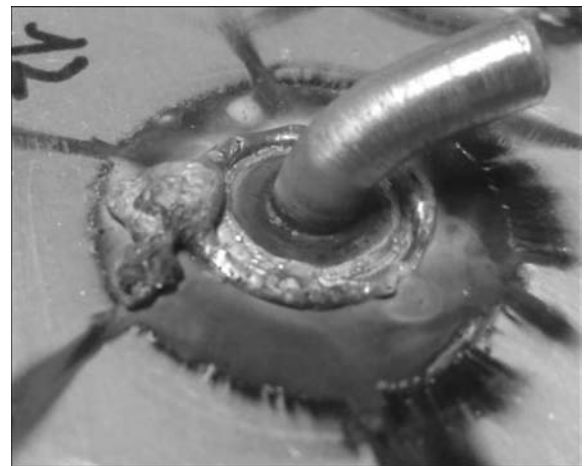


Figure 6. Joining of steel stud of 6 mm diameter to aluminum sheet of 3 mm thickness after impact bending testing on ISO 14555

cially developed Fortran-program. Calculation was carried out only for the zinc coating since no data about dependence of thermal-physical characteristics in liquid state on temperature were found for other metals except for zinc.

Figure 5 shows the effect of thickness of the zinc coating on thickness of molten metal of the stud body. It is obvious that increase of welding duration related to application of the studs with increased diameter of surface being joined should promote rise of coating thickness.

Experiments on welding of the studs, shown on Figure 4, were carried out on VKM-16i apparatus of «Soyer» company, thickness of zinc coating of the studs made 20, 30, and 50  $\mu\text{m}$ .

Insufficient filling of gap under the shoulder was observed in the joints with electroplated studs which have strip button that resulted in weak strength of the joint. The joint of satisfactory quality (Figure 6) was obtained at 970 A current, 22 V arc voltage, 0.2 s pulse duration, 1 A current of magnetic coil and 1.5 mm arc length (height of stud lifting).

## Conclusions

1. Minimization of formation of brittle transfer layer, consisting of intermetallic iron and aluminum compounds, is the main condition for obtaining of strong joint of steel stud with aluminum sheet necessary for automotive and shipbuilding as well as construction industries. Methods used at present time for joining of aluminum and steel parts are based on limitation of energy of heating of steel part and, respectively, reduction of iron content in liquid aluminum pool.

2. The method was developed for regulation of welding heating of the parts by means of deposition of metal layer having evaporation temperature lower than the melting temperature of base metal over surface being heated. Such materials for the steel stud can be magnesium, zinc, cadmium, tellurium as well as some alloys of these metals. Zinc has an advantage from economical point of view.

3. Obtaining of equal on strength joint with steel stud requires increase of diameter of stud surface being welded up to the size not less than 2.5 of diameter of main body of the stud. Such



studs should be welded using short-cycle welding method with magnetic rotation of the arc that allows reducing depth of penetration of aluminium sheet.

4. New shape of the stud was developed due to which joints corresponding to the indexes of satisfactory strength on ISO 14555 were obtained.

*The author expresses his sincere appreciation to «Soyer» company for help in performance of final part of the experiments.*

1. Kaleko, D.M. (1999) Arc-contact butt stud and threaded-rived nut welding. *Svarshchik*, **4**, 7–8.
2. Kaleko, D.M. (2012) Modern methods of welding aluminium alloys to steels (Review). *The Paton Welding J.*, **10**, 27–33.
3. Kaleko, D.M., Moravsky, V.E., Chvertko, N.A. (1984) *Capacitor-discharge percussion welding*. Kiev: Naukova Dumka.
4. Paton, B.E., Kaleko, D.M. *Stud for butt welding*. Pat. 100452 Ukraine. Int. Cl. B23k 9/20.
5. Vol, A.E. (1959) *Structure and properties of binary metallic systems*. Moscow: Fizmatgiz.
6. Nerodenko, M.M., Goncharov, A.B., Kirilyuk, V.F. et al. (1987) Application of heat-removing aluminium coatings in welding of zirconium alloy with 2.5 % niobium. *Avtomatich. Svarka*, **2**, 28–31.
7. Ryabov, V.F. (1983) *Welding of aluminium and its alloys with other metals*. Kiev: Naukova Dumka.
8. Sorokin, V.G., Volosinkova, A.V., Vyatkin, S.A. et al. (1989) *Reference book of steel and alloy grades*. Moscow: Mashinostroenie.
9. Kolachev, B.A., Livanov, V.A., Elagin, V.I. (1972) *Metals science and heat treatment of nonferrous metals and alloys*. Moscow: Metallurgiya.
10. Kaleko, D.M., Byshovets, V.N. *Method of arc-contact T welding and device for its realization*. Pat. 25037 Ukraine. Int. Cl. B23 k 9/20. Publ. 25.12.98.

Received 20.05.2013



# WET UNDERWATER WELDING OF LOW-ALLOY STEELS OF INCREASED STRENGTH

S.Yu. MAKSIMOV and I.V. LYAKHOVAYA

E.O. Paton Electric Welding Institute, NASU

11 Bozhenko Str., 03680, Kiev, Ukraine. E-mail: office@paton.kiev.ua

Conditions of welding directly in water environment limit greatly the feasibility of producing quality welded joints of low-alloy steels of increased strength. This is due to the fact that mechanical properties of weld metal are inferior to properties of base metal, and the initiation of cold cracks in the heat-affected zone (HAZ) is possible. Investigation of weld metal structure showed that depending on degree of alloying the weld areas, adjacent to the fusion line, can have different structures of transient compositions. The obtained results allowed working out requirements to the deposited metal composition to prevent the formation in HAZ of a brittle interlayer with an increased hardness, which is a place of initiation of cold cracks. Welded joints of steel 17G1S of 14 and 40 mm thickness, made under water using developed electrodes with rods of high-alloy steel, provide weld metal mechanical properties, corresponding to the requirements of class A of Specification AWS/ANSI D3.6 on underwater welding, and also resistance of welded joint against crack formation. Electrodes can be used in repair and construction of special-purpose metal structures, made of low-alloy steels of increased strength of up to 40 mm thickness. 8 Ref., 6 Figures, 1 Table.

**Keywords:** *wet underwater welding, low-alloy steels of increased strength, weld, structure, chemical composition, cracks, mechanical properties*

Wet welding is very attractive due to efficiency and simplicity in fulfillment [1, 2]. However, it encounters significant difficulties of a metallurgical nature. The hydrogen-oxygen atmosphere of a vapor-gas bubble contributes to oxidation of alloying elements and saturation of weld pool metal with hydrogen, and the accelerated cooling by surrounding water leads to its fixation in weld metal and formation of hardening structures in HAZ metal [3]. As a result, a risk of formation of cold cracks is greatly increased, in particular in welding of increased strength low-alloy steels of 17G1S or X60 type. The problem can be solved by applying electrode materials, providing the formation of austenitic structure of weld metal and, thus, decreasing the amount of hydrogen, diffusing into HAZ [4].

The preliminary experiments on welding with a flux-cored wire, having a sheath of nickel strip, confirmed, on the one hand, the feasibility of producing of quality welded joint on X60 type low-alloy steel of increased strength (without cracks in HAZ metal), and, on the other hand, revealed the difficulty in guaranteeing the required level of mechanical properties of weld metal. A large amount of hydrogen increases the weld metal resistance to plastic deformation and decreases the limiting characteristics of its ductility.

Such result is correlated with a known susceptibility of nickel to hydrogen embrittlement [6]. This phenomenon becomes more noticeable in the presence of oxygen as an impurity and increased rate of cooling [6] that is typical of the underwater welding conditions. In the author's opinion the presence of oxygen in nickel facilitates the intergranular fracture which occurs in this case at lower concentrations of hydrogen, as the hydrogen pressure is added by pressure of water vapors, forming in reduction of nickel oxides. Cracks, initiating along the grain boundaries, lead to fracture of specimens at tensile tests even at a negligible deformation.

Coming from the above-mentioned, the results of study of hydrogen brittleness of nickel alloys with iron and chromium represent interest. Authors of work [6] found that hydrogen brittleness of nickel alloys with iron and chromium is decreased with increase in content of the latter. They consider that this nature of effect of chemical composition is due to the change of electron state of alloys. Therefore, in our opinion, the application of electrode materials for underwater welding, providing the weld metal on the base of Fe-Ni-Cr alloying, can be rather successful. However, in one's time the electrodes with a core of stainless steel [7] were recognized as not promising because of a risk of crack formation in weld metal near the fusion line that was explained by dilution of electrode metal with base metal. Nevertheless, the authors of work [8] inform about the development of electrodes with a rod of Sv-

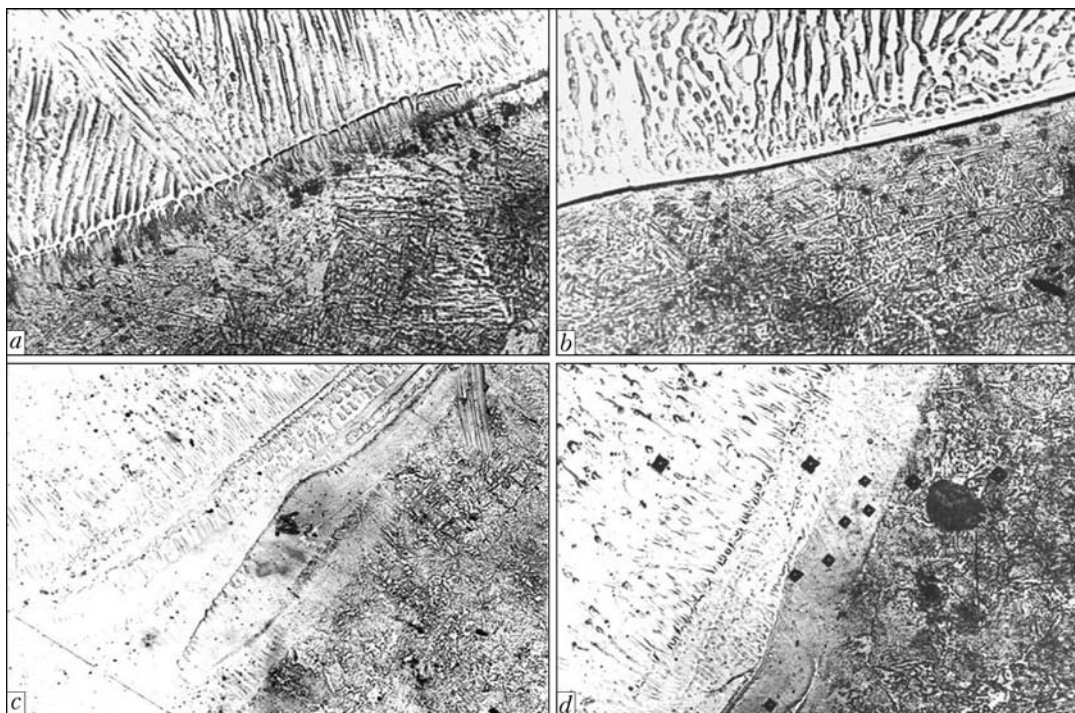


**Figure 1.** Microstructures ( $\times 650$ ) of fusion zone areas with a feathery structure (*a*), with distinctly expressed fusion line (*b*), with flowing-in of base metal (*c*) and with a parallel boundary (*d*)

10Kh16N25AM6 wire for underwater welding of high-strength steels, providing the quality welded joints with high mechanical properties and resistance against cold crack formation.

The aim of the present work was to study the structure, chemical composition and mechanical properties of welded joints of steel 17G1S of 14 and 40 mm thickness, made under water using electrodes with a rod of high-alloy steel, and to select the weld metal composition providing its mechanical properties at the level of base metal properties and welded joint resistance against the crack formation.

Taking into account the possible dilution of weld metal with base metal at the level of 40 %, the wires with chromium equivalent  $Cr_{eq} \cong 21-33$  % and nickel equivalent  $Ni_{eq} \cong 19-32$  % were selected as electrode rods for the preliminary experiments. Experimental electrodes of 4 mm diameter with rutile-fluorite coating were manufactured from these rods. Welding of butt specimens was made by a diver-welder in the laboratory basin at 1 m depth using the following conditions:  $I_w = 140-160$  A,  $U_a = 26-28$  V, direct current of reversed polarity. As a base metal the plates of 14 and 40 mm thickness of 17G1S type steel were used (wt. %: 0.18 C, 0.36 Si, 1.67 Mn).

It was found by the spectral analysis that the value  $Cr_{eq}$  in root welds was changed in the ranges of 12.0–15.5 %, and  $Ni_{eq} - 10.8-22.7$  %. According to obtained compositions, metal of all the welds in the Schaeffler's structural diagram is highly-alloyed Cr–Ni austenite. However, the

weld areas, adjacent to fusion line, represent a system of structures of transient compositions. Among them, austenite-martensite and martensite interlayers are of interest and hazard due to their increased hardness and brittleness and possibility of initiation of cracks in them during welding or under the service conditions. Width and length of these interlayers, as well as values of their hardness depend, on the one hand, on the degree of alloying of weld metals (margin of austenite content), and, on the other hand, on the degree of base metal penetration, i.e. on change of weld composition in dilution of base (pearlitic) and deposited (austenitic) metal.

The metallographic examinations revealed the variety of structures of a narrow zone of weld metal, adjacent to fusion line. Conditionally it is possible to distinguish four types of structures:

- so-called feathery structure, formed by weld metal, flowed-in between the fused grains of the base metal (Figure 1, *a*);
- regions with distinctly expressed fusion line. They are typical by the transition zone absence. Weld metal structure is radically differed from that of base metal (Figure 1, *b*);
- so-called flows-in («tongues») (Figure 1, *c*) of base non-fused metal, flowed into the weld and often characterized also by the increased hardness. The appearance of these structures is due to stirring of base metal under the direct influence by the welding arc. The less stable the welding condition, the larger fraction of these inclusions can be;

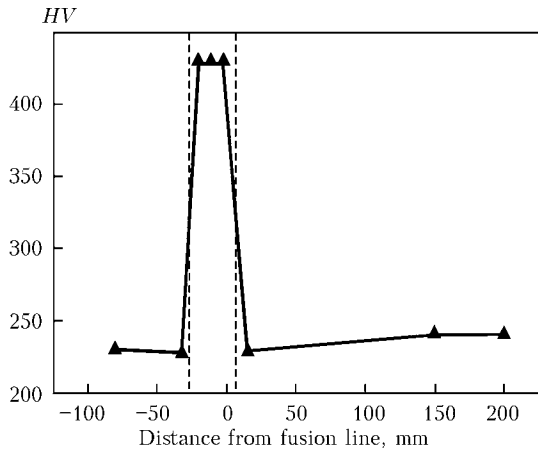


Figure 2. Distribution of microhardness in the presence of martensitic interlayer

- structure with the presence of so-called parallel boundary on the weld metal side (Figure 1, d) when a thin interlayer of increased hardness is arranged between the base and weld metal. Approximate diagram of distribution of microhardness in the presence of such interlayer is given in Figure 2.

Relations between the chemical composition of weld metal, weld arrangement in multilayer joint and structure type were not found. The most hazardous is the structure with a parallel boundary, in which the cold crack formation is possible at high hardness. This is typical of root welds. In final welds the hardness of these structures is significantly lower even at smaller amount of alloying elements.

To define by numerical method the conditions of prevention of brittle interlayer formation in weld metal, the effect of alloying degree per a fraction of forming martensite was investigated. For this purpose, the weld metal alloying with nickel in the ranges of 12–25 % and chromium in the range of 11–15 % was imitated. Results of

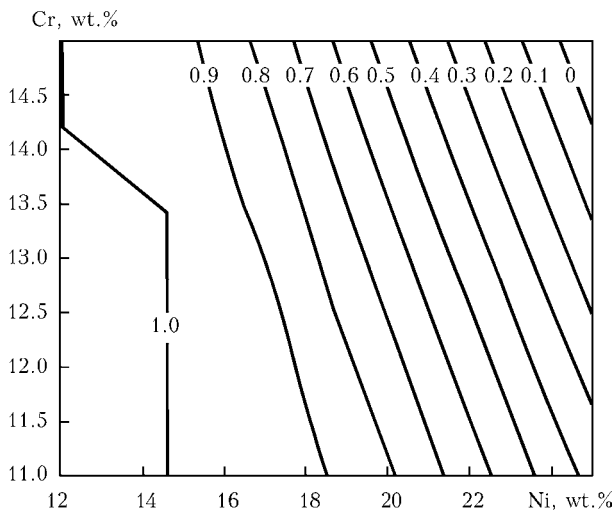


Figure 3. Effect of alloying of austenitic weld metal on martensite fraction in interlayer

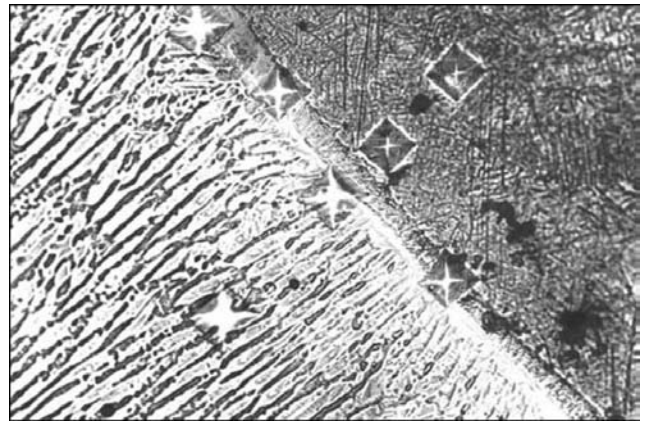


Figure 4. Parallel boundary with interlayer of low hardness (x650)

calculations (Figure 3) showed that to minimize a fraction of martensite, which is formed in weld metal interlayer near the fusion line during underwater welding, the nickel and chromium equivalents of the latter should lie above the line in state diagram, parallel to the line dividing the regions with austenitic and austenitic-martensitic structure, and passing through a point with coordinates  $Ni_{eq} = 24.2\%$  and  $Cr_{eq} = 14.3\%$ . Under these conditions the interlayer hardness is at the level of hardness of the surrounding metal (Figure 4).

Coming from the set requirements to the chemical composition, the electrodes with rods of wire Sv-10Kh16N25AM6 and additional alloying by coating were developed. To determine the

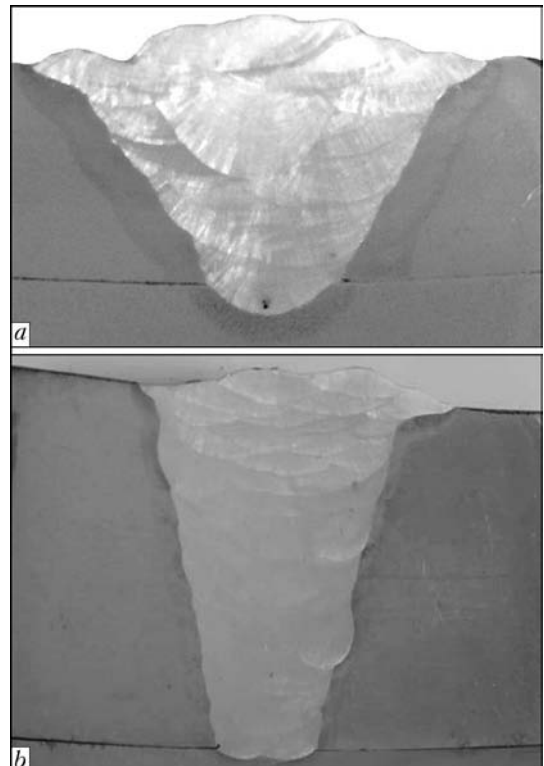


Figure 5. Macrosections of welded joints of 14 (a) and 40 mm (b) thickness

Mechanical properties of weld metal and base metal

Material	$\sigma_{0.2}$ , MPa	$\sigma_{ult}$ , MPa	$\delta$ , %	$\psi$ , %	KCV <sub>-20</sub> , J/cm <sup>2</sup>	Bending angle, deg, $R = 2t$
Weld, 14 mm	≥410	≥620	≥32	≥38	≥108	180
Weld, 40 mm	≥460	≥600	≥29	≥47	≥105	180
Steel 17G1S	340	510	23	–	–	–

mechanical properties, the butt specimens of 14 and 40 mm thickness with V-shaped grooving were welded. Tests were conducted in accordance with requirements of class A of Specification AWS/ANSI D3.6 on underwater welding. The obtained results are presented in Table. Macrosections, cut out from welded specimens, are given in Figure 5.

Metallographic examinations of macrosections of Tekken sample, made by the developed electrodes, showed the absence of cracks in welded joint (Figure 6).

Thus, the application of developed electrodes with Cr–Ni–Mn system of alloying guarantees producing of underwater welded joints of increased strength low-alloy steels without cracks in HAZ metal and with mechanical properties meeting the requirements of class A of Specification AWS/ANSI D3.6 on underwater welding.

In conclusion, as a result of carried out investigations it was found during wet underwater welding of low-alloy steels of increased strength that:

- brittle interlayers of increased hardness (up to 4500 MPa), susceptible to cold cracking are formed near the fusion line on the side of weld metal as a result of dilution with base metal;
- to prevent crack formation the required and sufficient range of alloying by chromium together with nickel should be determined by the following values:  $Cr_{eq} = 17.5\text{--}23\%$ ,  $Ni_{eq} = 18\text{--}28\%$ ;
- mechanical properties of welded joints of 14 and 40 mm thickness, made by the developed electrodes, meet the requirements of class A of Specification AWS/ANSI D3.6 on underwater welding.

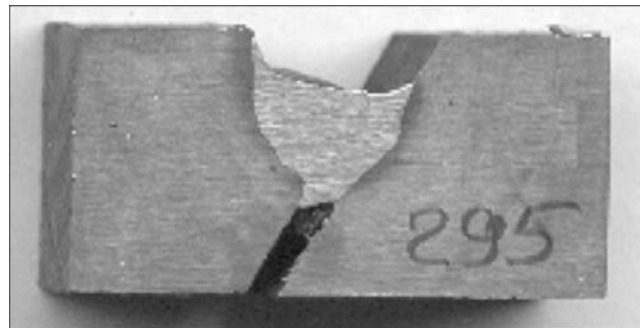


Figure 6. Macrosection of technological sample Tekken

1. McKeown, D., Abson, D. (2006) Wet welding repairs. *Shipping World and Shipbuilder*, 207(5), 24–26, 28.
2. Rowe, M., Liu, S. (2001) Recent developments in underwater wet welding. *Sci. and Technology of Welding & Joining*, 6(6), 387–396.
3. Dariusz, F., Grzegorz, R. (2011) Effect of shielded-electrode wet welding conditions on diffusion hydrogen content in deposited metal. *Welding International*, 25(3), 166–171.
4. Bartzsch, J., Daniel, S., Bouaifi, B. et al. (1997) Arc welding with austenitic filler metal for underwater application. In: *Proc. of 16th Intern. Conf. on Offshore Mechanics and Arctic Engin. – OMAE 1997* (Yokohama, Japan, 13–17 April, 1997).
5. Maksimov, S.Yu., Savich, I.M., Zakharov, S.M. et al. (2003) Structure and properties of the metal deposited under the water by flux-cored wire with a nickel sheath. *The Paton Welding J.*, 4, 18–21.
6. Moroz, L.S., Chechulin, B.B. (1967) *Hydrogen brittleness of metals*. Moscow: Metallurgiya.
7. Bailey, N. (1991) Welding under water – a metallurgical appraisal. In: *Proc. of 1st Int. Offshore and Polar Engin. Conf.* (Edinburg, UK, 11–16 August, 1991).
8. Maslennikov, P.S., Russo, V.L. (2000) New electrodes for underwater welding. *Svarochn. Proizvodstvo*, 11, 26–27.

Received 28.05.2013



# ELECTROSLAG SURFACING OF PARTS, MADE OF HIGH-CHROME CAST IRON, USING CAST IRON SHOT

Yu.M. KUSKOV, I.L. BOGAJCHUK, Ya.P. CHERNYAK and A.I. EVDOKIMOV

E.O. Paton Electric Welding Institute, NASU

11 Bozhenko Str., 03680, Kiev, Ukraine. E-mail: office@paton.kiev.ua

A lot of parts, used in machine building, metallurgy, mining and other industry branches and subjected to different types of wear in service, are manufactured of high-chrome cast irons. After base service the worn-out parts of this type are not subjected to restoration in practice by the known methods of arc surfacing. The present work deals with the possibility of restoration of worn-out parts, manufactured of high-chrome cast iron, using the technology of electroslag surfacing, developed at the E.O. Paton Electric Welding Institute. The peculiar feature of this technology is the application of a special device in surfacing, namely a current-carrying mould, allowing surfacing using a discrete filler material (shot). Here, the capability of «soft» and uniform heating of surface and layer being deposited by a slag, typical of various known methods of electroslag surfacing, the present technology provides a feasibility to produce a fine-grain deposited metal. This contributes to restoration of parts providing high service characteristics. Using the present technology, the experimental restoration electroslag surfacing of high-chrome cast iron layer on worn-out zones of plates of chamber of shotblast unit of «Bduhuis» company and blades of shotblast unit of «Carlo Banfi» company, made of high-chrome cast iron, were carried out. As a surfacing filler material the shot was used of the following chemical composition, wt.%: 2.5 C, 26.2 Cr, 0.7 Si, 0.7 Mn, 1.3 Ni, 0.9 Mo. It was found that the technology of electroslag surfacing using discrete surfacing materials in the form of shot of high-chrome cast iron allows manufacturing quality bimetal products with an optimum combination of deposited metal of high-hard carbides and ductile matrix in the structure. 5 Ref., 5 Figures.

**Keywords:** *high-chrome cast iron, electroslag surfacing, surfacing shot, deposited metal*

As to their structure the high-chrome cast-irons (15–30 % Cr) are the materials with an increased resistance to different kinds of wear [1–3]. As the abrasive-resistant materials they found the widest spreading in the machine building, metallurgy, mining industry, in particular at ore-dressing factories.

The advantage of these materials, due to the presence of a large amount of high-hard chromium carbides ( $HV \approx 14.5\text{--}16.0$  GPa) in the structure, is also a serious drawback at the same time. The latter is connected with the fact that it is almost impossible to repair the products, manufactured of high-chrome cast irons, after their coming out of service. In particular, the known method of repair of parts using arc surfacing is not acceptable in this case, because it is necessary to apply a complicated technology for its realization (heating above 600–700 °C, strict keeping of rate of temperatures decreasing both in surfacing and also in next cooling of the deposited product), nevertheless not guaranteeing the prevention of crack initiation both during

surfacing and also after it. As a result, these non-repairable products, in spite of their high cost, had to be sent to remelting in the form of production wastes.

The present work considers the method of restoration of this type of parts using the technology of electroslag surfacing (ESS). The main distinguishing feature of this technology from the arc technology is the absence of a local heating of surface being deposited. Therefore, no high gradients of temperature are occurred in different zones of the deposited metal and, respectively, high thermal stresses, connected with them, leading to the appearance of cracks both in base and also in deposited metals. The another feature of the technology considered is the application of discrete surfacing material, namely a shot. As the experience of application of high-chrome cast iron shot showed, the present technology in ESS of mill rolls, made of low-alloy white cast irons or high-strength ones allows producing the quality products of a high serviceability [4]. The cause of producing of deposited metal with high service characteristics (strength, wear resistance, shock-resistance, resistance to crack initiation both at normal and also increased temperatures, and also

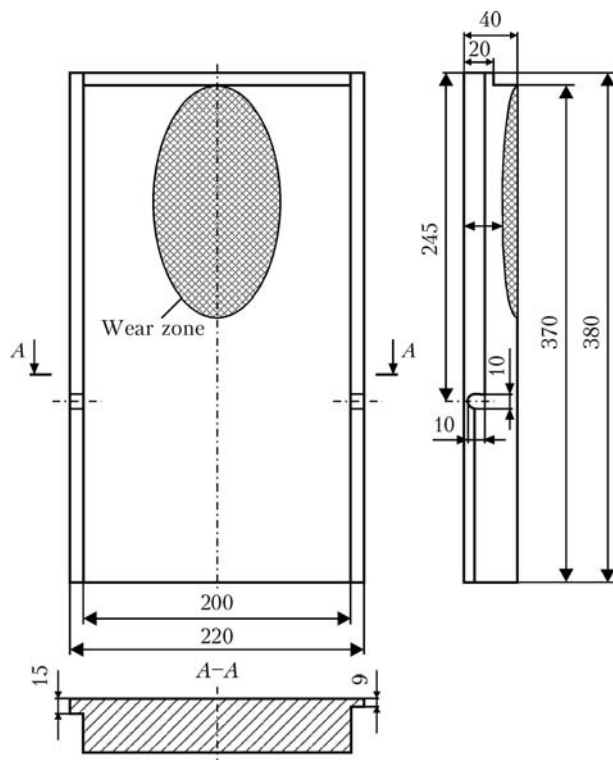


**Figure 1.** Scheme of upper plate of chamber of shotblast unit of «Bduhuis» company with a zone of abrasive wear

at thermal cycling) is the formation of a fine-grain metal in crystallization [5], having the matrix of increased ductility alongside with hard components (carbides). In other words, the present technology of surfacing allows producing a working layer in the form of a natural composite metal.

ESS was made of worn-out zones of plates of a chamber of shotblast unit of «Bduhuis» company (Figure 1) and blades of shotblast unit of «Carlo Banfi» company, manufactured of the high-chrome cast iron. As a surfacing filler material, the shot of OJSC «Torezhardalloy» was used, having the following chemical composition, wt.%: 2.5 C, 26.2 Cr, 0.7 Si, 0.7 Mn, 1.3 Ni, 0.9 Mo.

Specimens were cut out from deposited parts to evaluate the quality of deposited metal and carry out the metallographic examinations. It was found as a result of examinations of macrosections, that there were no pores, cracks and other defects in the deposited metal (layer thickness was 15–20 mm).

Metallographic examinations were made using microscope «Neophot-32». The digital image of microstructures was obtained by photcamera «Olympus C 5050». Hardness by Vickers was measured in microhardness meter M-400 of LECO company at 100 g load.

Microstructure of the deposited metal in surface layer of the specimen consists of chromium

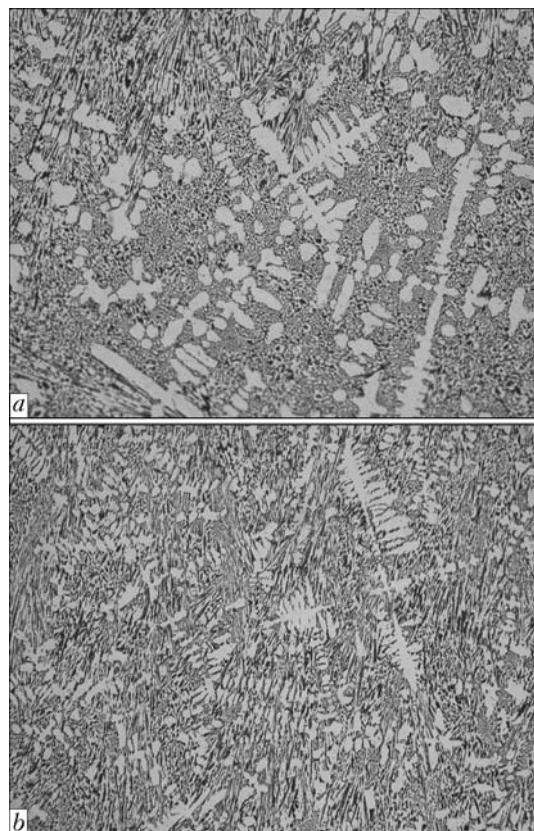


**Figure 2.** Microstructure ( $\times 125$ ) of deposited high-chrome cast iron in a specimen surface layer (a) and in the middle part of deposited layer (b)

carbides arranged fan-like in the form of plates of a lancet shape and carbides, having hexagonal faceting with a distinct boundary of mating with a matrix, as well as a carbide eutectics and austenite in the form of dendrites (Figure 2, a). Microhardness of austenite in this zone  $HV1$  is 2850–3090 MPa.

Metal in the middle part in height of the deposited metal is characterized by the presence of fine-dispersed carbides. In this zone the size of austenite dendrites is decreased, and the degree of their branching is increased (Figure 2, b). Microhardness of austenite zone  $HV1$  is also in-

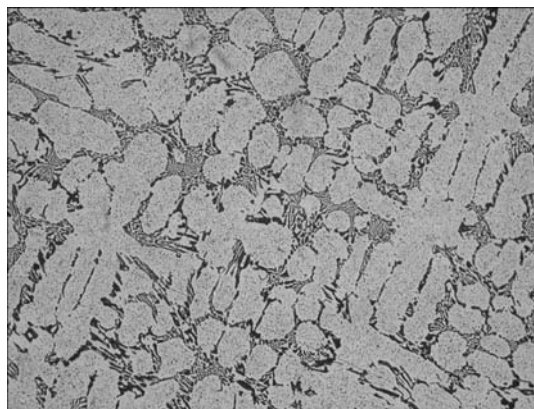


**Figure 3.** Microstructure ( $\times 125$ ) of high-chrome cast iron (base metal) at some distance from fusion zone

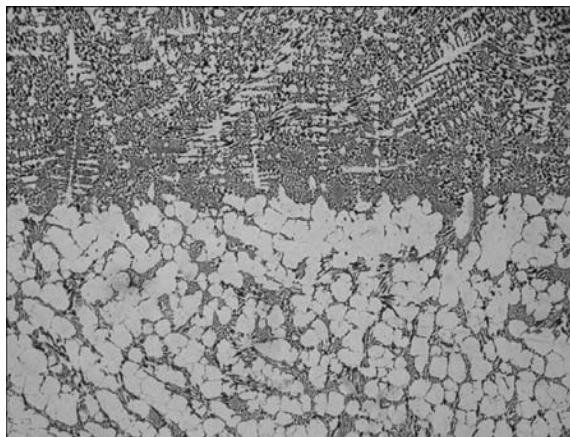


**Figure 4.** Microstructure ( $\times 100$ ) of fusion zone of high-chrome-cast irons

creased to 3830 MPa. The deposited metal has a typical fine-grained structure (Figure 2, *b*) as the application of filler particles in surfacing promotes the formation of local zones of crystallization in a molten metal.

The structure of base metal near the fusion zone is differed from the structure of the deposited metal. First of all it is cellular and consists of an austenitic matrix of hardness  $HV_1$ , equal to 3510–3830 MPa and precipitations of carbide eutectics along the boundaries of cells. The mean diameter of the cells is 25–44  $\mu\text{m}$ . Fine-dispersed precipitations of carbides are observed in the austenitic matrix (Figure 3). Microhardness  $HV_1$  of austenite with fine-dispersed precipitations of carbides is 6060–6420 MPa. Ratio of sizes of structure components in the deposited and base metal are well seen in Figure 4, where their fusion zone is presented. The width of this zone is rather large, i.e. 1400–1800  $\mu\text{m}$ .

One of the indices, characterizing the metal resistance against the abrasive wear, is its hardness. Therefore, hardness ( $HRC$ ) of the deposited specimen was measured in its height: from the base metal up to the deposited layer surface (Figure 5).

Maximum hardness of the deposited metal almost corresponds to the base metal hardness. In both cast irons the hardness reduction is observed when approaching the zone of their fusion: by 6–8 in deposited metal and by 13–15 units in the base metal. It should be noted that the lower hardness in the base metal is observed on the product working surface. This is due to the peculiarities of product casting, for example, its non-working side could, probably, be cooled at higher rates. It can be concluded from the above-mentioned that under the real service conditions

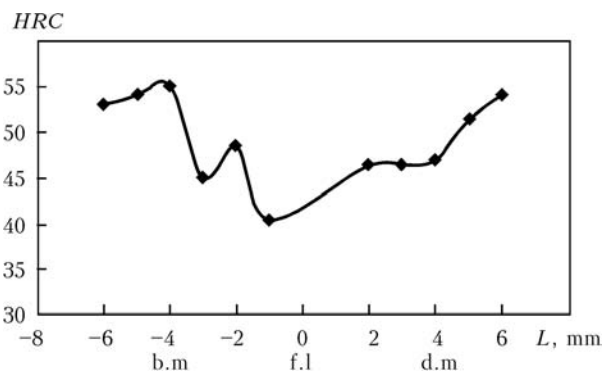


**Figure 5.** Hardness of specimen, deposited by ESS using shot of high-chrome cast iron (b.m – base metal, f.l – fusion line, d.m – deposited metal)

the as-repaired product should possess a wear resistance of not less than by 20 % exceeding that of the new product (coming only from the hardness values).

### Conclusions

1. Restoration of worn-out products, made of high-chrome cast irons, by ESS using cast iron shot, also containing the increased amount of chromium, allows manufacturing quality surfaced products.

2. Applying the offered surfacing with use of a water-cooled mould and discrete filler, it is possible to provide the optimum conditions of crystallization of molten metal (metal pool) with obtaining of fine-dispersed structure and increased service characteristics.

3. Application of ESS for some products as a technology of repair can increase their service life not only due to extension of this life, but also by imparting the higher service properties to the working surface.

4. Full-scale tests of restored different-purpose products by the offered method of ESS will allow defining the optimal fields of application of the offered technology and specifying of its advantages.

- (1969) *Materials in machine building*: Refer. Book. Vol. 4: Cast iron. Ed. by I.V. Kudryavtsev, A.A. Zhukov, A.D. Sherman. Moscow: Mashinostroenie.
- Garber, M.E. (1972) *Cast products from white wear-resistant cast iron*. Moscow: Mashinostroenie.
- Tsylin, I.I. (1983) *White wear-resistant cast irons. Structure and properties*. Moscow: Metallurgiya.
- Kuskov, Yu.M., Sarychev, I.S. (2004) Reduction electroslag surfacing of cast iron cylinders of mill 2000. *Svarochn. Proizvodstvo*, **1**, 39–43.
- Kuskov, Yu.M. (2001) Electroslag refining of different production waste using nonconsumable water-cooled electrode. *Elektrometallurgiya*, **2**, 24–28.

Received 15.05.2013



# PECULIARITIES OF INDUCTION BRAZING OF DIAMOND-HARD ALLOY CUTTERS TO BLADE OF BODY OF COMPLEX DRILL BIT

B.V. STEFANIV

E.O. Paton Electric Welding Institute, NASU  
11 Bozhenko Str., 03680, Kiev, Ukraine. E-mail: office@paton.kiev.ua

It is determined that application of existing technology for brazing of diamond-hard alloy plates (DHP) and hard alloy holder to bit blade does not provide necessary quality of parts due to overheating of brazed-in cutter in brazing of the next one that results in overheating of following diamond-hard alloy cutter (DHC) and degradation of diamond layer owing to graphitization. Different heat sources of bit blades for brazing were analyzed. Technology of induction brazing of DHC to drill bit blade providing necessary characteristics of diamond layer of DHC as a cutting tool was developed. Manufacturing process of induction brazing of DHC to drill bit blade allowing brazing of DHC to blade without overheating of its diamond layer and preserving its high level service characteristics was designed. It is shown that proposed technology of induction brazing of DHC to bit blade allows using brazing filler materials with brazing temperature not more than 680–700 °C without loss of this layer serviceability. Brazing filler materials of standard origin and developed at the E.O. Paton Electric Welding Institute of the NAS of Ukraine were tested in process of investigations. A conclusion that brazing filler materials of Ag–Cu–Zn–Ni–Mn and Ag–Cu–Zn–Sn–Ni–Mn systems are the most perspective for induction brazing of DHC to blade was made based on results of generalization of test complex. Technology of welding of blades to body of drill bit was developed which allows reducing spattering of electrode metal on diamond layer of DHC and improving weld formation. This technology of brazing of DHC to blades of body of complex drill bit was applied in full-size products and tested under real service conditions during on-land drilling of gas wells. 6 Ref., 1 Table, 5 Figures.

**Keywords:** *induction brazing, superhard materials, diamond-hard alloy cutter, diamond-hard alloy plate, hard alloy holder, bit, heat resistance, brazing filler material*

Technology of manufacture of drilling tool with diamond-hard alloy plates (DHP) in Ukraine was developed at the V.N. Bakul Institute for Superhard Materials of the NAS of Ukraine. However, domestic technology of manufacture of diamond drill bits, developed many years ago, does not fulfill current requirements. Brazing of DHP and hard alloy holders to blade was combined in known technology that did not allow controlling temperature of diamond layer. The situation was aggravated by application of induction heating with loop inductor which was used for subsequent brazing-in of hard alloy holder and DHP to the blade. In this case, non-uniform temperature field was created in brazing of the next DHC as well as reheating of brazed-in DHC during brazing of the following one took place. Moreover, induction heating was combined sometimes with flame heating that creates the danger of direct contact of diamond layer with torch flame. Development of new technol-

ogy requires investigation of various aspects of this process.

Aim of the present study lies in development of technology for brazing of DHC to blade and welding of blade to body of complex bit for providing minimum effect of heating on diamond layer properties, i.e. preservation of service characteristics of diamond layer of DHC as a cutting tool, increase of wear-resistance and value of headway of drill bit up to the level of foreign analogues.

The aim put by is achieved through development of new designs of drill tool [1, 2], i.e. setting of additional diamond-hard alloy cutters (DHC) on bit gage surface is used for drill bit and increase of dimensions of dovetail grooves for washing and lifting of cuttings and new brazing technology are applied for calibrator.

Present study provides the results of investigations on DHC joining to blade with the help of brazing. Different sources of heating of bit blades for brazing are analyzed. Selection of method and equipment providing necessary efficiency of the process, convenience and safety of equipment operation as well as control of brazing parameters has significant importance. Correct selection of equipment and method of brazing



## Classification of methods for brazing of hard alloy tool

Brazing method	Tool	Type of production
Brazing in continuous furnace with shielding atmosphere	All, except for large-size cutters of cutoff saws	Mass, large-scale, small-scale of different types of tool at large output
Brazing in chamber furnaces with atmosphere shielding	Same	Small-scale, piece
Induction brazing with operating frequency 2–66 kHz	Large-size and cutoff saws, drilling tool, road harrow	Any
Induction brazing with operating frequency 66–440 kHz	Cutoff cutters, drilling tool, cutoff saws with body thickness not more than 4 mm	»
Resistance soldering	Disc saws and cutters for treatment	Special
Flame brazing	Outsize drilling bit	Small-scale, piece production, repair

provides optimum conditions for formation of strong weld, elimination of high level of residual stresses, and, respectively, increase of service life and safety of tool in process of its operation.

Finished brazing filler materials are used for tool brazing, therefore, brazing is classified as a rule on method of heating. In turn, these methods are divided on methods of shielding of brazed joints from oxidation during brazing. Besides, their selection depends on scale of planned production, i.e. whether it will be small-scale production with large variety of products or large-scale production of single-type tool (Table).

Induction brazing is the most widespread method of manufacture of drilling tool, regardless large quantity of variants of performance of brazing process and variety of equipment. Further, the most attention is given to this method of brazing of drilling tool and the main principles of preparation to brazing, location of DHC, hard alloy inserts, brazing filler material, flux and positioning of tool in the inductor are considered.

Induction brazing is the most highly applied method of manufacture of hard alloy tool as in small-scale production and piece brazing as well as in large-scale production.

Efficiency of induction heating depends on electric parameters caused by characteristics of generator and inductor (current frequency, field intensity, proximity effect and etc.) and physical-chemical properties of tool and structural materials. Increase of frequency of generator current rapidly decreases depth of current penetration in material being brazed, i.e. gradient of temperatures on its surface and in depth is increased.

Heat conduction of hard alloy of tungsten group (VK) is 1.5 times higher than heat conductance of structural steel and 3 times than that of hard alloys of titanium-tungsten group (TK). It rises several times with increase of cobalt content. Specific electric resistance of hard alloys of TK group is 2 times higher of that in hard alloys

of VK group and temperature conductivity of hard alloy of TK group is 3.5 times lower than in hard alloy of VK group. This explains low heat resistance of hard alloy of TK group in comparison with VK group. On practice, this results in appearance of cracks in tool using hard alloys of TK group. These materials require keeping of conditions of uniform smooth heating and cooling of tool in process of brazing.

The most important in the process of brazing is not to allow band heating of hard alloy, in particular, of VK group, that can result in formation of cracks in the tool. TVCh generators of 10–66 kHz frequency are the most universal at the present time. Higher values of frequency can be used for small parts, however, there are some manufacturing difficulties with uniform heating control, that results in loss of process efficiency and appearance of critical residual stresses. Modern TVCh units can be equipped by programmer with controller providing high uniform heating of parts based on set program at speed corresponding to that of rejection of heat in the internal material layers. Heating speed of 40–100 °C/s is considered the optimum one that, except for mentioned above, can be achieved through corresponding selection of gap between the part and inductor (8–15 mm). Reduction of gap results in non-uniform heating.

Configuration of the inductor was chosen based on minimum temperature difference at heating of operating elements of blades for brazing. Uniformity of heating was determined in experimental way. The blind holes were drilled in blade housing for this. Distribution of temperature in the blind holes of the blade is determined with the help of thermal couples of TKhA type and several TRM202 devices at set specific heat power (Figure 1). Surface heating could not provide uniform distribution of temperatures in the surface layer. Temperature of body surface is always higher than set for internal boundary

of the layer. It can be seen from Figure that the lower time of heating, the higher is surface temperature and the lower is temperature in the deeper layers.

Double-loop inductor of special structure (Figure 2) providing uniform temperature field in area of cutter brazing was developed for brazing of DHC into blade working zone. Procedure of selection of size and shape of inductive drive (inductor) was determined in experimental way. In our case, the values of current in each wind depend on gap between part and inductive drive as well as geometry dimensions of winds. This effect is used in some cases for achievement of required temperature of heating of parts of different section and sizes.

As can be seen from Figure 2 showing also the curves of temperature distribution in body (housings) of blade being heated, the first loop of inductor heats working zone up to 680–700 °C and the second loop plays a role of preheating up to 580–600 °C. At induction heating the electromagnetic energy from outside comes inside the body through its surface and then transforms into the heat energy inside the body. Heat energy due to heat conduction effect moves from the places with high temperature to the places with low one. Temperature of separate points of the body is constantly changes. Dependence of temperature on geometry coordinates is determined by distribution of heat sources in the blade being heated, properties of material and time during which heating takes place.

Surface and deep heating are used in our case allowing obtaining uniform heating of the part in required zone without preheating of the separate areas. It is necessary to increase time of heating and reduce specific power supplied to the part for this. The effect of heat conduction is observed in our case as well providing transfer of heat to the less heated areas. In this situation a character of temperature distribution is different than in heat transfer from outside when using only effect of heat transfer. Since heat evolution mainly takes place in a layer of  $\Delta$  thickness (where  $\Delta$  is the depth of current penetration), then temperature in this layer has the highest increase. In deeper layers the temperature achieves smaller values during the same time. However, difference in temperatures is small [3] in scope of layer of  $\Delta$  thickness.

Performance of simultaneous brazing of all cutters to the blade became possible only with the help of high-frequency heating. When using this technology, the diamond layer of the cutter stays minimum time at high temperature and pre-

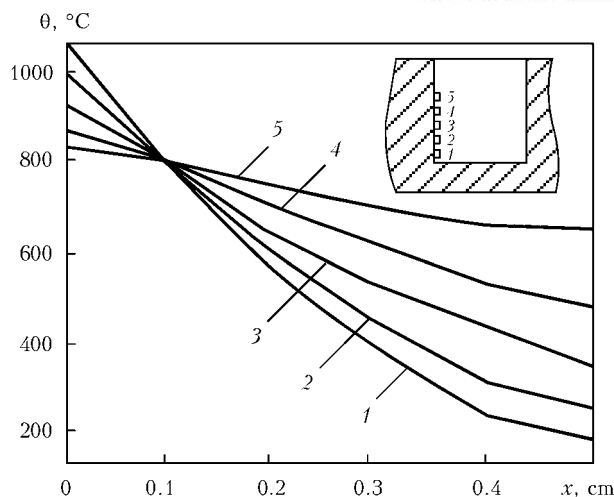


**Figure 1.** Distribution of temperature in steel body of the blade at set specific heat power under condition of obtaining of specified temperature of surface  $\theta = 800 \pm 20$  °C at 0.1 cm depth: 1 –  $t = 1.5$  s; 2 – 2.8; 3 – 3.2; 4 – 4.5; 5 – 10

serves required technological properties in operation. At that, temperature field in zone of the cutter brazing became smooth along the whole operating element of the blade, brazing temperature makes approximately 680–700 °C. It should be noted that developed compositions of brazing filler materials of Ag–Cu–Zn–Ni–Mn and Ag–Cu–Ni–Mn–Pd [4, 6] systems which were used in brazing of complex DHC, give good wetting of low-alloy steel of the blade and material of the cutters' substrate as well as provide safe join-

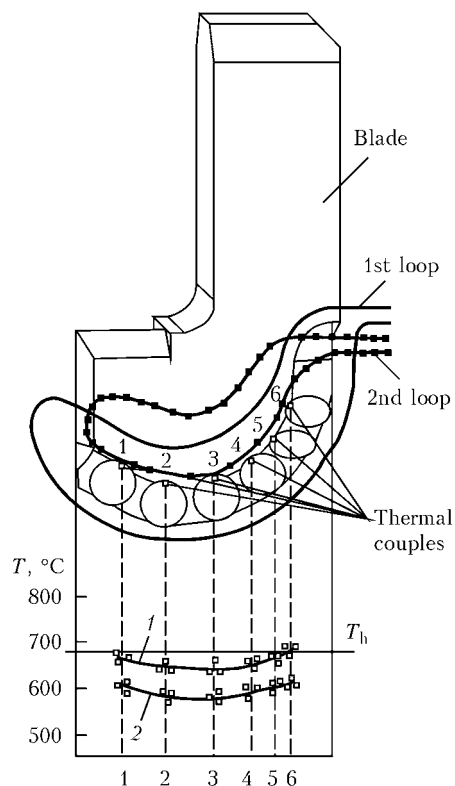


**Figure 2.** Scheme of location of double-loop inductor and distribution of temperatures in zone of brazing in connection of two loops (1) and one (2) loop



**Figure 3.** Microstructure ( $\times 300$ ) of brazed DHC + steel joint before drill bit testing: 1 – hard alloy VK8; 2 – brazed seam; 3 – steel 30Kh

ing of the latter to blade. Analysis of microstructure of brazed joint shows that brazing filler material of Ag–Cu–Zn–Ni–Mn system gives good wetting of hard alloy as well as steel, moreover fusion zone from both sides is smooth without formation of wide diffusion zones. Figure 3 shows microstructure of brazed DHC steel joint.

Results of mechanical tests showed that the brazing filler materials of copper–silver–zinc–tin system, alloyed by other elements (manganese, nickel, palladium etc.) provide sufficient shear strength (around 300 MPa) and good spreading of the brazing filler material over steel blade as well as hard alloy.

It should be noted that brazing filler materials of Ag–Cu–Zn–Ni–Mn and Ag–Cu–Ni–Mn–Pd systems are suitable on their technological properties for brazing of DHC to bodies of drill bits. The experiments were carried out using generator VChI4-10U4 of 10 kW power. The following devices were developed and manufactured for DHC to blade brazing:



**Figure 4.** Appearance of bit blade with brazed-in DHC

- single loop inductor for front end part of the operating blade where brazing of diamond-hard alloy inserts takes place;
- double loop inductor for front part of the operating blade where DHC brazing takes place;
- regulating device which holds the blade in set position relatively to the inductor.

Surfaces of the blade parts being joined are cleaned from dirt, grease and corrosion products before DHC to blade brazing. Checking of accuracy of value of gaps on diameter of hole in 0.05–0.1 mm range relatively to DHC was made. Then flux of PV-209 grade was spread in zone of brazing in a form of paste, manufactured by means of flux and water mixing in a form of pastry mixture at water to flux proportion 100:60 (wt.%) as well as inserts of brazing filler material and DHC were introduced in the blade holes. High-frequency heating of working zone of mating parts, i. e. DHC and brazing zone of operating elements of the blade was carried out up to complete melting of the brazing filler material and formation of outer fillet areas on whole section of DHC to blade holes. If incomplete braze penetration of DHC to blade holes is found, the brazing filler material in form of wire of 1.2–2.0 mm diameter was additionally introduced in the braze zone. The following parameters of heat source were used in DHC to blade brazing, i.e.  $I_{\text{main}} = 0.7 \text{ A}$ ;  $I_{\text{anode}} = 1.5\text{--}2.0 \text{ A}$ . Figure 4 shows appearance of blade with brazed-in DHC of drill bit.

Technology of joining of blades to body of drill bit, developed at the V.N. Bakul Institute for Superhard Materials of the NAS of Ukraine, was performed by manual arc welding. At that electrodes of ANO-4 grade of 4 and 5 mm diameters were used. Weld leg was reinforced with the help of manual arc welding by UONI-13/55 grade electrodes of 3 mm diameter. The main disadvantage of this technology is reheating of DHC in blade to body welding, at which degradation of diamond layer of DHC takes place, that, in turn, influences on chemical-physical properties of DHC. Significant spattering of electrode metal in zone of DHC being brazed is observed in process of welding. Technology of steel welding in shielding media [5] was used for elimination of these disadvantages in joining of blades to bit body. As a result reduction of electrode metal spattering on diamond layer of DHC and improvement of weld formation were achieved. Maintaining of optimum welding conditions helps to eliminate overheating of the operating elements of diamond-hard alloy plates at which secondary melting of the brazing filler material can take place.

According to proposed technology, joining of blades to body of drill bit was performed using semi-automatic welding in mixture of shielding gases (82 % Ar + 18 % CO<sub>2</sub>) by copped-coated wire Sv-08G2S of 1.2 mm diameter on Fronius device at welding current  $I_w = 180\text{--}200$  A and voltage  $U = 18\text{--}20$  V. No reinforcement of the weld legs was carried out, since metal filled in the gap between blade and bit body met strength characteristics of welded joint of bits, tested under real service conditions. Optimum welding conditions, quantity and sequence of weld deposition, time pauses for weld cooling and etc, were worked out. Particular attention was paid to welding of upper part of bit blade where welding arc is close to diamond layer of DHC.

Figure 5 shows new design of diamond drill bit with calibrator of 132 mm diameter for on-land drilling of gas and oil wells after brazing and welding. Industrial tests were successfully carried out using new designs and new brazing technology at Zasyadko Coal Mine.

Pilot-industrial batch of drill bits for underground and on-land drilling of wells for recovery of dispersed methane was manufactured using pilot batches of brazing filler materials of Ag-Cu-Zn-Ni-Mn and Ag-Cu-Zn-Ni-Mn-Pd [6] systems that allowed extending their service resource as well as several times increase value of well headway.

### Conclusions

1. New technology was developed for brazing of diamond-hard alloy cutters to blades, according to which all the cutters in contrast to known solutions are brazed in the blades simultaneously that eliminates secondary heating of the cutter and reduces danger of diamond layer degradation.

2. Technology of production of drill bits and calibrator developed at the E.O. Paton Electric Welding Institute was implemented at Zasyadko Coal Mine (Donetsk) for underground and on-land drilling of gas wells.

3. It is determined based on results of performed commercial investigations of diamond



**Figure 5.** Drill bit with calibrator for on-land drilling of wells

drill bits equipped with diamond-hard alloy cutters that application of indicated bits for on-land drilling of gas wells increases wear-resistance of drilling tool and speed of drill in comparison with serial bits of Russia and Ukraine.

1. Paton, B.E., Stefaniv, B.V., Khorunov, V.F. et al. *Diamond drill bit*. Pat. 92268 Ukraine. Int. Cl. E21B 10/46 E21B 10/54. Fil. 05.05.2009; Publ. 11.10.2010.
2. Paton, B.E., Stefaniv, B.V., Khorunov, V.F. et al. *Calibrator*. Pat. 92820 Ukraine. Int. Cl. E21B 10/26 E21B 7/28. Fil. 10.03.2009. Publ. 10.12.2010.
3. Glukhanov, N.P. (1989) *Physical principles of high-frequency heating*. Ed. by A.N. Shamov. Leningrad: Mashinostroenie.
4. Stefaniv, B.V. (2013) Development of the technology of brazing diamond-hard alloy cutters. *The Paton Welding J.*, **2**, 37–41.
5. Svetsinsky, V.G., Rimsky, S.T., Galinich, V.I. (1994) Welding of steels in shielding gas mixtures on argon base in industry of Ukraine. *Avtomatich. Svarka*, **4**, 41–44.
6. Khorunov, V.F., Maksimova, S.V., Stefaniv, B.V. (2012) Effect of palladium on structure and technological properties of Ag-Cu-Zn-Ni-Mn system brazing filler alloys. *The Paton Welding J.*, **9**, 20–25.

Received 24.05.2013



# THYRISTOR DIRECT CONVERTERS FOR SUPPLY OF RESISTANCE WELDING MACHINES

P.M. RUDENKO and V.S. GAVRISH

E.O. Paton Electric Welding Institute, NASU

11 Bozhenko Str., 03680, Kiev, Ukraine. E-mail: office@paton.kiev.ua

Machines for resistance and flash-butt welding, power of which can reach several hundreds of kilowatts, are widely used for manufacture of metallic structures and parts. In present time power supply schemes from alternating current main of 50 (60 Hz) frequency, single- and double phase, became the most wide spread for power supply of these machines. Now significant attention is paid to providing of electromagnetic compatibility of energy consumers, especially such powerful as resistance welding machines. This can be provided at uniform loading of three-phase main, including with the help of converters of frequency and number of phases. Aim of the present paper is development and analysis of frequency converters providing uniform loading of three-phase main for existing powerful resistance welding machines, the welding transformers of which are designed for supply from single-phase 50 Hz main. Shown are advantages and disadvantages of the converters operating on 30, 37.5 and 45 Hz frequencies. Pilot specimen of 37.5 Hz converter passed industrial tests during welding of railway rails. 5 Ref., 3 Figures.

**Keywords:** *resistance welding machines, converters of frequency and number of phases, uniform loading of three-phase main*

Machines for resistance and flash-butt welding are widely used in manufacture of metallic structures and parts. At that, each of them can have different power supply schemes [1–3], the following obtained the highest distribution, i.e.:

- from alternating current main of 50 (60 Hz) frequency, single- and double-phase;
- from converters of frequency and number of phases;
- from sources of rectified voltage of industrial frequency;
- from inverters of increased frequency with further rectifying;
- from condenser type sources.

Variety of power supply schemes is explained by the necessity of setting and working out of different welding cycles providing required quality of welded joints from different metals and alloys. Besides, great attention in present time is paid to electromagnetic compatibility of energy consumers, in particular, such powerful as resistance welding machines (GOST 13109–97). This can be provided at uniform loading of three-phase main, including with the help of converters of frequency and number of phases.

Thus, frequency converters which found application in resistance welding were developed by «Sciaky» company for the first time [1, 2]. However, regardless good technological indices, they did not found wide distribution due to bulky

and heavy welding transformer designed for very low frequency (approximately several hertz). A conclusion that required electric and technological characteristics can be obtained at higher frequencies was made based on analysis of frequency characteristics of similar machines, performed by V.K. Lebedev [2].

Converter operating at 30 Hz frequency without valves on secondary circuit of the welding machine and providing uniform loading of three-phase electric main was proposed [2]. The welding machines with such a converter have technological as well as energy advantages in comparison with the single-phase machines. They exceed direct current machines on efficiency and some other characteristics. However, these machines have specific disadvantages, i.e. increased mass and dimensions of the welding transformer in comparison with industrial frequency machines; impossibility of application of such a converter for power supply of existing single-phase resistance machines without reduction of supply voltage since in this situation open-circuit current of the welding transformer rises dramatically (in dozen times) that results in rise of electric losses and failures in operation of automatic regulation systems up to emergency modes.

Aim of the present work is development and analysis of frequency converters providing uniform loading of the three-phase main of existing powerful resistance machines, the welding transformers of which are designed for supply from single-phase 50 Hz main. The authors developed the algorithms for control of converters using 37.5 and 45 Hz at which these drawbacks are



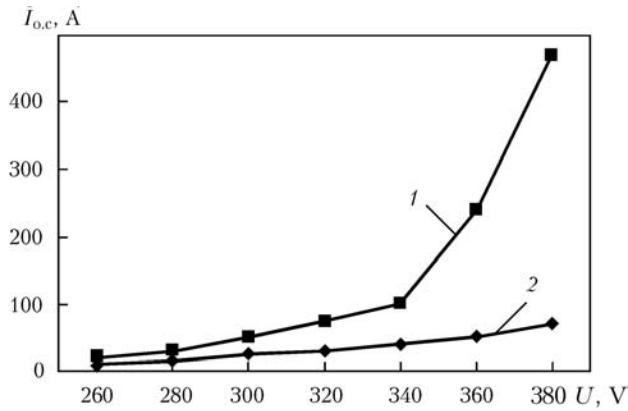


**Figure 2.** Dependence of open-circuit current on input voltage for welding transformers of K-190 (2) and K-1000 (1) machines at supply from 37.5 Hz frequency converter

Thus, experimental investigations of power transformer for resistance machine K-1000 showed 10 time increase of open-circuit current at supply from alternating current main of above 360 V voltage and frequency 37.5 Hz in comparison with supply of 50 Hz frequency voltage at the same effective voltage (Figure 2). Open-circuit current for machine K-190 makes 20A and for machine K-1000 is 35 A at supply from alternating current main of 50 Hz frequency, voltage  $U = 380$  V. It is obvious that operation of the transformers would be more complicated at 30 Hz voltage frequency.

Special measures should be taken, if the converter is supposed to be used for 50 (60) Hz transformers. At that, the main index, i.e. equal phase loading, should be preserved.

The most simple method for frequency increase is «insert» of multiple number of periods of voltage with 50 Hz frequency in a form of 37.5 Hz voltage after each voltage pulse of similar polarity in that linear voltage at which pulse ends [4]. In this case

$$K_e = [(2n + 1)/(2n + 1.333)]^2,$$

$$T_w = 40 + 60n, K_a = 1.41(2n + 1.333)/(2n + 1).$$

In particular, frequency of voltage makes 45 Hz at  $n = 1$  [5]

$$K_e = 0.81, T_w = 100 \text{ ms}, K_a = 1.56.$$

Indexes of efficiency on power and coefficient of amplitude approach to data for double-phase power since power is virtually carried out by series of 50 Hz pulses. At that, open-circuit current of welding transformer significantly reduces and three-phase selection of electric power allows obtaining uniform main load at 0.1 s averaging time.

Therefore, all considered algorithms have advantages as well as disadvantages. The algorithm using voltage of 37.5 Hz frequency is the most optimum for already existing welding machines.

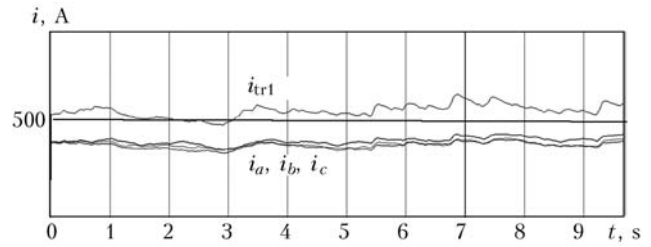


**Figure 3.** Oscillograms of currents  $i_a, i_b, i_c$  in A, B, C phases in the input of converter and current in the primary circuit of welding transformer  $i_{tr1}$  in welding of rails on K-1000 machine using converter of frequency and number of phases

Power source with 37.5 Hz voltage frequency passed industrial tests during resistance welding of large section parts. It was used in fusion welding more that two years on rail welding train (technological tests of the power source were guided by staff researcher of the E.O. Paton Electric Welding Institute A.V. Didkovsky). Welding of strings set in main rail track was carried at final stage of testing. In the first as well as second cases the quality of welded parts met the technical requirements for these parts.

Oscillography of phase currents in the input of converter of frequency and number of phases in welding (Figure 3) showed that they are equal between each other and reduces per 20 % in comparison with current in load (source output).

### Conclusions

1. Frequency converters with control algorithms on 37.5 and 45 Hz frequencies have electric advantages over power sources for resistance welding machines of industrial frequency due to consumption of electric energy from three phases.
2. Pilot tests of frequency converter on 37.5 Hz showed possibility and appropriateness of its application for flash-butt welding, in particular, of railways rails. At that, uniform load of three-phase electric main is provided.

1. Lebedev, V.K., Pismenny, A.A. (2001) Power systems of resistance welding machines. *The Paton Welding J.*, **11**, 28–32.
2. Lebedev, V.K., Pismenny, A.A. (1998) Improvement of power systems for resistance butt welding machines. In: *Welding and related technologies into the 21st century*. Kiev: Naukova Dumka.
3. Lebedev, V.K., Pismenny, A.A. (2003) Power system of flash-butt welding machines with a transistor inverter. *The Paton Welding J.*, **2**, 10–12.
4. Kuchuk-Yatsenko, S.I., Gavrish, V.S., Rudenko, P.M. et al. *Method of electric power supply of a.c. single-phase resistance machines*. Pat. 86279 Ukraine. Int. Cl. B23K 11/24. Publ. 10.04.2009.
5. Kuchuk-Yatsenko, S.I., Gavrish, V.S., Rudenko, P.M. et al. *Method of electric power supply of welding transformer of AC single-phase resistance machines*. Pat. 100064 Ukraine. Int. Cl. B23K 11/24. Publ. 12.11.2012.

Received 15.04.2013